CAIO FERNANDO RODRIGUES DOS SANTOS

Orthogonal and Minimum Energy High-Order Bases for the Finite Element Method

Bases Ortogonais de Alta Ordem e de Mínima Energia para o Método de Elementos Finitos

40/2015

CAMPINAS
2015

i

UNIVERSIDADE ESTADUAL DE CAMPINAS

FACULDADE DE ENGENHARIA MECÂNICA

CAIO FERNANDO RODRIGUES DOS SANTOS

Orthogonal and Minimum Energy High-Order Bases for the Finite Element Method

Bases Ortogonais de Alta Ordem e de Mínima Energia para o Método de Elementos Finitos

Doctoral Thesis presented to the School of Mechanical Engineering, University of Campinas, to obtain the Ph.D. degree in Mechanical Engineering in the area of Solid Mechanics and Mechanical Design.

Tese de Doutorado apresentada à Faculdade de Engenharia Mecânica da Universidade Estadual de Campinas, para obtenção do título de Doutor em Engenharia Mecânica na área de Mecânica dos Sólidos e Projeto Mecânico.

THIS VERSION CORRESPONDS TO THESIS FOR THE EXAM BY THE PHD CANDIDATE CAIO FERNANDO RODRIGUES DOS SANTOS, SUPERVISED BY PROF. DR. MARCO LÚCIO BITTENCOURT

Supervisor: Prof. Dr. Marco Lúcio Bittencourt

....

SUPERVISOR SIGNATURE

CAMPINAS

2015

UNIVERSIDADE ESTADUAL DE CAMPINAS

FACULDADE DE ENGENHARIA MECÂNICA

COMISSÃO DE PÓS-GRADUAÇÃO EM ENGENHARIA MECÂNICA

DEPARTAMENTO DE SISTEMAS INTEGRADOS

Ph.D. THESIS

Orthogonal and Minimum Energy High-Order Bases for the Finite Element Method

Bases Ortogonais de Alta Ordem e de Mínima Energia para o Método de Elementos Finitos

Author: **Caio Fernando Rodrigues dos Santos**
Supervisor: **Marco Lúcio Bittencourt**
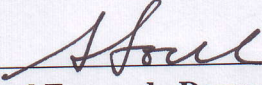
The following members of the Defense Committee have approved this Thesis:

Prof. Dr. Marco Lúcio Bittencourt, President
DSI/FEM/UNICAMP

Prof. Dr. Renato Pavanello
DMC/FEM/UNICAMP

Prof. Dr. Philippe Remy Bernard Devloo
DES/FEC/UNICAMP

Prof. Dr. Ney Augusto Dumont
DEC/PUC-RJ

Prof. Dr. Abimael Fernando Dourado Loula
LNCC

Campinas, 27 de Fevereiro de 2015.

v

Dedication

I dedicate this work to my mother Eunice, my father João Carlos, my brothers Carla and Carlos, my niece Ana Clara and my girlfriend Seica.

Acknowledgements

"Tudo chega com o tempo para quem sabe esperar".

François Rabelais

Abstract

SANTOS, Caio Fernando Rodrigues. Simultaneously Diagonal and Minimum Energy High-Order Bases Appied to Elastic Problems. 2015. 108p. Thesis (Doctoral). School of Mechanical Engineering, University of Campinas, Campinas.

In this work we present construction procedures of bases for the high-order finite element method (FEM) considering a procedures for the simultaneous diagonalization of the internal modes of the one-dimensional mass and stiffness matrices and orthogonalization of the boundary modes using minimum energy procedure. The concepts of minimum energy orthogonalization are used efficiently to construct one-dimensional boundary modes orthogonal to the internal modes of the shape functions. New one-dimensional bases for the high-order FEM are presented for the construction of the simultaneously diagonal and minimum energy basis for the Helmholtz norm. Furthermore, we present a calculation procedure for the $2D$ and $3D$ mass and stiffness matrices, as the combination of one-dimensional coefficients of the mass, stiffness and Jacobian matrices. This procedure is presented for quadrilateral and hexahedral distorted elements in projection, Poisson, plane state and general linear elasticity problems. The use of the one-dimensional matrices procedure allows a significant speedup compared to the standard procedure for distorted and undistorted meshes. Also, this procedure stores only one-dimensional shape functions and their derivatives calculated using one-dimensional integration points, which generates a reduction in memory consumption. The performance of the proposed bases was verified by numerical tests and the results are compared with those using the standard basis using Jacobi polynomials. Sparsity patterns, condition numbers and number of iterations using the conjugate gradient methods with diagonal preconditioner are also investigated. Furthermore, we investigated the use of the local mass matrix using simultaneously diagonal and minimum energy bases as preconditioner to solve the system of equations. The results are compared with the diagonal preconditioner and Symmetric Successive Over Relaxation (SSOR).

Keywords: Finite Element Method, Minimum Energy Orthogonalization, Simultaneously Diagonal Matrices.

Resumo

SANTOS, Caio Fernando Rodrigues. Bases Simultaneamente Diagonais de Mínima Energia de Alta Ordem Aplicado a Problemas de Elasticidade. 2015. 108p. Tese (Doutorado). Faculdade de Engenharia Mecânica, Universidade Estadual de Campinas, Campinas.

Nesse trabalho apresentamos os procedimentos de construção de bases para o Método de Elementos Finitos (MEF) de alta ordem considerando o procedimento de diagonalização simultânea dos modos internos da matriz de massa e rigidez unidimensionais e a ortogonalização dos modos de contorno usando procedimentos de mínima energia. Nesse caso, os conceitos de ortogonalização de mínima energia são usados como uma maneira eficiente de se construir modos de contorno ortogonais aos modos internos das funções de forma $1D$. Novas funções de forma unidimensionais para o MEF de alta ordem são apresentadas para a construção de bases simultaneamente diagonais de mínima energia para o operador de Helmholtz. Além disso, um procedimento para o cálculo das matrizes de massa e rigidez $2D$ e $3D$, como combinação dos coeficientes unidimensionais das matrizes de massa, rigidez e mista é apresentado para elementos quadrilaterais e hexaédricos distorcidos em problemas de projeção, Poisson, estado plano e estado geral em problemas de elasticidade linear. O uso de procedimentos via matrizes unidimensionais permite obter um speedup significativo em comparação com o procedimento padrão, para malhas distorcidas e não distorcidas. Com esse procedimento, é possível armazenar apenas as funções de forma unidimensionais e suas derivadas calculadas nos pontos de integração unidimensionais gerando uma redução no consumo de memória. O desempenho das bases propostas foi verificado através de testes numéricos e os resultados comparados com aqueles usando a base padrão com polinômios de Jacobi. Características como esparsidade, condicionamento numérico e número de iterações usando o método dos gradientes conjugados com precondicionador diagonal também são investigados. Além disso, investigamos o uso da matriz de massa local, utilizando bases simultaneamente diagonais de mínima energia, como pré-condicionador. Os resultados foram comparados com o uso do precondicionador diagonal e SSOR (Symmetric Successive Over Relaxation).

Palavras-chave: Método de Elementos Finitos, Ortogonalização de Mínima Energia, Matrizes Simultaneamente Diagonais.

List of Figures

SUMMARY

Contents

1 Introduction

The advance of numerical procedures has provided increasingly realistic and reliable modeling. These developments have contributed to make the use of computer simulation techniques a reality in various segments of engineering. In this context, the high-order finite element methods has emerged as a numerical analysis tool with characteristics as spectral convergence problems with smooth solution (Karniadakis and Sherwin, 1999). There has been works in several applications such as computational fluid dynamics (Lomtev *et al.*; Karniadakis and Sherwin, 1998; 1999), Heat transfer (Beskok and Warburton, 2001), electromagnetism (Demkowicz and Vardapetyan, 1998), nonlinear elasticity (Krause *et al.*; Bittencourt *et al.*; Dong and Yosibashi, 1995; 2007b; 2009), seismic imaging (Virieux *et al.*, 2012) among others.

1.1 High-Order Finite Element Methods

The systematic development of the finite element method (FEM) began in the decade of 1960 with the Turner's work (Turner, 1956), consolidating with the work done by (Clough; Oden; Clough, 1960; 1987; 2001). The method is based on the domain discretization and the use of polynomial functions for the approximation of the solution. We can distinguish three variants for the FEM. In h-version (Hughes; Johnson; Oden *et al.*, 1987; 1990; 1981), the convergence of the approximation is obtained by reducing the size h of mesh elements. In p-version (Babuska *et al.*; Babuska and Suri; Babuska and Suri; Szabó and Babuska, 1981; 1987; 1990; 1991), convergence is achieved by increasing the polynomial order P of the basis functions. This version is also known as the high-order FEM (p-FEM). There is still a mixed version or hp combining elements of versions h and p.

Generally in the high-order FEM, the choice of the basis functions influences the condition number and the sparsity pattern of the discretization system. Thus, the closer to a diagonal matrix is possible to represent the problem, the easier the solution of the initial value problem. In addition, if the matrix associated with the system of equations is ill-conditioned, rounding and truncation of operations can lead to very large errors in the solution (Karniadakis and Sherwin, 1999). Note that high performance is not only related to the use of distributed systems but also the construction of basis functions that allow the construction of better conditioned and sparser matrices.

To improve the properties of sparsity and conditioning of the matrix systems, obtained through interpolation using the high-order FEM, classic hierarchical functions using Legendre polynomials were used which exploited the tensor nature and orthogonality concepts of functions (Babuska *et al.*, 1981). In this case, the stiffness matrix obtained for structured elements becomes block diagonal. However, these functions exhibit an exponential increase in the condition number for unstructured elements with high-order polynomial expansion (Abdul-Rahman and Kasper, 2007).

The use of hierarchical functions was introduced in (Carnevali *et al.*, 1993) for triangles and tetrahedra. Moreover, orthogonality concepts were used to achieve local matrices with better conditioning compared to the sparsity of functions defined in (Szabó and Babuska, 1991).

In (Karniadakis and Sherwin, 1999), tensor product was used for the construction of hierarchical functions to quadrilaterals and hexahedra, using one-dimensional shape functions with orthogonal Jacobi polynomials. This basis is widely used in high-order applications such as fluid dynamics problems and in structural mechanics (Nogueira Jr and Bittencourt; Dong and Yosibash, 2007; 2009). The Jacobi polynomials have been extensively used in the construction of high-order shape functions due to their orthogonality, resulting in sparser one-dimensional matrices (Beuchler and Schöberl; Bittencourt *et al.*, 2006; 2007a).

In (Nogueira Jr. and Bittencourt, 2001), the advantages of using Jacobi polynomials to improve the computational efficiency of high-order bases were discussed. It was found an exponential increase in condition number for matrices using the bases functions proposed (Carnevali *et al.*, 1993), but lower than that shown in the functions introduced by (Szabó and Babuska, 1991).

(Bittencourt *et al.*, 2007a) showed that the appropriate choice of the weights of the Jacobi polynomials results in an increase in sparsity pattern of the mass and stiffness matrices. Furthermore, it has been found in (Bittencourt and Vazquez, 2009) that the choice of the weights for the Gauss-Jacobi, Gauss-Radau-Jacobi and Gauss-Lobatto-Jacobi quadratures optimizes the number of operations required for the integration of the mass and stiffness matrices.

Another technique widely used in the high-order FEM is the Schur complement, referenced in the literature also as static condensation or substructuring. The application of this procedure significantly improves the conditioning of the algebraic system and the performance of iterative methods for the solution systems of equations (Axelsson, 1994). In high-order methods that operation is

always performed.

In real problems, where in general the system matrices are large, local solution techniques has also been used successfully. In (Bittencourt and Vazquez, 2010), a technique based on eigenvalue decomposition of mass matrix of the elements was proposed. These concepts were used to develop local methods of explicit and implicit time integration by (Furlan, 2011). Recently in (Yu *et al.*, 2014), a semi-local technique was used to accelerate the solution of linear systems resulting from the discretization of in fluid-structure interaction with linear elasticity.

1.2 Objectives

The convergence rate of the approximated solution may be obtained improved by increasing the polynomial order of the shape functions in the high-order FEM. This feature combined with complex geometry make the method computationally expensive which restricts their application to problems with more variables. Thus, it becomes necessary to use efficient algorithms and is therefore fundamental to search for numerical and computational solutions to make high-order FEM more accessible to users.

In the study and implementation of algorithms for the high-order FEM, some computational aspects, such as the need for scalable algorithms and development of efficient solvers for parallel computing (Dong and Karniadakis, 2004; Dong and Yosibash, 2009; Bargos, 2009; da Costa, 2012; Augusto, 2012) must be considered, as illustrated in Fig. 1.1.
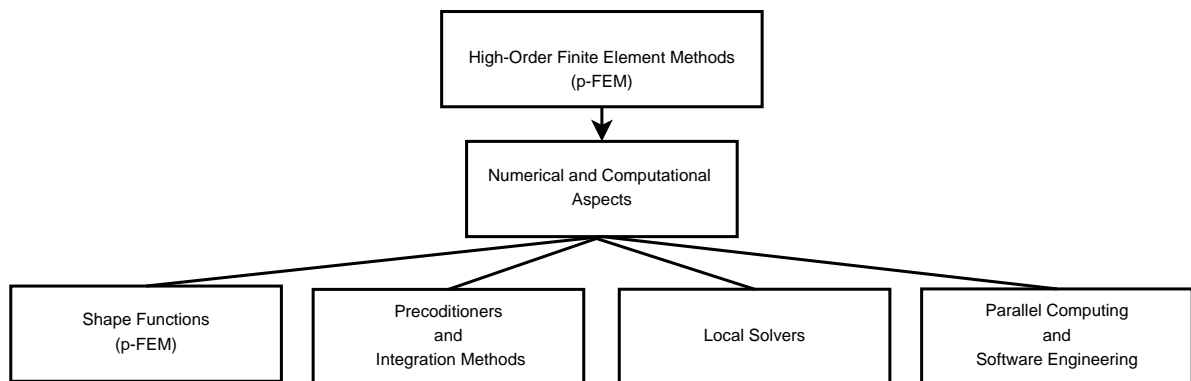
Figure 1.1: Technical aspects considered in the high-order FEM.

Moreover, numerical aspects, including the tensorial bases that producing elementary matri-

ces with good condition number and sparsity pattern, local transient solution procedures, precon-
ditioners, time integration methods are topics that have received extensive attention in the recent
high-order FEM literature (Noels *et al.*, 2004; Bittencourt *et al.*, 2007a; Bittencourt and Vazquez,
2009; Furlan, 2011; Zheng and Dong, 2011).

Therefore, the main focus of this work are:

○ Propose and implement of the simultaneously diagonal and minimum energy bases (SDME)
for the high-order FEM applied to projection problem, Poisson, Helmholtz and transient
linear elasticity using implicit and explicit methods for time integration.

○ Development and implementation of the procedure for calculating the two- and three-
dimensional mass and stiffness matrices using the product of coefficients of one-dimensional
mass, stiffness and mixed matrices for quadrilateral and hexahedral elements for projection,
Poisson, plane-state ($2D$) and general strain ($3D$).

○ Development of local preconditioners using the SDME bases for the high-order FEM.

1.3 Contributions

The main contributions proposed by this work include:

○ Implementation in the software (hp^2)FEM in MatLab of the simultaneously diagonal and
minimum energy bases for the high-order FEM.

○ Generalization of the minimum energy orthogonalization procedures for boundary modes
based on the appropriate choice of the norm.

○ Proposal of the new one-dimensional shape functions for the high-order FEM considering
the simultaneous diagonalization of the internal modes and the minimum energy orthogonal-
ization procedure based on the Helmholtz norm.

○ Study and testing with the SDME bases in projection, Poisson, Helmholtz and linear elasticity
problems using the implicit and explicit methods for time integration.

4

○ Procedure for calculation of the $2D$ and $3D$ mass and stiffness matrices for quadrilaterals and hexahedra structured elements in distorted meshes for problems of projection, Poisson, plane state ($2D$) and general strain ($3D$) for linear elastic problems

○ Local mass preconditioner using the SDME basis for the high-order FEM.

1.4   Organization of the Text

This work is organized as a collection of two papers developed for publication. It is arranged into chapters, which enables independent reading of the contributions.

In Chapter 2, we present the procedures for construction of the simultaneously diagonal and minimum energy bases. We also show that the minimum energy orthogonalization procedure can be generalized to the choice of the appropriate norm. This allows, to obtain basis functions for the high-order FEM considering simultaneously diagonal and minimum energy procedures according to the choice of the norm used in the construction of minimum energy procedures. The new bases are proposed considering the use of the Helmholtz norm in minimum energy procedure. Furthermore, the calculation of the two- and three-dimensional mass and stiffness matrices, respectively for quadrilateral and hexahedral elements, is made using the one-dimensional coefficients product of the mass, stiffness and Jacobian matrices for the general case of the undistorted and distorted meshes. This formulation was developed in (Vazquez, 2009) to undistorted elements. The performance of the high-order bases is verified through numerical tests for projection, Poisson, Helmholtz and transient linear elasticity using the explicit method of the central difference for time integration.

In chapter 3, we discuss the application of simultaneous diagonal and minimum energy bases using Helmholtz norm for use in transient elasticity problems with the implicit Newmark method for time integration. The influence of the λ parameter used in the construction of the bases is analyzed. We also present calculation procedures of two- and three-dimensional mass and stiffness matrices for quadrilateral and hexahedral structured elements, using the product of coefficients of one-dimensional matrices in a plane state and general $3D$ linear elasticity. The use of local mass matrix preconditioner is analyzed through numerical tests and compared using the diagonal preconditioner and SSOR (Symmetric Successive Over Relaxation).

The final chapter presents the conclusions and future works.

2 SIMULTANEOUSLY DIAGONAL AND MINIMUM ENERGY HIGH-ORDER BASES FOR STRUCTURED ELEMENTS

2.1 Introduction

In the high-order Finite Element Method (FEM), the convergence of the solution is obtained by increasing the polynomial order of the basis functions. The combination of this feature with geometrical complexity and the required discretization order fully demand the use of efficient algorithms for the solution of large systems of equations. The choice of the basis for the approximation space influences the accuracy and efficiency for the numerical calculation of the approximate solution. This comes from the fact that the basis influences the numerical conditioning and sparsity of the system matrices obtained after discretization. If the matrix associated with the system of equations is ill-conditioned, rounding and truncation operations can lead to very large errors in the solution (Karniadakis and Sherwin, 2005).

Tensor-based hierarchical functions with orthogonal Legendre polynomials were used in (Babuska *et al.*, 1981) to improve the properties of sparsity and conditioning of the matrix systems. In this case, the stiffness matrix obtained for structured elements is block diagonal. However, these functions exhibit an exponential increase in the condition number for unstructured elements with increasing of the polynomial order (Abdul-Rahman and Kasper, 2007).

Hierarchical shape functions for triangles and tetrahedra were presented in (Carnevali *et al.*, 1993). Orthogonality properties of the polynomial basis were used to obtain local matrices with better conditioning and sparsity compared to the functions defined in (Szabó and Babuska, 1991).

In (Karniadakis and Sherwin, 2005), tensor product of one-dimensional Jacobi orthogonal polynomials were considered to build hierarchical shape functions for structured and non-structured elements. The advantages of using Jacobi polynomials to improve the computational efficiency of high-order FEM expansion bases were also discussed in (Nogueira Jr. and Bittencourt, 2001). Modal bases have been used very often in high-order applications not only in fluid dynamics but also in structural mechanics (Nogueira Jr and Bittencourt, 2007; Dong and Yosibash, 2009).

The appropriate choice of the weights of Jacobi polynomials improves the sparsity of mass

and stiffness matrices (Karniadakis and Sherwin, 2005; Bittencourt *et al.*, 2007a). Furthermore, the choice of polynomials weights for the Gauss-Jacobi, Gauss-Radau-Jacobi, and Gauss-Lobatto-Jacobi quadratures also decreases the number of points required for the numerical integration of the mass and stiffness matrices (Bittencourt and Vazquez, 2009).

Sparsity of the elemental matrices is desirable because it influences the conditioning of the resulting algebraic system (Abdul-Rahman and Kasper, 2007). Techniques for simultaneous diagonalization of matrices were used to improve the conditioning and sparsity of the matrix systems in (Shen and Wang, 2007). In this case, $1D$ mass and Laplace stiffness matrices are made simultaneously diagonal. This technique was used in (Šolín and Vejchodský, 2008) to build internal bubble functions for the high-order FEM.

Schur complement, also referred to as static condensation, improves significantly the conditioning properties and performance of iterative methods for solving systems of equations. It has been used as an efficient way to condense the terms related to the internal modes of elements (Babuska and Guo, 1989). Preconditioners based on the element topology and domain decomposition techniques were developed in (Casarin, 1997). In (Vejchodský, 2010), the concept of minimum energy was presented as a simple way to construct boundary modes orthogonal to internal modes. This technique is applied directly to the construction of one-dimensional basis functions.

Simultaneous diagonalization techniques for the internal modes were employed in (Zheng and Dong, 2011) to build a high-order expansion basis for structured elements. The algorithm results in one-dimensional local internal mass and stiffness matrices simultaneously diagonal and with the same condition number. It is also known that the boundary modes influences strongly the performance and numerical conditioning of the system matrices after the Schur complement. The modification of the interior modes only does not affect the numerical performance of the Schur-complemented system (Zheng and Dong, 2011). An algorithm based on Gram-Schmidt orthogonalization was used to obtain one-dimensional boundary modes orthogonal to the internal modes. The obtained basis has large efficiency in terms of conditioning and number of iterations for convergence for mass, Poisson stiffness, and Helmholtz matrices using the conjugate gradient method, when compared to the standard basis proposed in (Sherwin and Karniadakis, 1995; Karniadakis and Sherwin, 2005). However, the extension to non-structured elements may be difficult.

In this paper, we present a new methodology for building higher-order expansion bases. Our proposal is to combine the good results in terms of sparsity and conditioning obtained from

the simultaneous diagonalization of internal modes with the minimum energy transformation of one-dimensional boundary modes. The construction of boundary modes is simpler that the Gram-Schmidt procedure and can be suited to different problems as will be considered for projection, Poisson, Helmholtz, and linear elasticity. A particular high-order basis is presented for the one-dimensional Helmholtz problem after application of simultaneous diagonalization and minimum energy directly to the one-dimensional Helmholtz matrix. In addition, we propose a procedure to calculate the mass and Poisson stiffness matrices for $2D$ and $3D$ elements in terms of the one-dimensional mass and stiffness matrices. This procedure only require one-dimensional quadratures. The performance of the proposed bases are investigated through numerical experiments using the conjugate gradient method with and without diagonal preconditioner. The results are compared to those ones obtained with the standard basis given in (Karniadakis and Sherwin, 2005). Explicit analyses of $3D$ linear elasticity problems are also presented and the number of iterations for convergence is compared with the standard basis for different polynomial orders.

2.2 Construction of One-dimensional Bases with Simultaneously Diagonalization and Minimum Energy

This work considers the one-dimensional modal basis refereed here as the standard basis and built with Jacobi orthogonal polynomials $\mathcal{P}_p^{\alpha,\beta}(\xi_1)$ (Bittencourt *et al.*, 2007a; Karniadakis and Sherwin, 2005). In general, the modal shape functions are related to the elemental topological entities as vertices, edges, and faces.

The one-dimensional standard basis of polynomial order P is defined in the local coordinate system ξ_1 as (Karniadakis and Sherwin, 2005)

$$\psi_p(\xi_1) = \begin{cases} \frac{1}{2}(1-\xi_1) & p = 0 \\ \frac{1}{2}(1+\xi_1) & p = 1 \\ \frac{1}{4}(1-\xi_1)(1+\xi_1)\mathcal{P}_{p-2}^{\alpha,\beta}(\xi_1) & 2 \le p \le P \end{cases}. \tag{2.1}$$

This is a hierarchical basis because the set of functions of order P is included in the set of order $P+1$. The vertex functions correspond to $p = 0$ and $p = P$; the internal functions are obtained for $0 < p < P$. The one-dimensional local coefficients of the mass and stiffness matrices

are respectively determined by

$$M_{pq} = \int_{-1}^{1} \psi_p(\xi_1)\psi_q(\xi_1)d\xi_1, \tag{2.2}$$

$$K_{pq} = \int_{-1}^{1} \psi_{p,\xi_1}(\xi_1)\psi_{q,\xi_1}(\xi_1)d\xi_1, \tag{2.3}$$

with $0 \leq p,q \leq P$ and ψ_{p,ξ_1} the derivative of ψ_p with respect to ξ_1.

The mass and stiffness matrices are symmetric and the submatrices of internal modes are positive-definite. The weights (α, β) of the Jacobi polynomials can be chosen in such way to obtain sparser matrices (Karniadakis and Sherwin, 2005). Fig. 2.1 illustrates the sparsity pattern of the local mass and stiffness matrices for $\alpha = \beta = 1$ and $P = 10$. The mass matrix is pentadiagonal and the vertex and internal blocks of the stiffness matrix are decoupled.
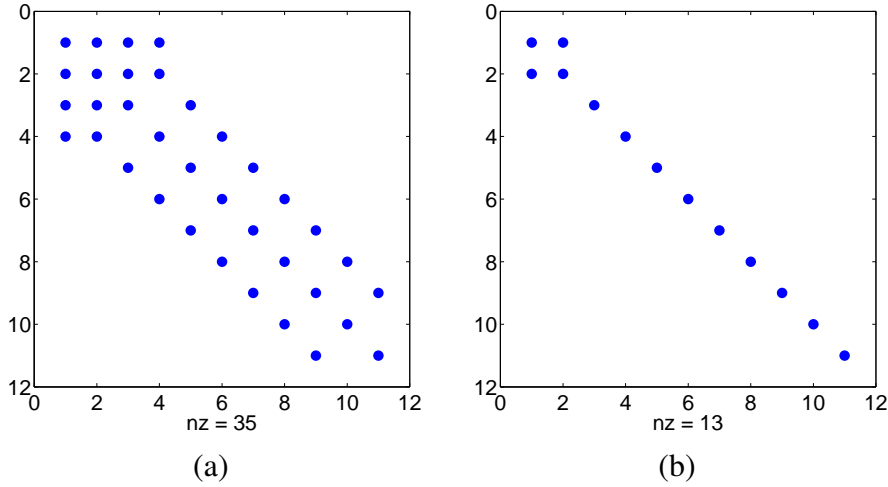
Figure 2.1: Sparsity patterns of the one-dimensional local mass (a) and stiffness (b) matrices obtained with the standard basis ($\alpha = \beta = 1$) and polynomial order $P = 10$ (nz is the number of non-zero coefficients).

We can partition the element system of equation related to the mass matrix

$$[M]\{a\} = \{f\} \tag{2.4}$$

in terms of the blocks relative to vertex (v) and internal (i) modes as

10

$$\begin{bmatrix} [M_{vv}] & [M_{vi}] \\ [M_{vi}]^T & [M_{ii}] \end{bmatrix} \left\{ \begin{matrix} \{a_v\} \\ \{a_i\} \end{matrix} \right\} = \left\{ \begin{matrix} \{f_v\} \\ \{f_i\} \end{matrix} \right\}, \tag{2.5}$$

The L_2-inner product of functions f and g is defined as $\langle f,g \rangle_{L_2} = \int_{-1}^{1} f(\xi)g(\xi)d\xi$. Therefore, the coefficients of the vertex block are given by $M_{vv} = \langle \psi_p, \psi_q \rangle_{L_2} (p,q = 0,1)$; for the coupling block, $M_{vi} = \langle \psi_p, \psi_q \rangle_{L_2} (p = 0,1; q = 2,...,P)$; and for the internal block, $M_{ii} = \langle \psi_p, \psi_q \rangle_{L_2} (p,q = 2,...,P)$.

It is possible to write Eq. (2.4) in terms of the vertex coefficients only after the Schur complement as

$$[M_s]\{a_v\} = \{f_s\}, \tag{2.6}$$

where

$$[M_s] = [M_{vv}] - [M_{vi}][M_{ii}]^{-1}[M_{vi}]^T \quad \text{and} \quad \{f_s\} = \{f_v\} - [M_{vi}][M_{ii}]^{-1}\{f_i\}. \tag{2.7}$$

The internal coefficients are obtained as

$$\{a_i\} = [M_{ii}]^{-1}\left(\{f_i\} - [M_{vi}]^T\{a_v\}\right). \tag{2.8}$$

The Schur complement has the advantage of reducing the number of equations to obtain for the coefficients of the approximated solution, and decreases the condition number of the associated matrix (Axelsson, 1994).

2.2.1 Diagonalization of Internal Modes

We consider the transformation of the internal modes for the basis given in Eq. (2.1) according to (Shen and Wang, 2007; Šolín and Vejchodský, 2008) as

$$\phi_p(\xi_1) = \sum_{q=2}^{P} y_{pq}\psi_q(\xi_1). \tag{2.9}$$

The coefficients y_{pq} are determined in such way that the blocks $\left[M'_{ii}\right]$ and $\left[K'_{ii}\right]$ related to the internal modes of the new mass and stiffness matrices are diagonal and given by

$$
\begin{aligned}
\left[M'_{ii}\right] &= [Y]\,[M_{ii}]\,[Y]^T, \\
\left[K'_{ii}\right] &= [Y]\,[K_{ii}]\,[Y]^T.
\end{aligned}
\tag{2.10}
$$

Given the symmetric and positive-definite internal mass matrix $[M_{ii}]$, we can diagonalize it as

$$
[X]^T\,[M_{ii}]\,[X] = [\Lambda_M],
\tag{2.11}
$$

where $[X]$ is the eigenvector matrix of $[M_{ii}]$ and $[\Lambda_M]$ is the diagonal matrix with the eigenvalues of $[M_{ii}]$. Using these matrices and the internal stiffness matrix $[K_{ii}]$, we can define

$$
[L] = \left([X]\left[\Lambda_M^{-\frac{1}{2}}\right]\right)^T [K_{ii}]\left([X]\left[\Lambda_M^{-\frac{1}{2}}\right]\right).
\tag{2.12}
$$

This matrix is also symmetric and positive-definite and can be diagonalized analogously to $[M_{ii}]$ as

$$
[Z]^T\,[L]\,[Z] = [\Lambda_S],
\tag{2.13}
$$

where $[Z]$ is the matrix of the eigenvectors and $[\Lambda_S]$ is the diagonal matrix with eigenvalues of $[L]$. Thus, matrix $[Y]$ can be written as

$$
[Y] = \left([X]\left[\Lambda_M^{-\frac{1}{2}}\right][Z]\left[\Lambda_S^{-\frac{k}{2}}\right]\right)^T,
\tag{2.14}
$$

where k is a parameter that influences the condition number of the matrices related to the internal modes. Replacing $[Y]$ in Eq. (2.10), we have

$$
[Y]\,[M_{ii}]\,[Y]^T = \left[\Lambda_S^{-k}\right] \quad \text{and} \quad [Y]\,[K_{ii}]\,[Y]^T = \left[\Lambda_S^{1-k}\right].
\tag{2.15}
$$

For $k = 0$, the internal block of the mass matrix is the identity matrix. The same fact is observed for the stiffness matrix with $k = 1$. The same condition number of the internal mass and stiffness matrices are obtained for $k = 1/2$, as illustrated in Fig. 2.2. The condition number for $[M'_{ii}]$ is 1 for any polynomial order and $k = 0$. For $[K_{ii}]$, the smallest condition number is also 1 but obtained for $k = 1$. From Eq. (2.15), it may be observed that the simultaneous diagonalization procedure for $k = 0$ is equivalent to solving the generalized eigenvalue problem for $[M_{ii}]$ and $[K_{ii}]$.
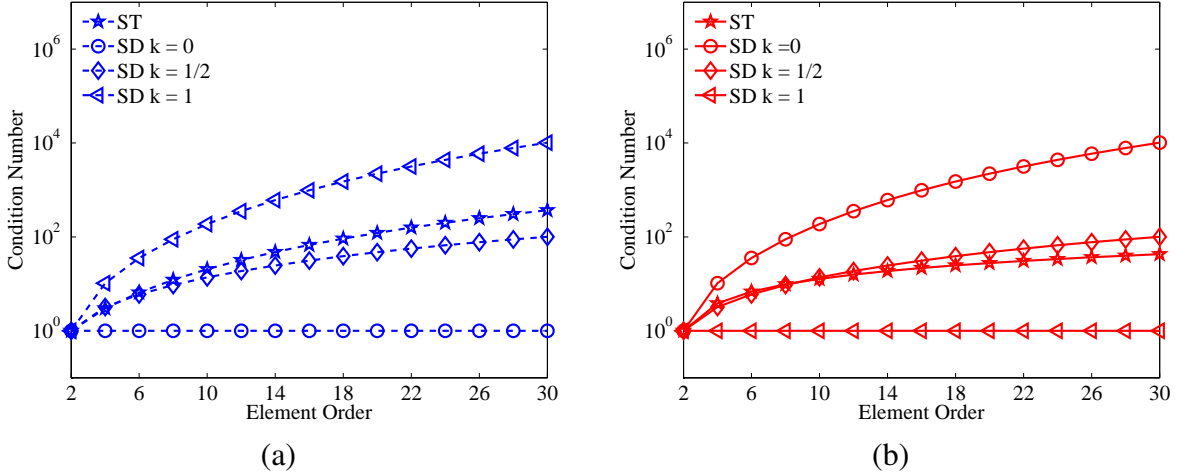
Figure 2.2: Comparison of the condition numbers of the $1D$ internal mass (a) and stiffness (b) matrices for the standard basis (ST) and the simultaneous diagonalization basis (SD) for different values of the parameter k.

The different choices for the parameter k in Eq. (2.15) do not change the order of the functions associated with the internal modes. Fig. 2.3 illustrates the behavior of the one-dimensional functions for different values of k. Note that the internal functions with polynomial order P include the basis functions with polynomial order $P - 1$. Therefore the transformation applied to the internal modes preserve the hierarchy of the basis.

The internal modes form a linear space and the $1D$ linear vertex modes have the best approximation in the space of the interior modes with respect to some norm. One way to calculate this approximation is to determine an orthogonal basis for the internal modes and then make the projection of the linear vertex modes on that basis. The difference between the vertex modes and the best approximation is basically the application of the Gram-Schimdt procedure (Zheng and Dong, 2011). This procedure was used to construct vertex modes orthogonal to the internal modes. Fig.2.4 shows the behavior of the one-dimensional vertex and internal modes for the standard and to the basis given in (Zheng and Dong, 2011) for $P = 3$. The vertex modes have polynomial order P.
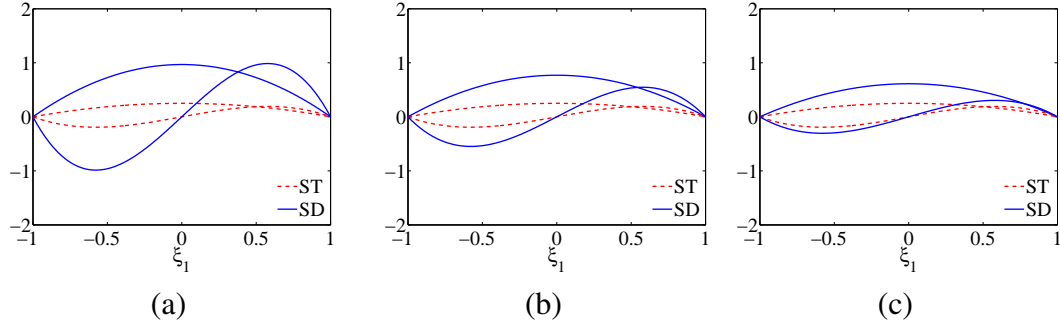
Figure 2.3: $1D$ interior basis functions after simultaneous diagonalization for different values of the parameter $k = 0$ (a), $k = 1/2$ (b) and $k = 1$ (c) with polynomial order $P = 3$.
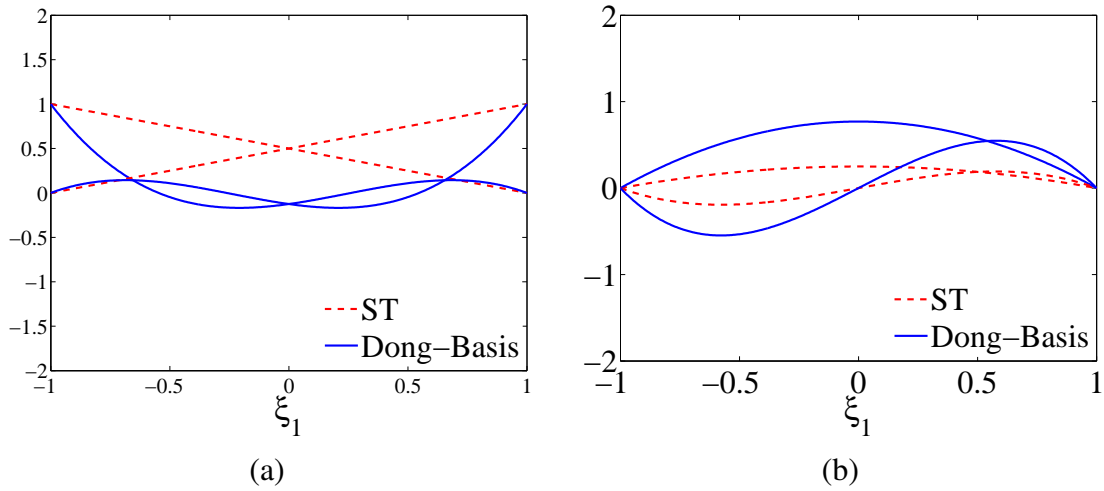
Figure 2.4: $1D$ Dong's basis with $k = 1/2$ and polynomial order $P = 3$ to vertex (a) and interior modes (b).

In the next section we will introduce the concept of minimum energy orthogonalization to the boundary modes. This formulation is used to construct the one-dimensional vertex modes. The main advantage when compared to (Zheng and Dong, 2011) is the convenient choice of the norm used in the orthogonalization procedure. However, the same bases obtained in (Zheng and Dong, 2011) are recovered for $k = 1/2$.

2.2.2 Minimum Energy Basis

Consider a splitting of the approximation space V into the direct sum $V = V^v \oplus V^i$, where V^v and V^i are nontrivial subspaces associated respectively to the boundary and internal modes (Vejchodský, 2010). The basis $\psi \in V$ are defined as

$$\psi = \psi^v \oplus \psi^i, \tag{2.16}$$

where ψ^v are boundary modes in V^v and ψ^i the internal modes in V^i.

The minimum energy extension $\psi^{me} \in V$ of $\psi^v \in V^v$ with respect to V^i is uniquely defined as

$$\psi^{me} := \psi^v - \psi^*, \tag{2.17}$$

where ψ^* is the projection of ψ^v into ψ^i such that

$$\langle \psi^{me}, \psi^i \rangle_{L_2} = 0, \quad \forall \psi^i \in V^i. \tag{2.18}$$

Eq. (2.18) implies that ψ^{me} is the component of ψ^v orthogonal to the subspace V^i. It is possible show that $\|\psi^{me}\|_E \leq \|\psi^v\|_E$, where $\|v\|_E^2 = \langle v,v \rangle_E$ stands for the energy norm (Vejchodský, 2010), and ψ^{me} is called minimum energy basis. Let $\psi^v = \{\psi_1, ..., \psi_{N_v}\}$ and $\psi^i = \{\psi_1,..., \psi_{N_i}\}$. The minimum energy extensions of the standard basis functions is computed as

$$\psi_k^{me} = \psi_k^v - \sum_{j=1}^{N_i} \alpha_{kj} \psi_j^i, \quad k = 1,...,N_v. \tag{2.19}$$

From Eq. (2.18) and (3.11), the coefficients α_{kj}^M for the mass norm are uniquely determined

15

as

$$\langle \psi_k^v, \psi_l^i \rangle_{L_2} - \sum_{j=1}^{N_i} \alpha_{kj}^M \langle \psi_j^i, \psi_l^i \rangle_{L_2} = 0, \quad \forall \psi_l^i \in V^i. \tag{2.20}$$

Using the partitioning given in Eq. (2.5), the previous condition can be written in matrix form as

$$\left[\alpha^M \right] = \left[M_{vi} \right] \left[M_{ii} \right]^{-1}. \tag{2.21}$$

The modes ψ^{me} can be used as boundary modes in V. With this formulation the submatrix $[M_{vv}^{me}] \in \Re^{N_v \times N_v}$ with entries $(M_{vv}^{me})_{ij} = \langle \psi_i^{me}, \psi_j^{me} \rangle$ is just the Schur complement of the standard mass matrix

$$[M_{vv}^{me}] = [M_{vv}] - [M_{vi}] [M_{ii}]^{-1} [M_{vi}]^T. \tag{2.22}$$

We consider the simultaneous diagonalization of the internal modes of the mass and stiffness matrices to construct the one-dimensional internal modes together with the minimum energy orthogonalization for the boundary modes. This allows to generalize the orthogonalization procedure for the boundary modes based on the choice of the appropriate norm according to the considered problem.

Assuming linear vertex functions, the orthogonalization of the vertex and internal modes using the L_2-norm results in the same basis proposed in (Zheng and Dong, 2011). Therefore, for $\alpha_{kj} = \alpha_{kj}^M$, the minimum energy procedure is equivalent to the Gram-Schimidt orthogonalization.

Fig. 2.5 shows the sparsity patterns of the local $1D$ mass and stiffness matrices after the application of the SD and ME procedures. The boundary and internal blocks of the mass matrix are decoupled and the same blocks of the stiffness matrix become coupled. In this case, the Schur complement is obtained directly from the one-dimensional basis construction.

Using the energy norm, Eq. (2.20) is given by

$$\langle \psi_k^v, \psi_l^i \rangle_E - \sum_{j=1}^{N_i} \alpha_{kj}^K \langle \psi_j^i, \psi_l^i \rangle_E = 0, \quad \forall \psi_l^i \in V^i, \tag{2.23}$$

16
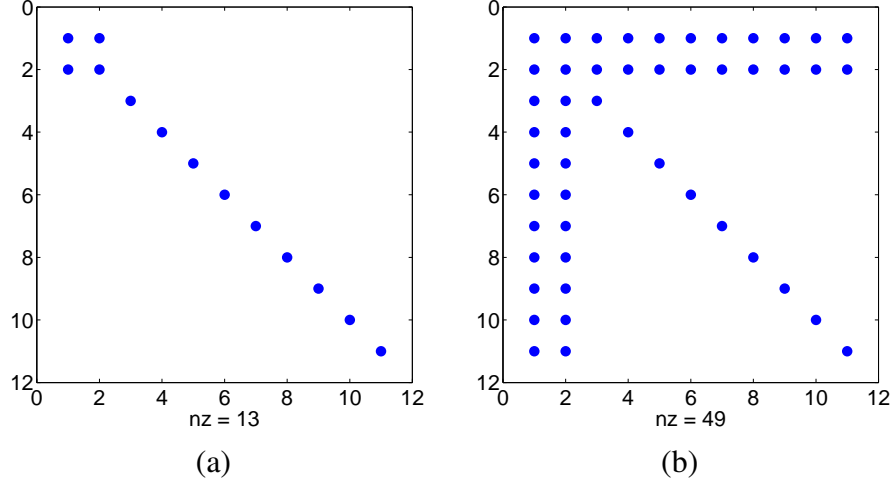
Figure 2.5: Sparsity patterns of the mass (a) and stiffness matrices (b) with polynomial order $P = 10$ for the SDME basis using $\left[\alpha^M\right]$.

The element local stiffness matrix may be partitioned in terms of boundary and internal modes as

$$[K] = \left[\begin{array}{cc} [K_{vv}] & [K_{vi}] \\ [K_{vi}]^T & [K_{ii}] \end{array} \right],$$ (2.24)

where $(K_{vv})_{ij} = \langle \psi_{i,\xi_1}, \psi_{j,\xi_1} \rangle_E$ $(i,j = 1, \ldots, N_v)$; $(K_{vi})_{ij} = \langle \psi_{i,\xi_1}, \psi_{j,\xi_1} \rangle_E$ $(i = 1, \ldots, N_v$ and $j = N_v + 1, \ldots, N_i)$; $(K_{ii})_{ij} = \langle \psi_{i,\xi_1}, \psi_{j,\xi_1} \rangle_E$ $(i,j = N_v + 1, \ldots, N_i)$.

Condition Eq. (2.23) may be expressed matricially as

$$\left[\alpha^K\right] = [K_{vi}][K_{ii}]^{-1}.$$ (2.25)

The submatrix $[K_{vi}] = 0$ for the standard Jacobi basis. Thus, the previous procedure does not alter the linear modes of the standard basis (ST). Fig. 2.6 shows the behavior of the vertex and internal modes of the simultaneously diagonal and minimum energy basis with $\left[\alpha^K\right]$ and $P = 3$. This results is similar to the Basis-LV presented in (Zheng and Dong, 2011) for $k = 1/2$.

Note that the choice of coefficients matrix $[\alpha]$ allows to recover the bases proposed in the literature considering the simultaneous diagonalization for the internal modes and orthogonalization for the vertex modes. We consider now the use of the minimum energy procedure for the Helmholtz problem.

17
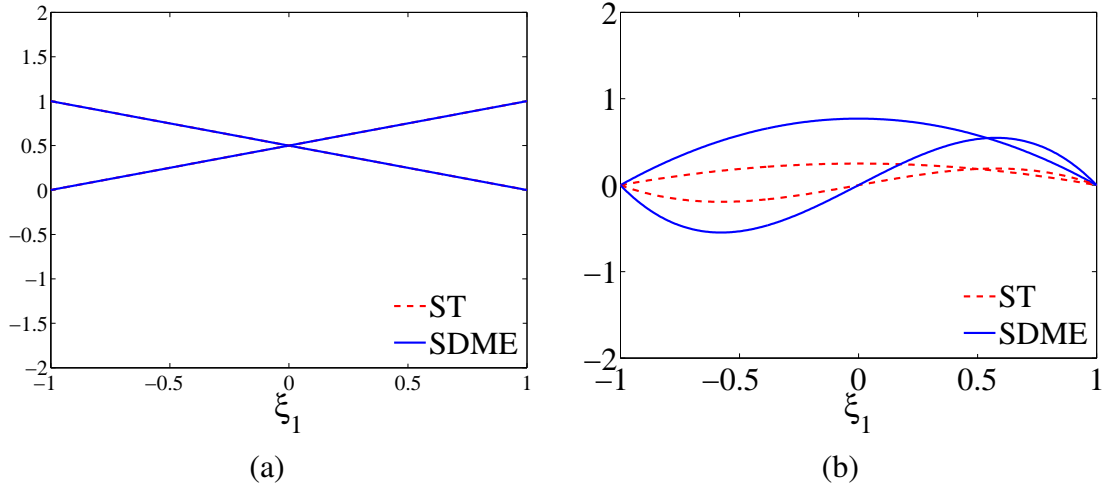
Figure 2.6: $1D$ SDME basis with $\left[\alpha^K\right]$, $k = 1/2$ and polynomial order $P = 3$ to vertex (a) and interior modes (b).

In this case, the energy norm for a function $v \in V$ is $\|v\|_E^2 = \langle v,v\rangle_E = \langle v',v'\rangle_{L_2} + \lambda\langle v,v\rangle_{L_2}$. Similarly as discussed for the mass and stiffness matrices the element local Helmholtz matrix can be partitioned as

$$[H] = [K] + \lambda\,[M] = \begin{bmatrix} [H_{vv}] & [H_{vi}] \\ [H_{vi}]^T & [H_{ii}] \end{bmatrix}. \tag{2.26}$$

A condition similar to Eq. (2.20) is obtained and the coefficients $\left[\alpha^H\right]$ are calculated as

$$\left[\alpha^H\right] = [H_{vi}]\,[H_{ii}]^{-1}. \tag{2.27}$$

This choice obtains a one-dimensional Helmholtz matrix with orthogonal vertex and internal modes as shown in Fig. 2.7. In this case, the local stiffness and mass matrices have vertex and internal blocks coupled and the orthogonalization of boundary modes and their derivatives cannot be made independently. However, when we add them to obtain the Helmholtz matrix, boundary and internal blocks are uncoupled.

The construction of the vertex modes of the SDME basis depends on the parameter λ. Fig. 2.8 shows the behavior of the boundary and internal modes for the standard element and different λ values and for polynomial order $P = 3$. For larger λ, Fig. 2.8(a), the behavior of the vertex modes
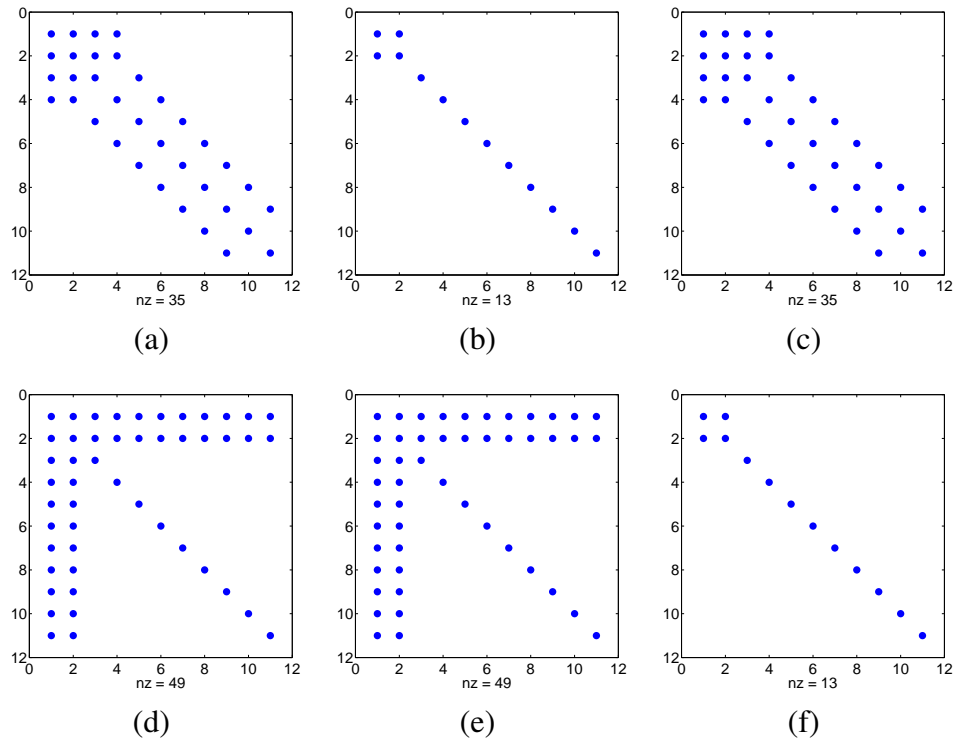
Figure 2.7: Sparsity patterns of the mass (a), stiffness (b), and Helmholtz (c) one-dimensional local matrices for $P = 10$ using the standard basis (ST). Sparsity patterns of the mass (d), stiffness (e), and Helmholtz (f) one-dimensional local matrices for $P = 10$ using the simultaneous diagonalization and minimum energy basis (SDME) with $\lambda = 1$.

is similar to using $\left[\alpha^M\right]$. For smaller λ, Fig. 2.8(e), the behavior of the vertex modes is similar $\left[\alpha^K\right]$.
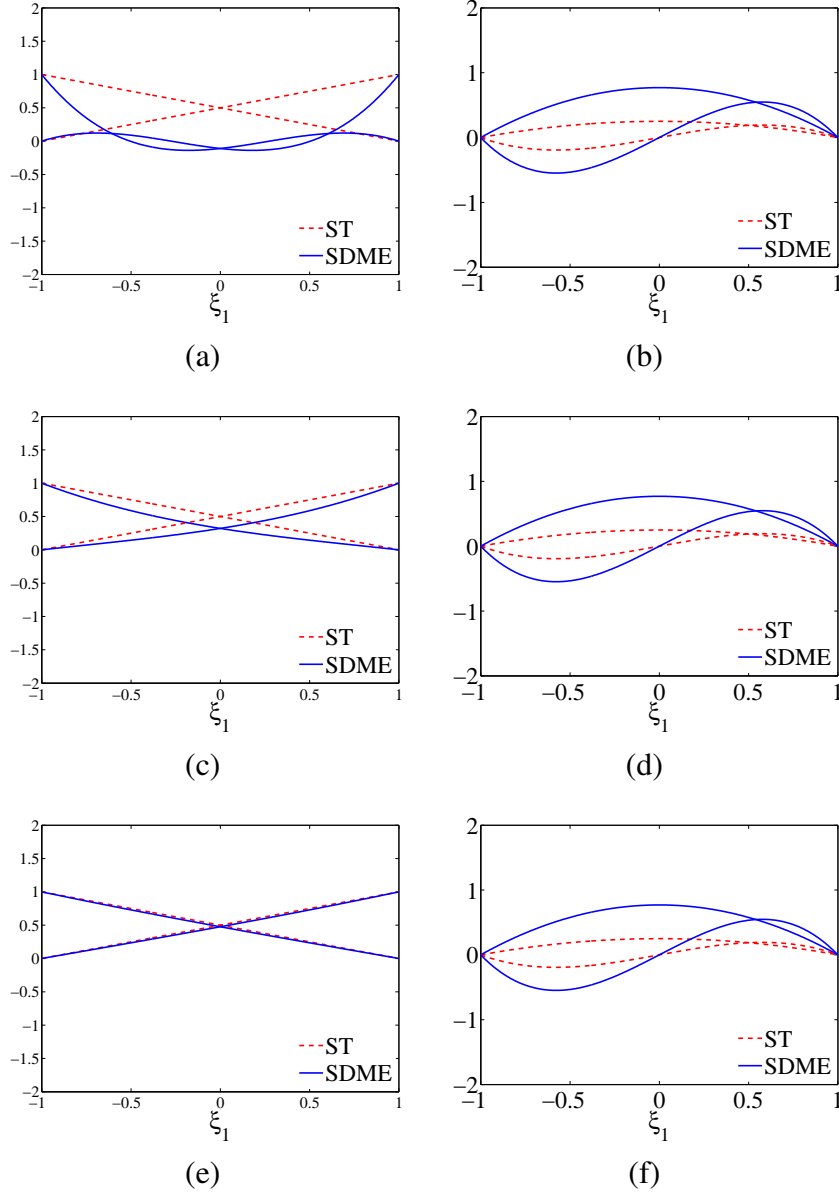
Figure 2.8: $1D$ SDME bases with $\left[\alpha^H\right]$, $k = 1/2$ and polynomial order $P = 3$. Vertex (a) and internal (b) modes with $\lambda = 100$. Vertex and internal modes to $\lambda = 1$ in (c) and (d). Vertex and internal modes for $\lambda = 0.1$ in (e) and (f).

Fig. 2.9 shows the behavior of the boundary and internal modes for the standard element with $\lambda = 100$ and for polynomial order $P = 10$. For high-order polynomial functions, the behavior of the vertex modes is similar to step function.

20
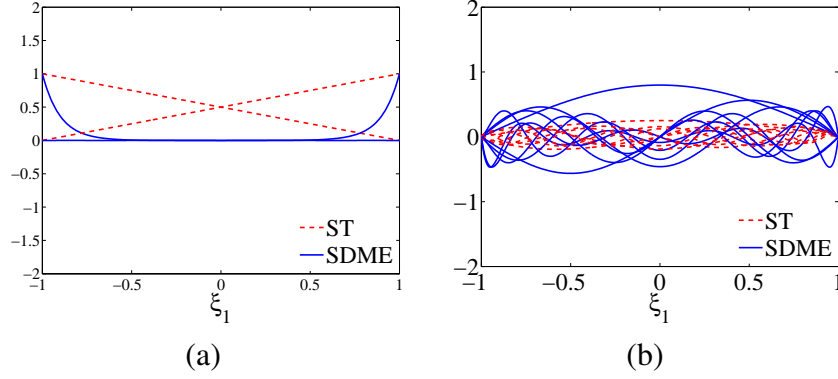
Figure 2.9: $1D$ SDME bases with $\left[\alpha^H\right]$, $k = 1/2$ and polynomial order $P = 10$. Vertex (a) and internal (b) modes with $\lambda = 100$.

In the next section, we will present the condition numbers in terms of the polynomial order for the one-dimensional projection, Poisson, and Helmholtz problems. For each case we consider the different norms used in the construction of the SDME bases.

2.3 Simultaneous Diagonalization and Minimum Energy Bases for Projection and Poisson Problems

In the FEM, the global interpolation functions $\{\psi^i\}_{i=1}^n$ define a functional space and the approximated solution for a function u is $u_{ap} = \Sigma_{i=1}^n a_i \psi_i$. Solving a $1D$ projection problem means to obtain the coefficients a_i that minimize the error $e = u - u_{ap}$, where u is a continuous function defined in the domain $\Omega = \{x | 0 \leq x \leq l\}$.

The solution of the projection problem is obtained by solving the system of equations (Karniadakis and Sherwin, 2005)

$$[M]\{a^m\} = \{f^m\}, \tag{2.28}$$

where

$$f_i^m = \int_\Omega u\psi_i d\Omega, \tag{2.29}$$

and $[M]$ is the global mass matrix obtained by the assembling of element matrices.

Fig. 2.10 illustrates the construction of the SDME basis for the projection problem. The diagonalization of the internal modes are made using the matrix $[Y]$ given in Eq. (2.14). Fig. 2.11

21

shows a comparison of the condition numbers of the one-dimensional local mass matrices using the standard (ST) and the SDME bases with $\left[\alpha^M\right]$ for different values of k according to the polynomial order. Notice that the condition numbers obtained using the SDME basis with $k = 1/2$ is better than those obtained with the standard basis and equal to those ones obtained with the basis presented in (Zheng and Dong, 2011).
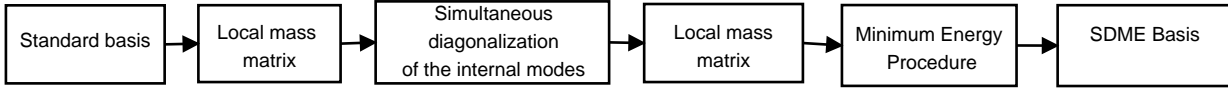
Figure 2.10: Scheme of construction of the 1D SDME basis for projection problems.
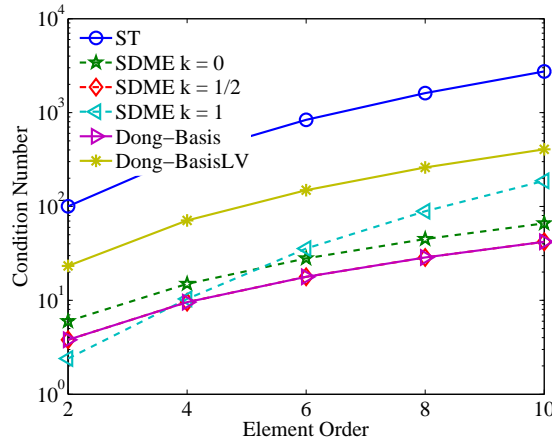
Figure 2.11: Numerical conditioning of the $1D$ mass matrices using the standard basis (ST) and the simultaneously diagonal and minimum energy basis (SDME) according to the polynomial order.

The one-dimensional Poisson problem with homogeneous Dirichlet boundary conditions is defined in the domain $\Omega = \{x | 0 \leq x \leq l\}$ as

$$
\begin{aligned}
\frac{d^2 u(x)}{dx^2} &= q(x) \quad && \Omega \\
u(x) &= 0 \quad && \partial\Omega_D
\end{aligned}, \tag{2.30}
$$

where $\partial\Omega_D$ is the part of the boundary $\partial\Omega$ where Dirichlet boundary conditions are applied, i.e., $x = 0$ and $x = l$.

The coefficients of the approximated solution are obtained by the system of equations

$$
[K]\left\{a^k\right\} = \left\{f^k\right\}, \tag{2.31}
$$

where

$$f_i^k = \int_\Omega q\psi_i d\Omega. \tag{2.32}$$

$[K]$ is the global stiffness matrix and q is the body load intensity.

Fig. 2.12 illustrates the construction of the SDME basis for the Poisson problem. In this case, the boundary and internal blocks of the element local stiffness matrix for the Jacobi standard basis are already decoupled and the coefficients $[\alpha^K]$ are zero. Therefore, the application of the minimum energy procedure has no effect on the coupling block of the boundary and internal modes. This construction is similar to that presented in (Zheng and Dong, 2011) for the Basis-LV, where only the internal modes are changed. For the bases here proposed, the choice of $[\alpha]$ influences the coupling blocks of the mass and stiffness matrices. The advantage of the proposed bases is that we can select the most appropriate $[\alpha]$ according to the considered problem. The choice of $[\alpha^M]$ for the construction of the one-dimensional minimum energy basis does not decouple internal and boundary modes of the one-dimensional stiffness matrix. However, the one-dimensional mass matrix has the internal and boundary modes uncoupled.
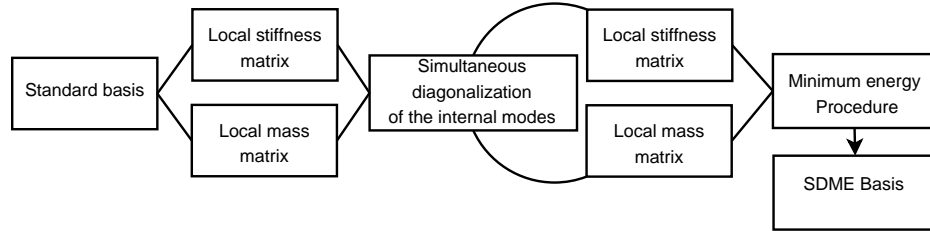
Figure 2.12: Scheme of construction of the 1D minimum energy basis for the Poisson problem.

Fig. 2.13 illustrates the behavior of the condition number of the one-dimensional local stiffness matrices using the standard (ST) and simultaneously diagonal and minimum energy (SDME) bases for different values of k in terms of the polynomial order. Note that after $P = 4$, the condition numbers are larger with the proposed minimum energy basis with $k = 1/2$. For $k = 1$, the condition number is smaller than those ones obtained with the other bases. The choice of parameter $k = 1/2$ is especially convenient for $2D$ and $3D$ problems.
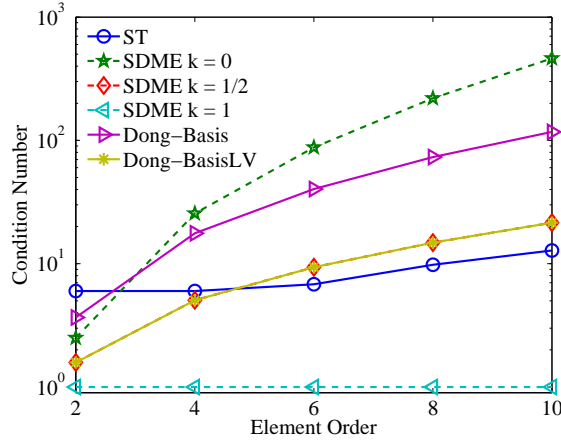
Figure 2.13: Numerical conditioning of the $1D$ stiffness matrix using the standard (ST) and the SDME bases, for different values of the parameter k, in terms of the polynomial order.

2.4 Minimum Energy Basis for Helmholtz Problem

The general equation for the one-dimensional Helmholtz problem is given by (Karniadakis and Sherwin, 2005)

$$
\begin{aligned}
\frac{d^2u(x)}{dx^2} - \lambda u(x) + f(x) &= 0, \quad x \in \Omega \\
u(x) &= u_0, \quad x \in \partial\Omega_D
\end{aligned}
, \tag{2.33}
$$

where $u(x)$ is a continuous and smooth function in the domain $\Omega = \{x | 0 \leq x \leq l\}$, λ a positive real constant, $f(x)$ a known function and u_0 a non-homogeneous Dirichlet condition. Multiplying Eq. (2.33) by an arbitrary smooth test function $v(x)$, which satisfies the homogeneous Dirichlet conditions on the boundary $\partial\Omega_D$, and further applying integration by parts, we obtain the weak form of Eq. (2.33) as

$$
\int_\Omega \frac{\partial u(x)}{\partial x}\frac{\partial v(x)}{\partial x}d\Omega + \lambda \int_\Omega u(x)v(x)d\Omega = \int_\Omega f(x)v(x)d\Omega + \left.\frac{\partial u(x)}{\partial x}v(x)\right|_{\partial\Omega_N}, \tag{2.34}
$$

and $\partial\Omega_N$ is the Neumann boundary.

Applying the Galerkin discretization, $u(x) = \sum_{i=1}^{n} a_i \psi^i(x)$ and $v(x) = \sum_{j=1}^{n} b_j \psi_j(x)$, we can write the associated system of equations for Eq. (2.34) as

$$
[H]\left\{a^h\right\} = \left\{f^h\right\}, \tag{2.35}
$$

24

where

$$f_i^h = \int_\Omega f(x)\psi_i(x)d\Omega + \left.\frac{\partial\psi_i(x)}{\partial x}\psi_j(x)\right|_{\partial\Omega_N}, \tag{2.36}$$

and

$$[H] = [K] + \lambda[M]. \tag{2.37}$$

$[M]$ and $[K]$ are the mass and stiffness matrices, respectively, and $[H]$ the Helmholtz matrix used for the construction of the SDME bases.

The difference here regarding the construction of the SDME basis is that the orthogonalization is applied directly to the Helmholtz matrix as indicated in Fig. 2.14.
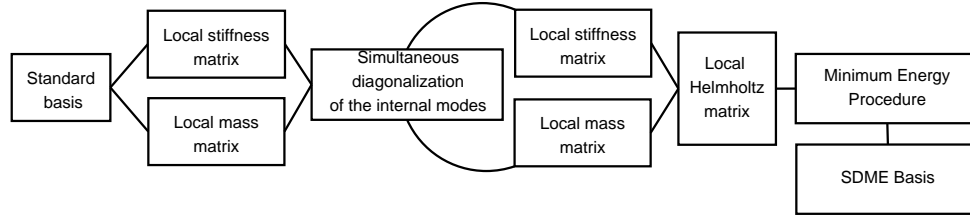
Figure 2.14: Scheme of construction of the $1D$ SDME basis for the Helmholtz problem.

Fig. 2.15 shows the behavior of the condition number of the one-dimensional local Helmholtz matrix, using the standard (ST) and the simultaneously diagonal and minimum energy (SDME) bases with $\left[\alpha^H\right]$ for different values of k and $\lambda = 1$, in terms of the polynomial order. The choice of k in Eq. (2.14) is important in determining the behavior of the condition number of the one-dimensional Helmholtz matrix. In this case, for $k = 1/2$, the condition number of the matrix using the SDME basis is larger than the standard basis for polynomial order larger than $P = 4$. For $k = 1$, the condition number is 1 for any polynomial order. Note that in this case, the condition number for any polynomial order used is smaller than the those ones obtained with the bases presented in (Zheng and Dong, 2011). For $P = 2$, the condition number for Basis-LV and SDME with $k = 1/2$ are not equal. This difference is observed because for $\lambda = 1$ the vertex modes is not similar. For smaller values of λ and larger values of P, these results are similar.

Fig 2.16 shows the behavior of the condition number of the one-dimensional local Helmholtz matrix, using the standard (ST) and the simultaneously diagonal and minimum energy (SDME) bases for different values of k and λ values for the polynomial order $P = 10$. Note that for larger values of λ, the condition numbers of the SDME basis with $k = 1/2$ is similar to that presented in (Zheng and Dong, 2011). For smaller values of λ, the condition number is similar to those ones
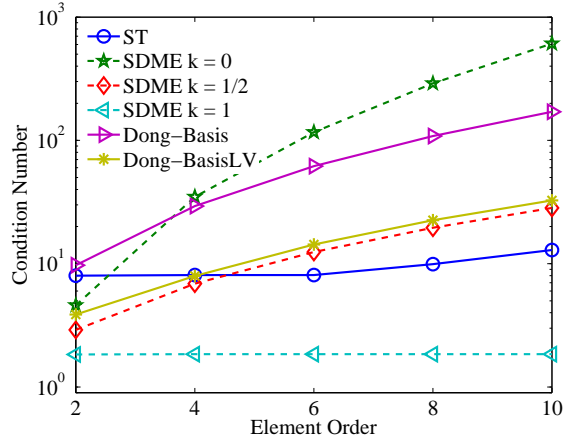
Figure 2.15: Numerical conditioning of the one-dimensional Helmholtz matrices using the standard (ST) and the simultaneously diagonal and minimum energy (SDME) bases $\left[\alpha^H\right]$ in terms of the polynomial order for $\lambda = 1$.

of the Basis-LV. However, for the given range of λ, the condition number of the SDME bases are better than the other bases.
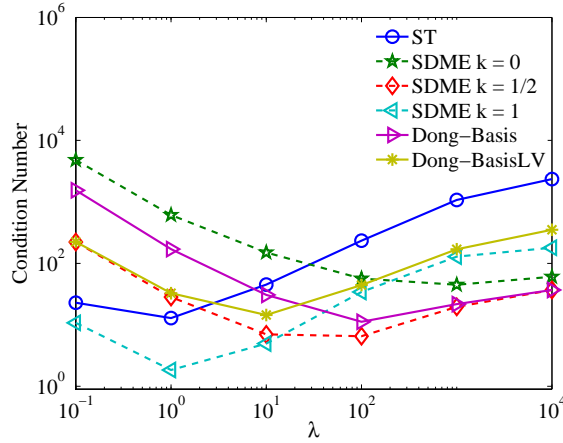
Figure 2.16: Numerical conditioning of the one-dimensional Helmholtz matrices using the standard (ST) and simultaneously diagonal and minimum energy (SDME) bases with $\left[\alpha^H\right]$ in terms of λ for polynomial order $P = 10$.

2.5 Construction of Basis for Quadrilaterals and Hexahedra

In this section, we discuss the extension of the proposed $1D$ bases to quadrilaterals ($2D$) and hexahedra ($3D$) structured elements using the tensor product of one-dimensional functions.

26

The shape functions for squares are given by (Karniadakis and Sherwin, 2005; Bittencourt *et al.*, 2007a)

$$N_i(\xi_1,\xi_2) = \varphi_p(\xi_1)\varphi_q(\xi_2), \quad 0 \le p,q \le P. \tag{2.38}$$

Similarly, the shape functions for hexahedra can be obtained as

$$N_i(\xi_1,\xi_2,\xi_3) = \varphi_p(\xi_1)\varphi_q(\xi_2)\varphi_r(\xi_3), \quad 0 \le p,q,r \le P, \tag{2.39}$$

where p, q, and r are tensor product indices associated with the topological entities of the element; P the polynomial order in directions ξ_1, ξ_2 and ξ_3; $i = 1,\ldots,(P+1)^2$ for squares and $i = 1,\ldots,(P+1)^3$ for hexahedra.

Due to the tensorial nature of the shape functions defined in Eqs. (2.38) and (2.39), sum-factorization has been used as an effective procedure to calculate the elemental operators (Karniadakis and Sherwin, 2005). Another possibility is to calculate the coefficients of the $2D$ and $3D$ elemental operator as a combination of the coefficients of the $1D$ mass and stiffness matrices and the Jacobian matrix. This procedure requires to work the expressions of the operator as presented in the next section for general distorted element. A similar procedure was indicated in (Vos *et al.*, 2010) for the mass matrices of the elements with constant Jacobian.

2.5.1 Tensor product of one-dimensional matrices for quadrilaterals

The one-dimensional local mass, stiffness, and mixed matrices will be respectively denoted here as $\left[M^{1D}\right]$, $\left[K^{1D}\right]$ and $\left[D^{1D}\right]$. Their coefficients are defined by

$$M_{ij}^{1D}(\xi_1) = \int_{-1}^{1} \varphi_i(\xi_1)\varphi_j(\xi_1)d\xi_1, \tag{2.40}$$

$$K_{ij}^{1D}(\xi_1) = \int_{-1}^{1} \varphi_{i,\xi_1}(\xi_1)\varphi_{j,\xi_1}(\xi_1)d\xi_1. \tag{2.41}$$

$$D_{ij}^{1D}(\xi_1) = \int_{-1}^{1} \varphi_{i,\xi_1}(\xi_1)\varphi_j(\xi_1)d\xi_1. \tag{2.42}$$

The coefficients of the mass and stiffness matrices for quadrilateral elements are given, respectively, by

$$M_{ij}^{2D} = \int_{-1}^{1}\int_{-1}^{1} N_i(\xi_1,\xi_2)N_j(\xi_1,\xi_2)|J|d\xi_1 d\xi_2, \tag{2.43}$$

$$K_{ij}^{2D} = \int_{-1}^{1}\int_{-1}^{1} [N_{i,x}N_{j,x} + N_{j,y}N_{i,y}]|J|d\xi_1 d\xi_2, \tag{2.44}$$

where $|J|$ is the Jacobian of the mapping between the local and global reference coordinate systems; $N_{i,x}$ and $N_{i,y}$ denote the shape function derivatives for the global coordinates x and y. The local and global derivatives are related by the inverse Jacobian matrix as

$$\left\{\begin{array}{c} N_{i,x} \\ N_{i,y} \end{array}\right\} = \left[\begin{array}{cc} j_{11} & j_{12} \\ j_{21} & j_{22} \end{array}\right] \left\{\begin{array}{c} N_{i,\xi_1} \\ N_{i,\xi_2} \end{array}\right\}, \tag{2.45}$$

where j_{11}, j_{12}, j_{21}, and j_{22} are coefficients of the inverse Jacobian matrix.

Substituting Eq. (2.38) in Eq. (2.43), we obtain the coefficients of the two-dimensional mass matrices in terms of coefficients of the one-dimensional mass matrices as

$$\begin{aligned} M_{ij}^{2D} &= \int_{-1}^{1}\varphi_a(\xi_1)\varphi_p(\xi_1)\left(\int_{-1}^{1}\varphi_b(\xi_2)\varphi_q(\xi_2)|J|d\xi_2\right)d\xi_1 \\ &= \Sigma_{k=1}^{n_1}\Sigma_{l=1}^{n_2}M_{ap}^{1D}(\xi_{1_k})M_{bq}^{1D}(\xi_{2_l})W_lW_k|J_{kl}|, \end{aligned} \tag{2.46}$$

where n_1, n_2, W_k, and W_l are, respectively, the number of integration points and weights in local directions ξ_1 and ξ_2.

Analogously, we obtain the coefficients of the two-dimensional Poisson stiffness matrix for quadrilaterals in terms of the coefficients of the one-dimensional matrices replacing Eqs. (2.38) and (2.45) in Eq. (2.44). Therefore,

$$\begin{aligned} K_{ij}^{2D} &= \Sigma_{k=1}^{n_1}\Sigma_{l=1}^{n_2}\left[(j_{11}^2 + j_{21}^2)_{kl}K_{ap}^{1D}(\xi_{1_k})M_{qb}^{1D}(\xi_{2_l}) + (j_{12}^2 + j_{22}^2)_{kl}M_{pa}^{1D}(\xi_{1_k})K_{qb}^{1D}(\xi_{2_l})\right. \\ &+ \left.(j_{11}j_{12} + j_{21}j_{22})_{kl}(D_{pa}^{1D}(\xi_{1_k})D_{qb}^{1D}(\xi_{2_l}) + D_{qb}^{1D}(\xi_{2_l})D_{pa}^{1D}(\xi_{1_k}))\right]|J_{kl}|W_lW_k. \end{aligned} \tag{2.47}$$

For undistorted elements, the terms of the Jacobian are constant and can be factored from the

28

integral sign. Thus, Eqs. (2.46) and (2.47) can be rewritten as

$$M_{ij}^{2D} = |J| \left[\left(\Sigma_{k=1}^{n_1} M_{ap}^{1D}(\xi_{1_k}) W_k \right) \left(\Sigma_{l=1}^{n_2} M_{bq}^{1D}(\xi_{2_l}) W_l \right) \right] = |J| M_{ap}^{1D}(\xi_1) M_{bq}^{1D}(\xi_2), \qquad (2.48)$$

$$
\begin{aligned}
K_{ij}^{2D} &= |J| \left[(j_{11}^2 + j_{21}^2) \left(\Sigma_{k=1}^{n_1} K_{ap}^{1D}(\xi_{1_k}) W_k \right) \left(\Sigma_{l=1}^{n_2} M_{qb}^{1D}(\xi_{2_l}) W_l \right) \right. \\
&\quad + \left. (j_{12}^2 + j_{22}^2) \left(\Sigma_{k=1}^{n_1} M_{pa}^{1D}(\xi_{1_k}) W_k \right) \left(\Sigma_{l=1}^{n_2} K_{qb}^{1D}(\xi_{2_l}) W_l \right) \right] \\
&= |J| \left[(j_{11}^2 + j_{21}^2) K_{ap}^{1D}(\xi_1) M_{qb}^{1D}(\xi_2) + (j_{12}^2 + j_{22}^2) M_{pa}^{1D}(\xi_1) K_{qb}^{1D}(\xi_2) \right].
\end{aligned}
\qquad (2.49)
$$

2.5.2 Tensor product of one-dimensional matrices for hexahedra

Similarly, the coefficients of the mass and stiffness matrices for hexahedra can be obtained from the coefficients of the one-dimensional matrices. The coefficients of the mass and Poisson stiffness matrices for hexahedra are given, respectively, by

$$M_{ij}^{3D} = \int_{-1}^{1} \int_{-1}^{1} \int_{-1}^{1} N_i(\xi_1,\xi_2,\xi_3) N_j(\xi_1,\xi_2,\xi_3) |J| d\xi_1 d\xi_2 d\xi_3, \qquad (2.50)$$

$$K_{ij}^{3D} = \int_{-1}^{1} \int_{-1}^{1} \int_{-1}^{1} (N_{i,x} N_{j,x} + N_{i,y} N_{j,y} + N_{i,z} N_{j,z}) |J| d\xi_1 d\xi_2 d\xi_3. \qquad (2.51)$$

The global derivatives $N_{i,k}$, with $k = x, y, z$, are determined by the inverse Jacobian matrix as

$$
\left\{ \begin{array}{c} N_{i,x} \\ N_{i,y} \\ N_{i,z} \end{array} \right\} = \left[\begin{array}{ccc} j_{11} & j_{12} & j_{13} \\ j_{21} & j_{22} & j_{23} \\ j_{31} & j_{32} & j_{33} \end{array} \right] \left\{ \begin{array}{c} N_{i,\xi_1} \\ N_{i,\xi_2} \\ N_{i,\xi_3} \end{array} \right\}. \qquad (2.52)
$$

Substituting Eq. (2.39) in Eq. (2.50), the three-dimensional mass matrix can be written in terms of the one-dimensional mass matrices as

$$
\begin{aligned}
M_{ij}^{3D} &= \int_{-1}^{1} \varphi_a(\xi_1) \varphi_p(\xi_1) \left(\int_{-1}^{1} \varphi_b(\xi_2) \varphi_q(\xi_2) \left(\int_{-1}^{1} \varphi_c(\xi_3) \varphi_r(\xi_3) |J| d\xi_3 \right) d\xi_2 \right) d\xi_1 \\
&= \Sigma_{k=1}^{n_1} \Sigma_{l=1}^{n_2} \Sigma_{m=1}^{n_3} M_{ap}^{1D}(\xi_{1_k}) M_{bq}^{1D}(\xi_{2_l}) M_{cr}^{1D}(\xi_{3_m}) |J_{klm}| W_m W_l W_k,
\end{aligned}
\qquad (2.53)
$$

where n_1, n_2, n_3, W_k, W_l, and W_m are respectively the number of integration points and weights in the local directions ξ_1, ξ_2 and ξ_3.

Analogously, we obtain the coefficients of the three-dimensional Poisson stiffness matrix in terms of the one-dimensional coefficients replacing Eqs. (2.39) and (2.52) in Eq. (2.51). Therefore,

$$
\begin{aligned}
K_{ij}^{3D} = & \ \Sigma_{k=1}^{n_1}\Sigma_{l=1}^{n_2}\Sigma_{m=1}^{n_3} \left[(j_{11}^2 + j_{21}^2 + j_{31}^2)_{klm} K_{ap}^{1D}(\xi_{1_k}) M_{bq}^{1D}(\xi_{2_l}) M_{cr}^{1D}(\xi_{3_m}) \right. \\
& + \ (j_{12}^2 + j_{22}^2 + j_{32}^2)_{klm} M_{ap}^{1D}(\xi_{1_k}) K_{bq}^{1D}(\xi_{2_l}) M_{cr}^{1D}(\xi_{3_m}) \\
& + \ (j_{13}^2 + j_{23}^2 + j_{33}^2)_{klm} M_{ap}^{1D}(\xi_{1_k}) M_{bq}^{1D}(\xi_{2_l}) K_{cr}^{1D}(\xi_{3_m}) \\
& + \ J1_{klm}(D_{ap}^{1D}(\xi_{1_k}) D_{qb}^{1D}(\xi_{2_l}) M_{cr}^{1D}(\xi_{3_m}) + D_{pa}^{1D}(\xi_{1_k}) D_{bq}^{1D}(\xi_{2_l}) M_{cr}^{1D}(\xi_{3_m})) \\
& + \ J2_{klm}(D_{ap}^{1D}(\xi_{1_k}) M_{bq}^{1D}(\xi_{2_l}) D_{rc}^{1D}(\xi_{3_m}) + D_{pa}^{1D}(\xi_{1_k}) M_{bq}^{1D}(\xi_{2_l}) D_{cr}^{1D})(\xi_{3_m}) \\
& + \left. J3_{klm}(M_{ap}^{1D}(\xi_{1_k}) D_{bq}^{1D}(\xi_{2_l}) D_{rc}^{1D}(\xi_{3_m}) + M_{ap}^{1D}(\xi_{1_k}) D_{qb}^{1D}(\xi_{2_l}) D_{cr}^{1D}(\xi_{3_m})) \right] |J_{klm}| W_m W_l W_k,
\end{aligned}
\tag{2.54}
$$

where

$$
\begin{aligned}
J1_{klm} &= (j_{11}j_{12} + j_{21}j_{22} + j_{31}j_{32}), \\
J2_{klm} &= (j_{11}j_{13} + j_{21}j_{23} + j_{31}j_{33}), \\
J3_{klm} &= (j_{12}j_{13} + j_{22}j_{23} + j_{32}j_{33}).
\end{aligned}
\tag{2.55}
$$

The terms of the Jacobian matrix for undistorted elements are constant and can be factored from the integral sign. Thus, Eqs. (2.53) and (2.55) can be rewritten as

$$
\begin{aligned}
M_{ij}^{3D} &= |J| \left[(\Sigma_{k=1}^{n_1} M_{ap}^{1D}(\xi_{1_k}) W_k)(\Sigma_{l=1}^{n_2} M_{bq}^{1D}(\xi_{2_l}) W_l)(\Sigma_{m=1}^{n_3} M_{cr}^{1D}(\xi_{3_m}) W_m) \right] \\
&= |J| \left[M_{ap}^{1D}(\xi_1) M_{bq}^{1D}(\xi_2) M_{cr}^{1D}(\xi_3) \right],
\end{aligned}
\tag{2.56}
$$

$$
\begin{aligned}
K_{ij}^{3D} = |J| & \left[(j_{11}^2 + j_{21}^2 + j_{31}^2) K_{ap}^{1D}(\xi_1) M_{bq}^{1D}(\xi_2) M_{cr}^{1D}(\xi_3) \right. \\
& + \ (j_{12}^2 + j_{22}^2 + j_{32}^2) M_{ap}^{1D}(\xi_1) K_{bq}^{1D}(\xi_2) M_{cr}^{1D}(\xi_3) \\
& + \left. (j_{13}^2 + j_{23}^2 + j_{33}^2) M_{ap}^{1D}(\xi_1) M_{bq}^{1D}(\xi_2) K_{cr}^{1D}(\xi_3) \right].
\end{aligned}
\tag{2.57}
$$

For straight-side elements, mapping is calculated by using only the vertex shape functions of the standard basis.

2.5.3 Sparsity of the matrices

In this section, we present the sparsity patterns for the mass, Poisson stiffness, and Helmholtz matrices obtained with the standard (ST) and the simultaneously diagonal and minimum energy (SDME) bases for two and three-dimensional elements. The degrees of freedom are numbered beginning with boundary modes followed by the internal modes of the elements.

To study the sparsity patterns for $2D$ and $3D$ undistorted elements, we consider the domains $\Omega = [0,1] \times [0,1]$ and $\Omega = [0,1] \times [0,1] \times [0,1]$. The distorted elements illustrated in Fig. 2.17 are also considered.
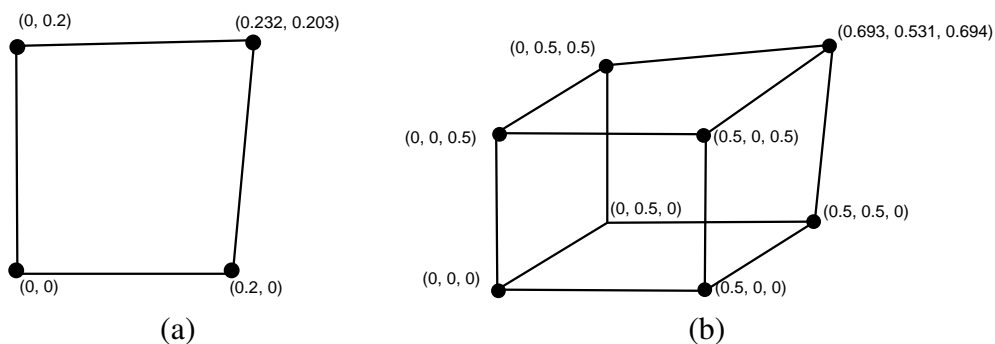
Figure 2.17: Distorted $2D$ (a) and $3D$ (b) elements.

Fig. 2.18 shows the sparsity patterns of the mass matrices obtained using the ST and SDME bases for two-dimensional elements with $\left[\alpha^M\right]$ and polynomial order $P = 10$. Note that the mass matrix obtained with the SDME basis is much sparser. Moreover, it is observed that the boundary and internal modes of the mass matrix with SDME basis are decoupled as shown in Fig. 2.18(b). The same behavior is obtained for the sparsity patterns of the mass matrix for $3D$ elements as illustrated in Fig. 2.19. In both cases, the distortion of the elements generates coupling of boundary and internal coefficients of the mass matrix.

Figs. 2.20 and 2.21 illustrate the sparsity patterns of the Poisson stiffness matrices for the $2D$ and $3D$ elements. As discussed in the previous section, the stiffness matrices for two and three-dimensional elements can be obtained using the one-dimensional mass and stiffness matrices. Using $\left[\alpha^K\right]$, the boundary and internal blocks of the one-dimensional mass matrices are coupled. Consequently, the $2D$ and $3D$ stiffness matrices have coupled internal and boundary modes as may be seen in Figs. 2.20(b) and 2.21(b). For the distorted element, the sparsity pattern obtained using
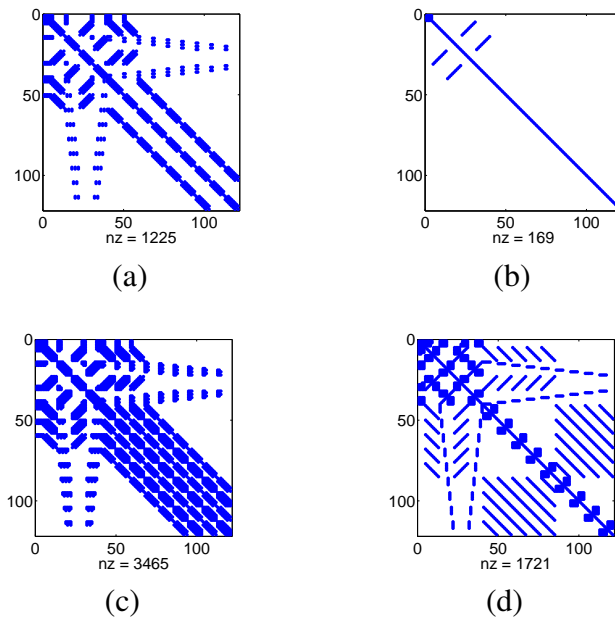
Figure 2.18: Sparsity patterns of $2D$ mass matrices using the standard (a) and simultaneously diagonal and minimum energy bases (b) for undistorted element and polynomial order $P = 10$. Sparsity patterns of $2D$ mass matrices using the standard (c) and simultaneously diagonal and minimum energy bases (d) for distorted element and polynomial order $P = 10$. All results with SDME used $\left[\alpha^M\right]$.
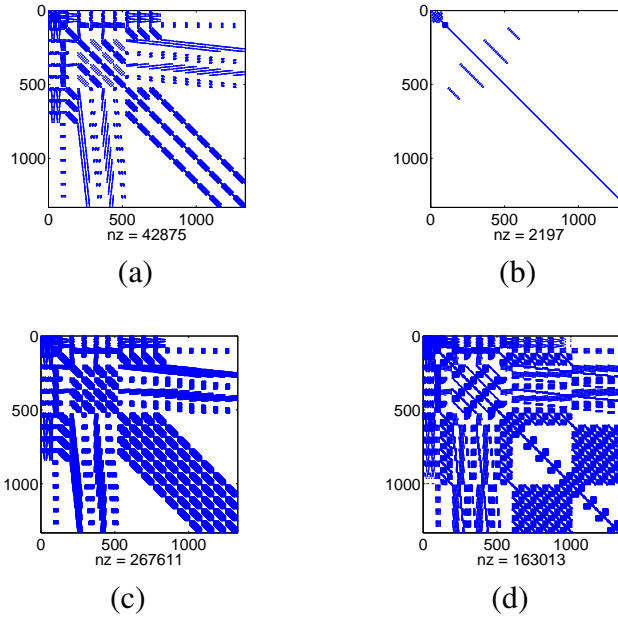
Figure 2.19: Sparsity patterns of $3D$ mass matrices with standard (a) and SDME bases (b) for undistorted element and polynomial order $P = 10$. Sparsity patterns of $3D$ mass matrices with standard (c) and SDME bases (d) for distorted element and polynomial order $P = 10$. All results with SDME used $\left[\alpha^M\right]$.

the SDME basis is completely full. Observe that using the SDME basis, the block of internal modes of the stiffness matrices maintains a diagonal profile for the $2D$ and $3D$ undistorted elements, which makes easier the calculation of the Schur complement.
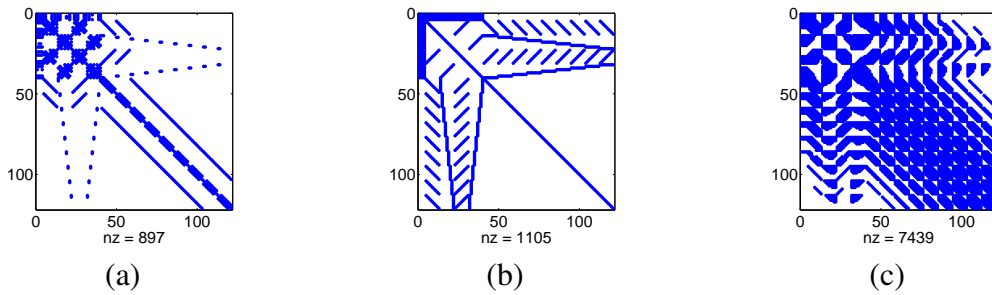
Figure 2.20: Sparsity patterns of $2D$ Poisson stiffness matrices with standard (a) and SDME bases (b) for undistorted element and polynomial order $P = 10$. Sparsity pattern of $2D$ stiffness matrices with standard basis (c) for distorted element and polynomial order $P = 10$.

The sparsity patterns for Helmholtz matrices obtained for the undistorted and distorted elements of Fig. 2.17 are shown in Figs. 2.22 and 2.23. In this case, the SDME basis is constructed

(a) (b) (c)
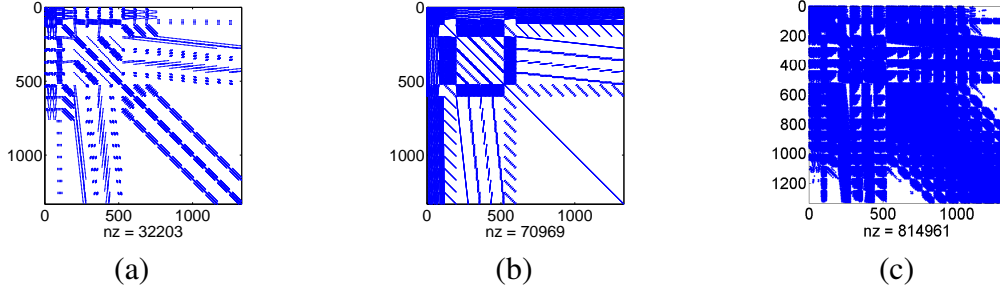
Figure 2.21: Sparsity patterns of $3D$ Poisson stiffness matrices with standard (a) and SDME bases (b) for undistorted element and polynomial order $P = 10$. Sparsity pattern of $3D$ stiffness matrices with standard basis (c) for distorted element and polynomial order $P = 10$.

such that the one-dimensional mass and stiffness matrices have coupled boundary and internal modes. However, when added to the construction of the one-dimensional Helmholtz matrices, the boundary and internal modes are uncoupled. As shown in Figs. 2.22(b) and 2.23(b), the boundary and internal modes are coupled for $2D$ and $3D$ elements.

(a) (b) (c)
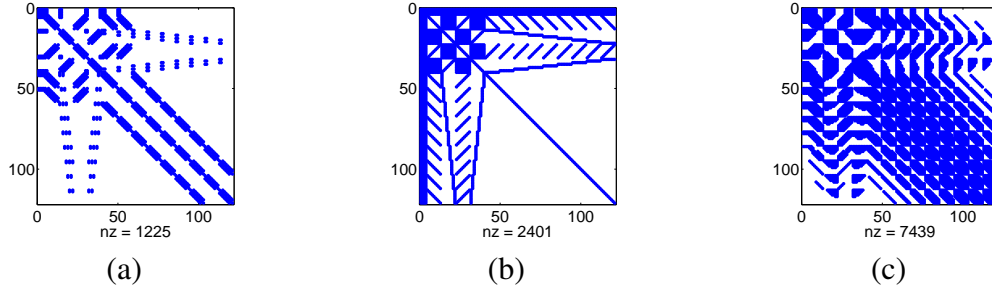
Figure 2.22: Sparsity patterns of $2D$ Helmholtz matrices with standard (a) and minimum energy bases (b) for undistorted element and polynomial order $P = 10$. Sparsity pattern of $2D$ Helmholtz matrices with standard basis (c) for distorted element and polynomial order $P = 10$.

2.6 Numerical results

The following norms are used, respectively, to study the convergence of the $3D$ projection, Poisson, and Helmholtz problems.

$$\|u\|_{L_2} = \left(\int_\Omega u^2 d\Omega \right)^{\frac{1}{2}}, \tag{2.58}$$

34
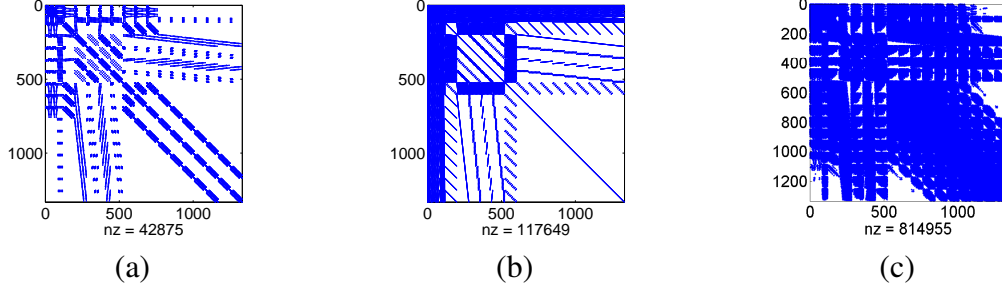
Figure 2.23: Sparsity patterns of $3D$ Helmholtz matrices with standard (a) and SDME bases (b) for undistorted element and polynomial order $P = 10$. Sparsity pattern of $3D$ Helmholtz matrices with standard basis (c) for distorted element and polynomial order $P = 10$.

$$\|u\|_E = \left(\int_\Omega (\nabla u)^2 d\Omega \right)^{\frac{1}{2}}, \tag{2.59}$$

$$\|u\|_H = \left(\int_\Omega (\nabla u)^2 + \lambda u^2 d\Omega \right)^{\frac{1}{2}}. \tag{2.60}$$

The standard basis (ST), standard basis with diagonal preconditioner (DP-ST), the simultaneously diagonal and minimum energy basis (SDME), and the simultaneously diagonal and minimum energy basis with diagonal precontitioner (DP-SDME) were considered. We used the conjugate gradient method with tolerance 10^{-11} for solving the systems of equations after applying the Schur complement. For $3D$ domains, meshes with 8 hexahedra were used.

In all examples, the relative percentage reduction I in the number of iterations is given by

$$I = \frac{(n_{ST} - n_{SDME})}{n_{ST}} 100, \tag{2.61}$$

where n_{ST} and n_{SDME} are the number of iterations using the ST and SDME bases. The relative percentage reduction in number of iterations obtained using the diagonal preconditioner is indicated by DPI. We compute the relative percentage reduction in solution time as

$$I = \frac{(t_{ST} - t_{SDME})}{t_{ST}} 100, \tag{2.62}$$

where t_{ST} and t_{SDME} are the solution time using the ST and SDME bases. The relative percentage reduction in solution time obtained using the diagonal preconditioner is indicated by DPI.

2.6.1 Projection Problem

Consider the function $u(x,y,z) = e^{2x}\sin(\pi y + 1)^2$ in the domain $\Omega = [0,1] \times [0,1] \times [0,1]$. The undistorted and distorted meshes with 8 hexahedra illustrated in Fig. 2.24 were used.

(a)   (b)
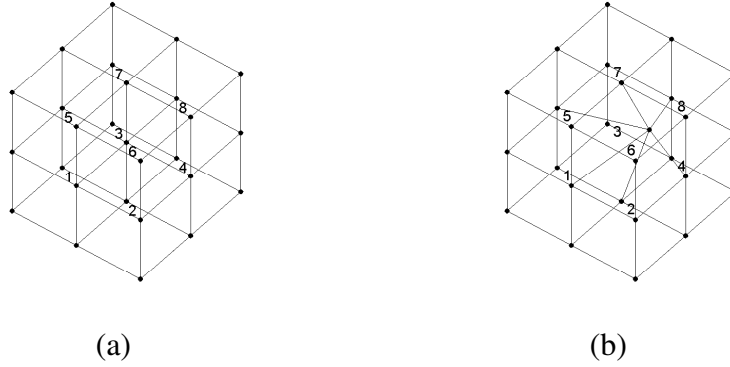
Figure 2.24: Undistorted (a) and distorted (b) meshes with 8 hexahedra.

The sparsity patterns of the global mass matrices for the distorted and undistorted meshes are shown in Fig. 2.25. It is observed in Fig. 2.25(c) that the boundary and internal blocks of the mass matrix are uncoupled for the undistorted mesh when using $\left[\alpha^M\right]$ for construction of the simultaneously diagonal and minimum energy bases. The number of non-zero coefficients for the distorted meshes is about half of the number for the standard basis.

Figs. 2.26(a) and 2.26(c) show the number of iterations required for convergence using the conjugate gradient method in terms of the polynomial order for the undistorted and distorted meshes respectively. In this case and without diagonal preconditioner, the choice of the parameter $k = 0$ for the simultaneouly diagonalization of the internal modes is better than the choice $k = 1/2$ with undistorted mesh. With distorted mesh, for the range of polynomial order used, the number of iterations with the choice $k = 1/2$ was smaller than that observed with the choice of the $k = 0$. When using diagonal preconditioner, the number of iterations is similar for both k parameters, even in distorted mesh. The condition numbers of the mass matrices are also shown in terms of polynomial order in Figs.2.26(b) and 2.26(d). In both cases, the SDME basis presented the best performance for the condition number of the global mass matrices after Schur complement.

This improvement can be also seen for the relative percentage reduction of the number of iterations for convergence. In Fig. 2.27(a), there is a reduction of more than 80% for the range
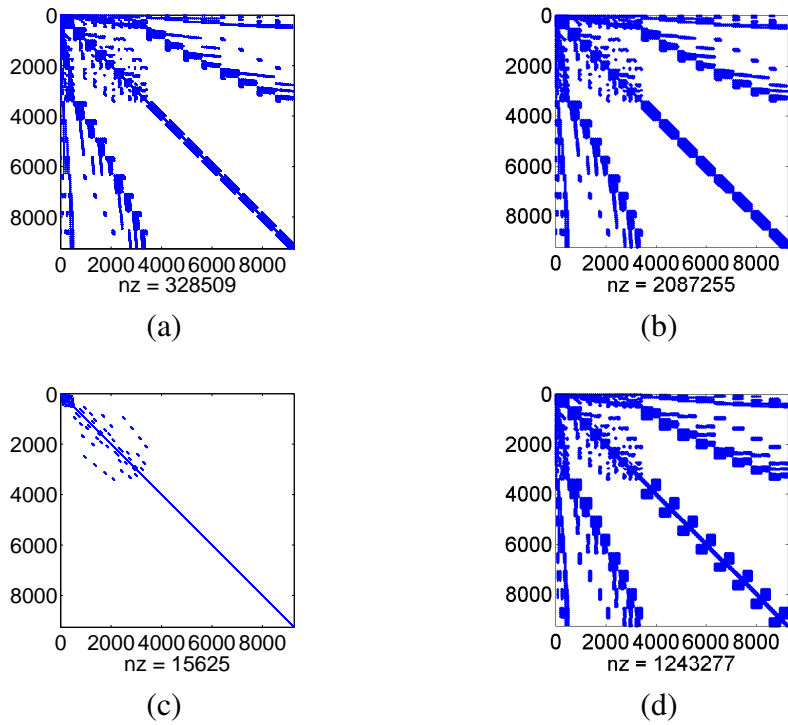
Figure 2.25: Sparsity patterns of global mass matrices for the $3D$ projection problem with undistorted mesh using ST (a) and SDME (c) bases with $\left[\alpha^M\right]$. Sparsity patterns of global mass matrices for the $3D$ projection problem with distorted mesh using ST (b) and SDME (d) bases for polynomial order $P = 10$.
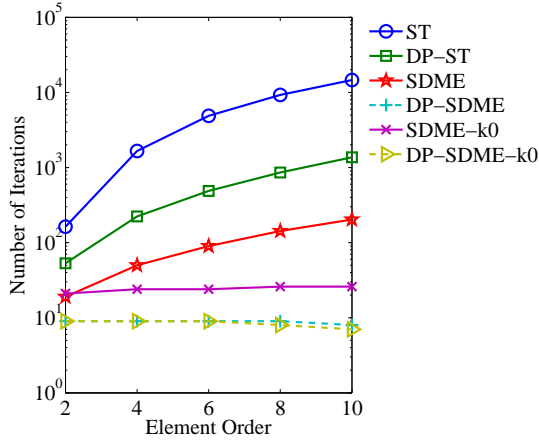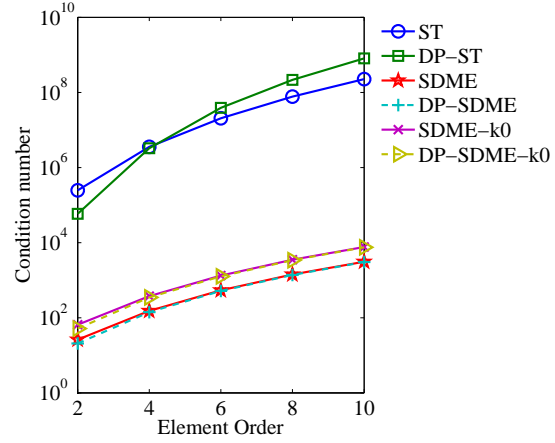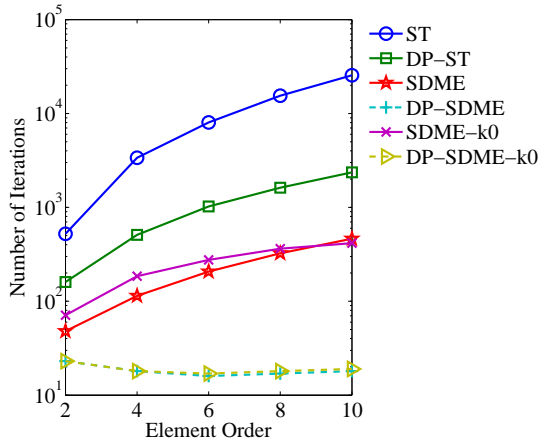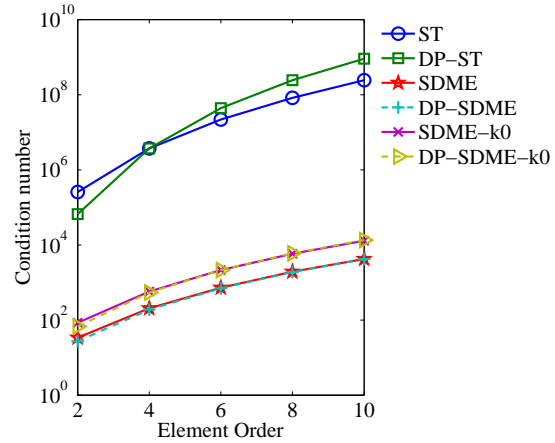
Figure 2.26: Number of iterations for convergence for the $3D$ projection problem with undistorted (a) and distorted (c) meshes. Condition number of the global mass matrices for the $3D$ projection problem with Schur complement to the simultaneously diagonal and minimum energy basis with undistorted (b) and distorted (d) meshes.

of polynomial order used for the SDME basis compared to the ST basis. For the problem with distorted mesh, the reduction in the number of iterations was also significant and similar to that one of the undistorted mesh as shown in Fig. 2.27(b).

(a) (b)
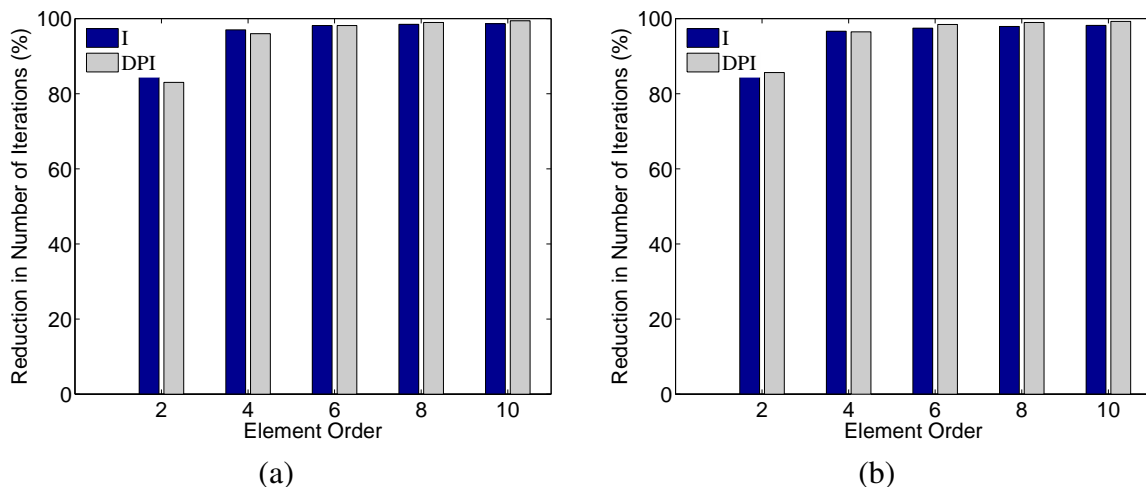
Figure 2.27: Relative percentage reduction in the number of iterations compared with and without the use of diagonal preconditioner for the $3D$ projection problem with undistorted (a) and distorted (b) meshes.

This results confirm the efficiency of the procedure of the simultaneous diagonal and minimum energy. The results are similar to those ones obtained with the Dong's basis and $k = 1/2$. In next section we present the results in Poisson problems.

2.6.2 Poisson Problem

In this section, we consider the solution of Poisson problem in $3D$ meshes. The results for the $2D$ case are similar and will not be presented here. We used also the fabricated solution $u(x,y) = \sin(\pi x)\sin(\pi y)$, with homogeneous boundary conditions, in the domain $\Omega = [0,1] \times [0,1] \times [0,1]$ and the undistorted mesh with 8 hexahedra illustrated in Fig. 2.24(a).

The sparsity patterns of the global stiffness matrices are shown in Fig. 2.28. It is observed that the stiffness matrices obtained using the SDME basis have a similar profile to the ST basis, but with a greater number of non-zero coefficients. As discussed in Section 2.3, the procedure for the construction of the SDME basis with $\left[\alpha^K\right]$ for Poisson problems does not decouple the

internal and boundary blocks of the one-dimensional mass matrices. This affects the sparsity of the stiffness matrices in $2D$ and $3D$ problems. As shown in Eqs. (2.47) and (2.55), the $2D$ and $3D$ stiffness matrices are defined in terms of the one-dimensional mass matrices, which in this case have internal and boundary blocks coupled. This makes the global stiffness matrix denser than that one obtained with the standard basis. But the internal block is still diagonal and the calculation of the Schur complement does not require the matrix inversion.
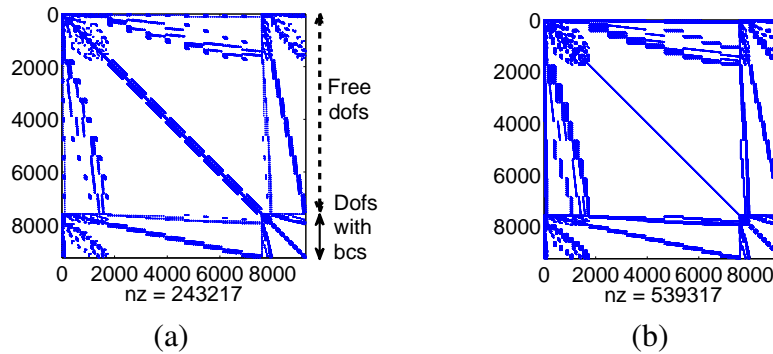
Figure 2.28: Sparsity patterns of the global stiffness matrices for the $3D$ Poisson problem with undistorted mesh using the ST (a) and SDME (b) bases and polynomial order $P = 10$. The matrix blocks related to the free dofs and boundary conditions are indicated.

Regarding the condition numbers of the global matrices for the $3D$ undistorted mesh, the SDME basis showed better conditioning, as shown in Fig. 2.29(b). The SDME basis was also superior to the ST basis in terms of CG iterations as illustrated in Fig. 2.29(a). The choice of the parameter $k = 1$ did not have no advantage over $k = 1/2$. The construction of the $2D$ or $3D$ stiffness matrix is dependent of the one-dimensional mass and stiffness matrices. For $k = 1$, the condition number of the one-dimensional mass matrix is larger than the one with $k = 1/2$. This fact affects the increase in the condition number for the $3D$ stiffness matrix.

The relative percentage reduction in the number of iterations was about 70% comparing the SDME and ST bases without the use of preconditioner and 30% with the use of diagonal preconditioner for polynomial order $P = 10$, as illustrated in Fig. 2.30(b). The relative percentage reduction in solution time reached 50% comparing the bases without preconditioner and was slightly above 10% using diagonal preconditioner for the polynomial order $P = 10$.

We also considered the same problem using the hexahedra distorted mesh shown in Fig. 2.24(b). The global stiffness matrices with the SDME basis have more non-zero coefficients as
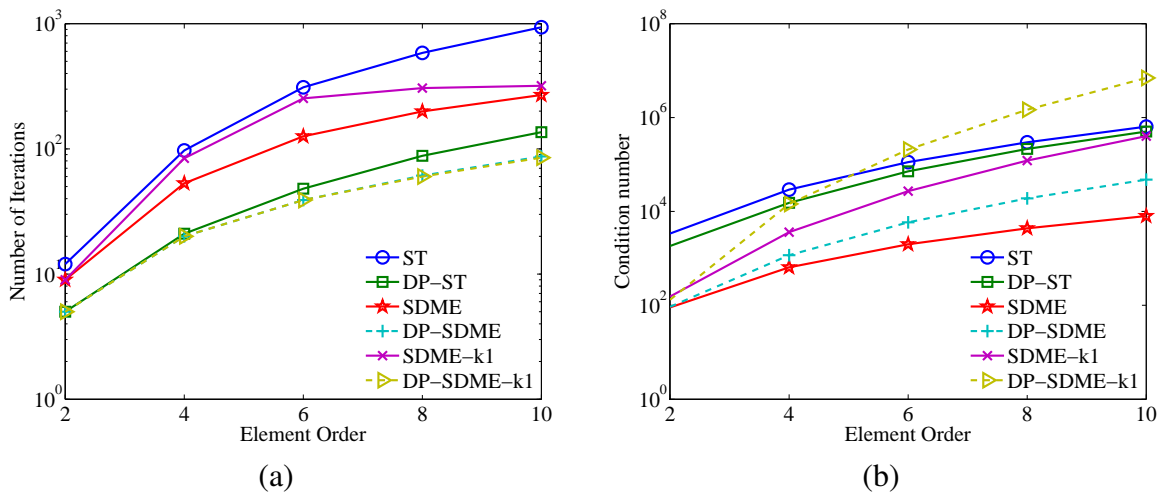
Figure 2.29: Number of CG iterations for the $3D$ Poisson problem with undistorted mesh (a). Condition number of the global stiffness matrices for the $3D$ Poisson problem after Schur complement and with undistorted mesh (b).
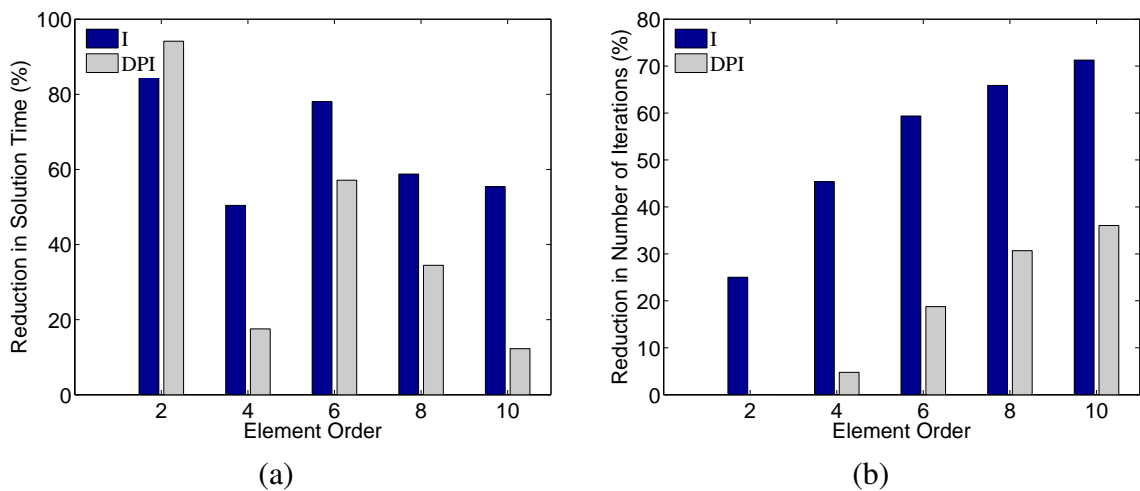
Figure 2.30: Relative percentage reduction in solution time (a) and number of iterations (b) with and without the use of diagonal preconditioner for the $3D$ Poisson problem with undistorted mesh.

illustrated in Fig. 2.31. Fig. 2.32 illustrates the behavior of the number of iterations for convergence and the condition number of the global stiffness matrices after Schur complement, in terms of the polynomial order used in the approximation. Note that the use of diagonal preconditioner with SDME basis reduced the number of iterations required for convergence as compared to the use of diagonal preconditioner applied to the ST basis, as show in Fig. 2.32(a). This reduction was observed in terms of the number of iterations, as shown in Fig. 2.33(b) for polynomial orders $P = 6, 8, 10$.

(a) (b)
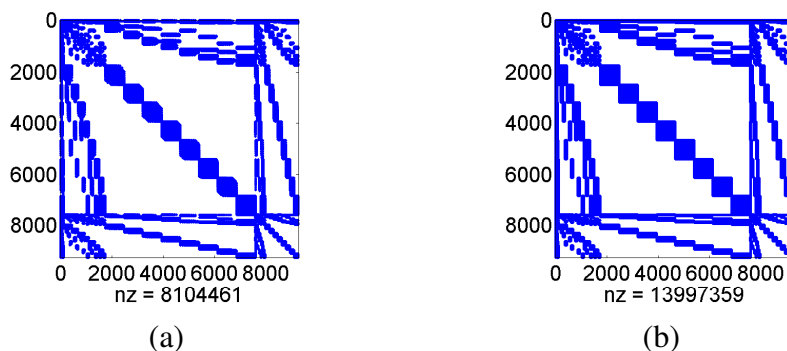
Figure 2.31: Sparsity patterns of the global stiffness matrices for the $3D$ Poisson problem with distorted mesh using ST basis (a) and SDME basis (b) and polynomial order $P = 10$.

(a) (b)
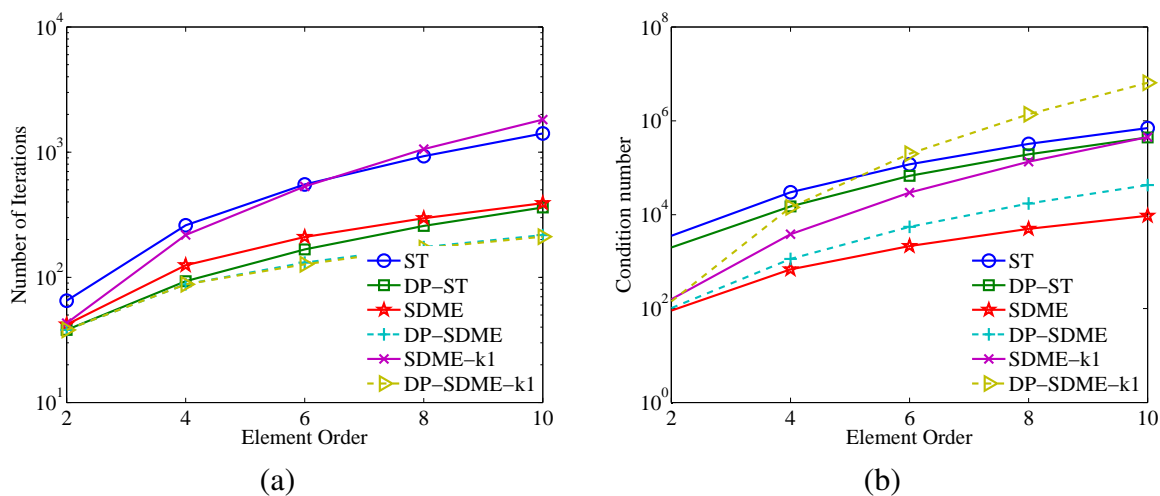
Figure 2.32: Number of iterations for the $3D$ Poisson problem with distorted mesh (a). Condition number of the global stiffness matrices for the $3D$ Poisson problem and distorted mesh (b).

However, the diagonal preconditioner worked well for both bases in terms of the number of iterations when compared to the standard CG as illustrated in Figs. 2.33(b) and 2.32(a).
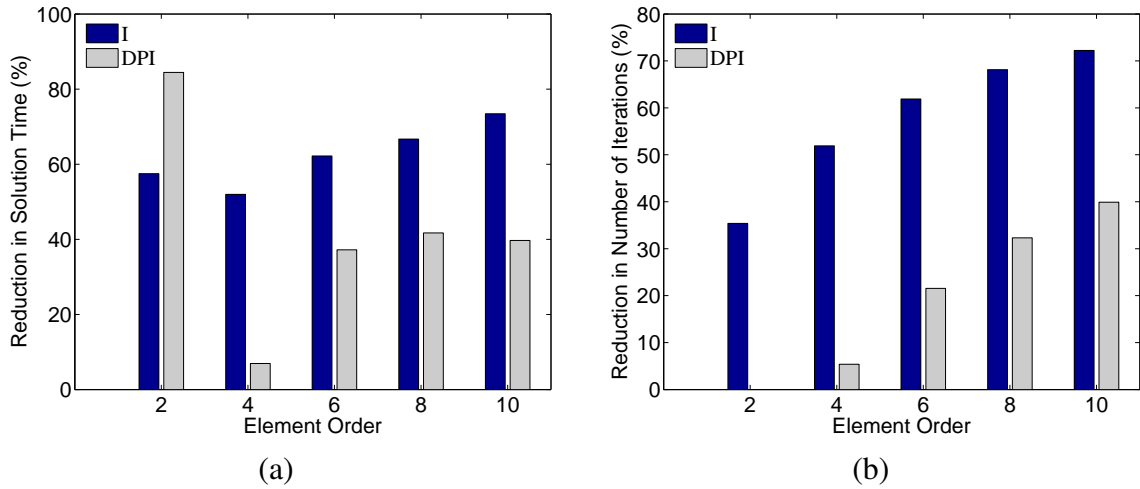
Figure 2.33: Relative percentage reduction in the solution time (a) and the number of iterations (b) with and without the use of diagonal preconditioner for the $3D$ Poisson problem with distorted mesh.

This results shows the equivalence for the SDME basis with $\left[\alpha^K\right]$ and the Basis-LV presented in (Zheng and Dong, 2011). In next section we present the results obtained with $\left[\alpha^H\right]$ for construction the SDME basis.

2.6.3 Helmholtz problem

We consider the fabricated solution $u(x,y) = \sin(\pi x)\sin(\pi y)$ to the $3D$ domain using the distorted mesh illustrated in Fig. 2.24(b). The Dirichlet conditions were imposed on the boundaries with $\lambda = 1$. For the construction of the SDME basis, we used $\left[\alpha^H\right]$ and $k = 1/2$.

The approximation errors in terms of polynomial order are shown in Fig. 2.34. By increasing the polynomial order, the error decreases exponentially until $P = 8$. The machine accuracy is achieved using the SDME basis with diagonal preconditioner (DP-SDME).

The sparsity patterns for the $3D$ Helmholtz problems, using distorted mesh, are shown in Fig. 2.35. We observe a larger number of non-zero coefficients for the Helmholtz matrices using the SDME basis.
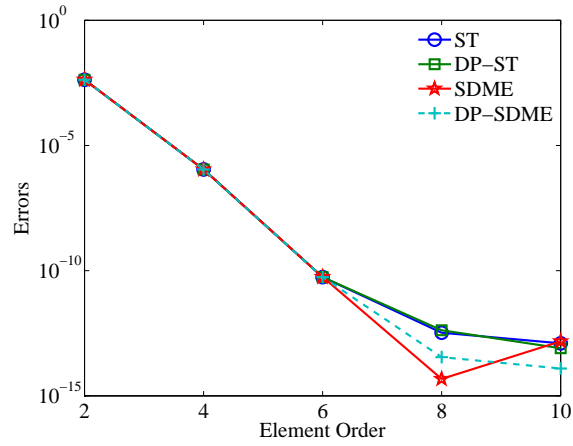
Figure 2.34: Approximation error for the SDME and ST bases in $3D$ Helmholtz problems with distorted mesh.

(a)

(b)
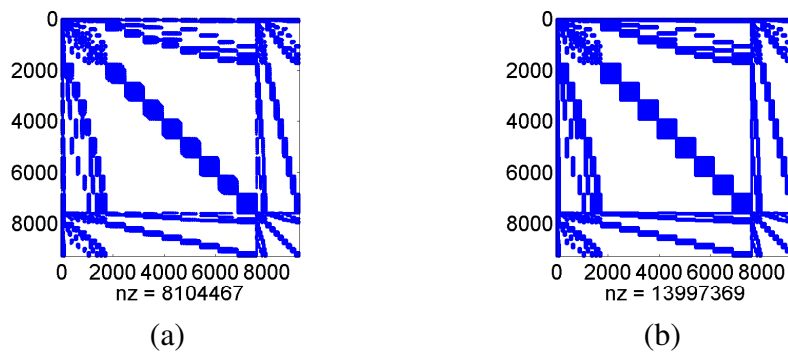
Figure 2.35: Sparsity patterns for the $3D$ Helmholtz matrices using the ST (a) and SDME (b) bases with distorted mesh and polynomial order $P = 10$.

Fig. 2.36 illustrates the behavior of the number of iterations and the relative percentage reduction in the number of iterations for the undistorted mesh and $\lambda = 1$. The proposed SDME basis presented a reduction of the number of iterations compared to the ST basis, according to Figs. 2.36(a). Fig. 2.36(b) illustrates the relative percentage reduction in the number of iterations for convergence for the conjugate gradient methods with the distorted mesh. The relative percentage reduction in the number of iterations using the SDME basis with the diagonal preconditioner was about 40% when using the polynomial order $P = 8$.

<center>(a)   (b)</center>
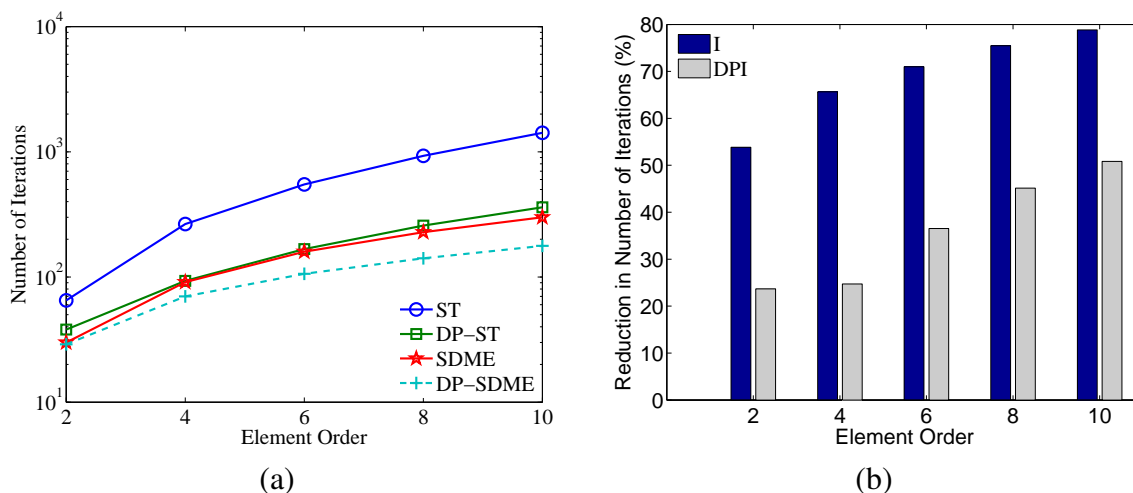
Figure 2.36: Number of iterations (a) and relative percentage reduction in the number of iterations with and without diagonal preconditioner (b) in terms of the polynomial order for the $3D$ Helmholtz problem with distorted mesh.

The solution time in terms of the polynomial approximation order is given in Fig. 2.37 for distorted mesh. We observed a reduction in time required for convergence of the solution for SDME basis. In this case, the solution time for the proposed basis was lower than the ST basis as shown in Fig. 2.37(a). The relative percentage reduction in solution time was over 70% using SDME basis without diagonal preconditioner and $P = 10$ as illustrated in Fig. 2.37(b). Using the preconditioner, the relative reduction in solution time was over 40% for the same polynomial order.

We solved the Helmholtz equation with different λ values for the distorted mesh (Fig. 2.24(b)) using the fabricated solution $u(x,y) = \sin(\pi x)\sin(\pi y)$. Fig. 2.38 shows the number of iterations of the conjugate gradient solver obtained with the SDME with $\left[\alpha^H\right]$ and ST bases using diagonal preconditioner. For comparison, we included the results obtained with SDME using $\left[\alpha^M\right]$ (SDME-M). Note that for small λ values, the number of iterations using the SDME basis is smaller when compared with the ST basis but still larger than SDME-M as shown Fig. 2.38(a). For large λ values,

<center>45</center>
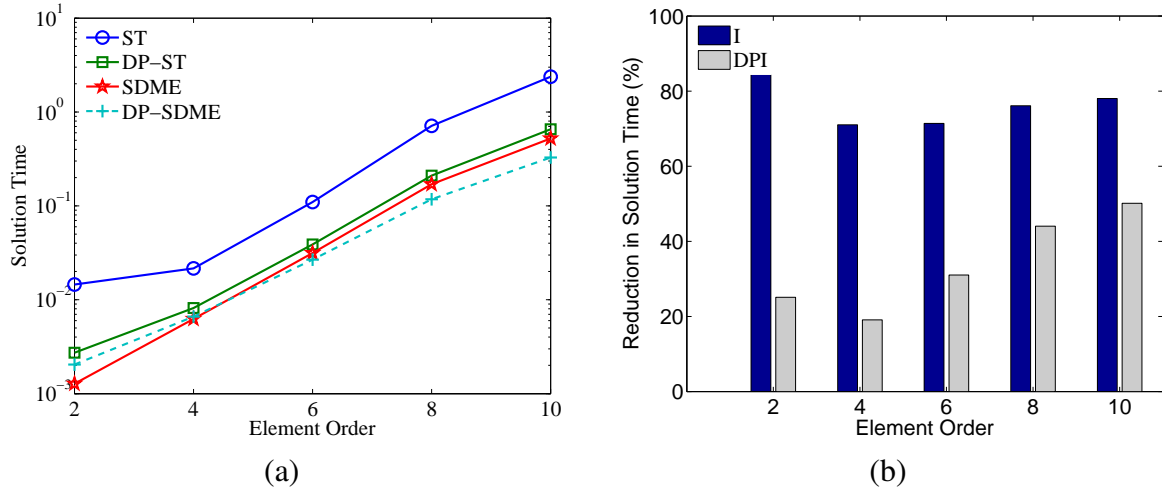
Figure 2.37: Solution time (a) and relative percentage reduction in solution time (b) for the $3D$ Helmholtz problem in terms of the polynomial order with distorted mesh.

the difference is even more remarkable when comparing to the ST basis and better than the SDME-M basis. This results indicates the efficiency of the basis for large λ values and $\left[\alpha^H\right]$.
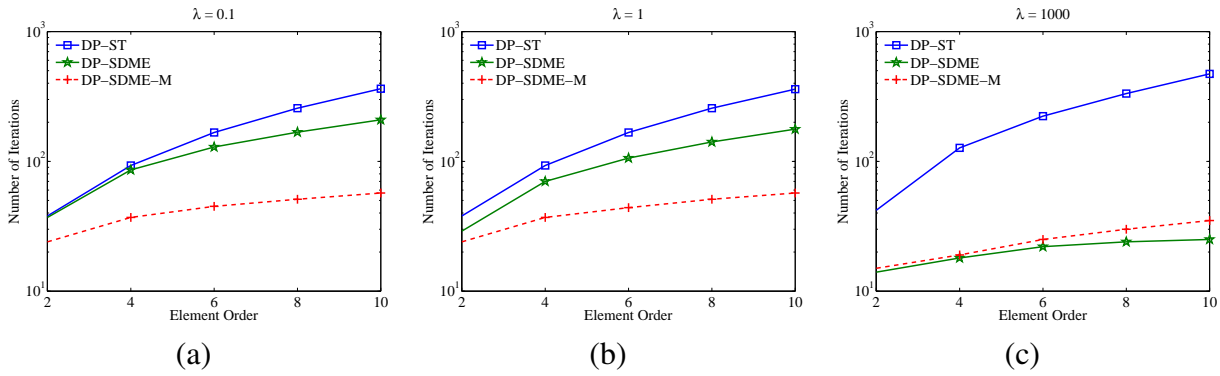
Figure 2.38: Number of iterations in terms of the polynomial order for the $3D$ Helmholtz problem with distorted mesh and different values of λ.

2.6.4 Linear elasticity

Consider the domain $\Omega = [-1, 1] \times [-1, 1] \times [-1, 1]$ discretized with 4 elements as shown in Fig. 2.39. We adopt Young modulus $E = 1$, density $\rho = 1$, and Poisson ratio $\nu = 0.25$ and assume the following fabricated solution for the displacement field as a function of time t
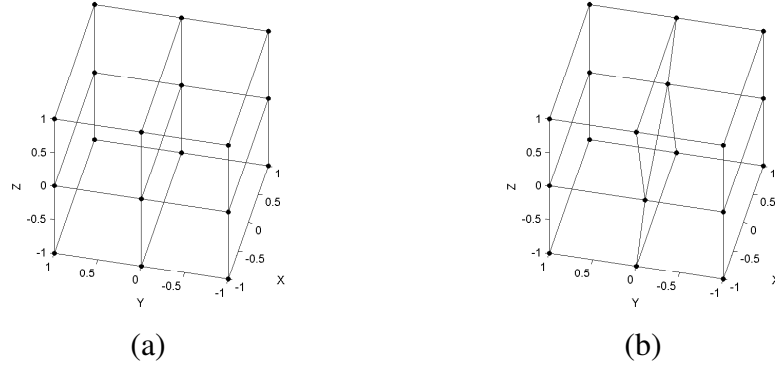
Figure 2.39: Undistorted (a) and distorted (b) meshes for $3D$ linear elasticity.

$$
\begin{aligned}
u_x &= (1 - x^2)(1 - y^2)(1 - z^2)\sin(2\pi t), \\
u_y &= 0, \\
u_z &= 0.
\end{aligned}
\tag{2.63}
$$

For small strain, the body force field is given by

$$
\begin{aligned}
f_x &= \frac{4\sin(2\pi t)}{5}\left\{(x^2 - 1)(y^2 - 1)\left[1 + 5\pi^2(z^2 - 1)\right] + \left[(x^2 - 1) + 3(y^2 - 1)\right](z^2 - 1)\right\}, \\
f_y &= \frac{\sin(2\pi t)}{5}\left[16xy(z^2 - 1)\right], \\
f_z &= \frac{\sin(2\pi t)}{5}\left[16xz(y^2 - 1)\right].
\end{aligned}
\tag{2.64}
$$

Homogeneous boundary conditions are applied on all faces of the domain and the initial conditions in terms of displacement and velocity are given by

$$
\begin{aligned}
u_x &= 0, \\
u_y &= 0, \\
u_z &= 0, \\
\dot{u}_x &= 2\pi(1 - x^2)(1 - y^2)(1 - z^2)\cos(2\pi t), \\
\dot{u}_y &= 0, \\
\dot{u}_z &= 0.
\end{aligned}
\tag{2.65}
$$

For the meshes shown in Fig. 2.39, the solution time was obtained using the explicit central difference method with time interval $[t_0; t_f] = [0; 0.12]$ and $\Delta t = 0.0012$. In such cases, we used $\left[\alpha^M\right]$

and $k = 1/2$ for the construction of the shape functions.

We also considered the Schur complement and diagonal preconditioner. The number of iterations was obtained as the sum of the number of iterations at each time step. As shown in Fig. 2.40, the number of iterations in terms of polynomial order is always smaller with the SDME basis to the range of P used. The reduction in the number of iterations is larger than 95% for distorted meshes and 98% for undistorted meshes and $P = 4$. These results indicate a higher efficiency of the use of SDME basis.

(a)   (b)
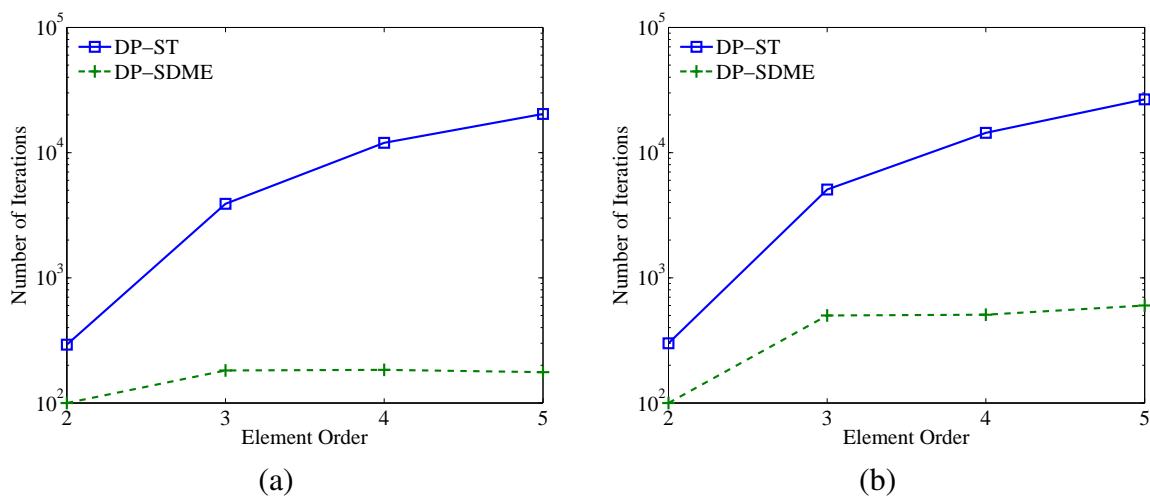
Figure 2.40: Number of iterations for convergence using undistorted (a) and distorted (b) meshes in $3D$ linear elasticity.
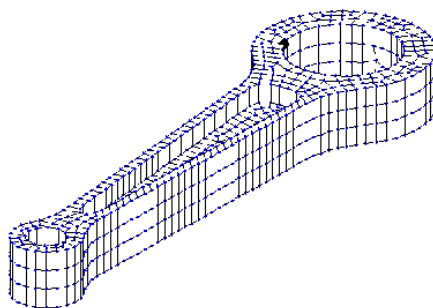
Figure 2.41: Mesh used for the conrod.

We also consider a conrod of an internal combustion engine discretized with a mesh of 768 hexahedra, as shown in Fig. 2.41. The internal nodes of the small end were fixed. The surface pres-

sures in directions x and y are applied on the internal surface of the big end. The load corresponds to a complete combustion engine cycle and was obtained using a dynamic rigid body model for the piston-conrod crankshaft system (Carbonara *et al.*, 2009).

The explicit central difference method was used with time interval $[t_0; t_f] = [0; 5.454 \times 10^{-3}]$ and $\Delta t = 6.06 \times 10^{-7}$. Furthermore, Schur complement and diagonal preconditioner were applied to obtain the solution at each time step. In our analyzes the number of iterations per load case was significantly smaller when using the SDME-M basis. The average number of iterations was 23.24 per load case for the standard basis and polynomial order $P = 2$. Using SDME basis this number was 2.22. The reduction in the number of iterations per load case was about 90%. Similar results was obtained for polynomial order $P = 3$. In this case, the average number of iterations was 27.18 for standard and 1.65 for SDME bases.

2.7 Conclusion

In this paper we presented the construction of high-order bases for structured elements considering the procedure of simultaneous diagonalization for internal modes and minimum energy orthogonalization to boundary modes. We shown that the procedure of orthogonalization can be generalized with the choice of the appropriate norm. This feature allows, in accordance with norm, obtain some high-order bases proposed in the literature, considering the simultaneously diagonal of internal modes and orthogonalization of the boundary modes procedure. The new basis functions is proposed when use the Helmholtz norm for construction the boundary modes with minimum energy orthogonalization. This particular basis for the one-dimensional Helmholtz problem uncoupled vertex and internal matrix blocks and is dependent of the parameter λ. For a given choice this parameter, exhibits a smaller condition number comparing with standard or Dong bases. Similar results is obtained for $3D$ Helmholtz problems and larger efficiency in terms of the number of iterations and numerical conditioning of the global matrices compared to the standard basis.

For construct the $2D$ and $3D$ mass and Poisson stiffness matrices, we presented the construction in terms of the one-dimensional mass and stiffness matrices for quadrilateral and hexahedral structural elements in distorted domains. This procedure interesting because consumes less memory for the solver, since we only need to store the one-dimensional shape functions and their derivatives calculated on one-dimensional integration points.

Numerical experiments for undistorted and distorted $3D$ meshes were made to verify the efficiency of this bases functions in projection, Poisson, Helmholz and linear elasticity problems. In projection and Poisson problems the application of the procedure of the minimum energy with $\left[\alpha^M\right]$ and $\left[\alpha^K\right]$ is more efficient in terms of the condition number and number of interations for solver when comparing to standard bases. This results are similar to presented in literature. We also shown that for $3D$ projection problems, the choice of the parameter $k = 0$ in procedure of the simultaneous diagonalization can improve the number of interations for convergence. For $3D$ Poisson problems the use of the parameter $k = 1$ in procedure of the simultaneous diagonalization not improve the number of iterations for convergence because the condition number of the one-dimensional mass matrix is larger than obtained with $k = 0$.

In transient linear elastic problems with explicit central difference methods, the use of the $\left[\alpha^M\right]$ is convenient due to dependence of the mass matrix to solver. The diagonal preconditioner was used to improved the performance of the bases.

The procedure proposed has been extended to non-structured elements.

2.8 Acknowledgements

50

3 TRANSIENT LINEAR ELASTIC ANALYSIS USING MINIMUM EN-ERGY HIGH-ORDER EXPANSION BASES

3.1 Introduction

The use of high-order shape functions for the FEM is convenient because of the higher convergence rate obtained with the increase of the polynomial order for problems with smooth solutions. There has been an increasing number of elasticity applications the high-order FEM method in the literature, such as Reissner-Mindlin plates, problems with large displacements and strains, elastoplasticity, nearly-incompressible, hyperelasticity, contact, dynamic, and powder metallurgy (Krause *et al.*, 1995; Nogueira Jr and Bittencourt, 2007; Gharti *et al.*, 2012; Yu *et al.*, 2012; Dong and Yosibash, 2009; Konyukhov and Schweizerhof, 2009; Heisserer *et al.*, 2008).

Pioneering work involving the high-order FEM for three-dimensional linear elasticity is attributed to (Zienkiewicz *et al.*, 1970), where hierarchical high-order shape functions were used in regions with elevated gradients of the considered domain. Since then, several families of shape functions for the high-order FEM were proposed in the literature. Regarding unstructured elements, hierarchical shape functions were derived for triangular elements using barycentric coordinates (Peano, 1976). The use of orthogonal Legendre polynomials to construct shape functions was proposed by (Babuska *et al.*, 1981), which obtained a block-diagonal stiffness matrix and improved the sparsity profile and numerical conditioning of the matrix system. In fact, as shown by (Abdul-Rahman and Kasper, 2007), the condition number for unstructured elements has an exponential increase with the polynomial order. Other works, such as (Carnevali *et al.*, 1993) used orthogonality properties to obtain local matrices with better conditioning and sparsity profiles.

The use of the tensor product of one-dimensional Jacobi orthogonal polynomials to build hierarchical shape functions for structured and unstructured elements was introduced by (Karniadakis and Sherwin, 2005). Moreover, a study comparing some modal basis and the applicability of the high-order FEM for nonlinear and linear elastic problems using three-dimensional unstructured meshes is presented in (Nogueira Jr and Bittencourt, 2007).

The choice of the weights of Jacobi polynomials to construct basis functions can influence the sparsity of the element mass and stiffness matrices. Therefore, an appropriate choice can re-

sult in better properties regarding sparsity profiles and numerical conditioning (Bittencourt *et al.*, 2007a). Moreover, the weights of the Gauss-Jacobi, Gauss-Radau-Jacobi, and Gauss-Lobatto-Jacobi quadratures have an important correlation with the number of required points to integrate the element matrices numerically (Bittencourt and Vazquez, 2009).

Techniques such as Schur complement and simultaneous diagonalization were implemented as an effective way to obtain better sparsity and numerical conditioning of mass and stiffness matrices (Babuska and Guo, 1989; Shen and Wang, 2007). Schur complement allows better conditioning and improves the performance of iterative solvers for the linear system of equations (Babuska and Guo, 1989). In (Šolín and Vejchodskỳ, 2008) simultaneous diagonalization was used to construct internal functions for the high-order FEM which makes simultaneously diagonal the one-dimensional Laplace stiffness and mass matrices. Also, in (Vejchodskỳ, 2010), a minimum energy orthogonalization technique was presented to construct one-dimensional basis functions. As the Schur complement, the application of the minimum energy procedure results in the orthogonality between the boundary and internal modes.

A modification of the construction of the one-dimensional high-order shape functions for structured elements was proposed by (Zheng and Dong, 2011) using simultaneous diagonalization. In this case, the internal shape functions were constructed in such way that the respective internal mass and stiffness matrices have the same condition number and are simultaneously diagonal. The Gram-Schmidt orthogonalization was used to decouple the boundary and internal modes when constructing the mass matrix. This is important to obtain an efficient high-order basis in terms of conditioning and number of iterations required by the conjugate gradient method to solve the global matrix system.

Traditionally, sum factorization and differentiation collocation have been used as effective procedures to obtain the two- and three-dimensional shape functions and their derivatives from the values of the one-dimensional shape functions and their derivatives on the integrations points. In this paper, we present an alternative procedure to calculate the coefficients of the two- and three-dimensional mass and elastic stiffness matrices in terms of the product of the local one-dimensional element matrices. The advantages of this procedure are the use of only one-dimensional shape functions and their derivatives, one-dimensional integration rules and better computational performance. We refer to this method as $1D$ matrices, while the fully tensorial procedure is referred as standard.

In this paper, we present a simulataneously diagonal and minimum energy high-order expansion basis applied to transient elastic analysis using structured elements. For this purpose, the internal modes are constructed in such way that the internal $1D$ mass and stiffness matrices have the same condition number. The minimum energy orthogonalization with Helmholtz and mass norms is used to decouple the boundary and internal modes for a transient three-dimensional problem in linear elasticity using the Newmark method. We perform numerical tests to show the performance when using the $1D$ matrices procedure. We investigate the performance of the proposed basis, comparing it to the standard basis with Jacobi polynomials given in (Karniadakis and Sherwin, 2005). We also use the $1D$ matrices procedure to construct the element matrices in terms of the one-dimensional mass, stiffness and mixed matrices. Furthermore, we propose the use of the local undistorted mass matrix as a preconditioner and compare it with the use of the diagonal and symmetric successive over relaxation (SSOR) preconditioners.

3.2 Minimum Energy High Order Basis

In this section we present the construction of shape functions based on simultaneously diagonalization and minimum energy procedures. A special construction for the one-dimensional basis functions using the Helmholtz norm is considered for application in dynamic problems using the Newmark method.

3.2.1 One-dimensional basis function

Consider the one-dimensional local element in the domain $-1 \leq \xi_1 \leq 1$. The hierarchical standard one-dimensional basis of polynomial order P is defined as

$$
\psi_p(\xi_1) = \begin{cases} \frac{1}{2}(1 - \xi_1) & p = 0 \\ \frac{1}{2}(1 + \xi_1) & p = 1 \\ \frac{1}{4}(1 - \xi_1)(1 + \xi_1)\mathcal{P}_{p-2}^{\alpha,\beta}(\xi_1) & 2 \leq p \leq P \end{cases} , \tag{3.1}
$$

where $\mathcal{P}_p^{\alpha,\beta}(\xi)$ is the Jacobi polynomial of order P and weights (α, β). The Jacobi basis is related to the element topological entities such as vertices, edges and faces. The one-dimensional local

coefficients of the mass and stiffness matrices are respectively determined by

$$M_{pq} = \int_{-1}^{1} \psi_p(\xi_1)\psi_q(\xi_1)d\xi_1, \tag{3.2}$$

$$K_{pq} = \int_{-1}^{1} \psi_{p,\xi_1}(\xi_1)\psi_{q,\xi_1}(\xi_1)d\xi_1, \tag{3.3}$$

with $0 \leq p,q \leq P$ and ψ_{p,ξ_1} the derivative of ψ_p with respect to ξ_1.

The construction of the new shape functions $\phi_p(\xi)$ for the interior modes is performed in the following way

$$\phi_p(\xi) = \sum_{q=2}^{P} y_{pq}\psi_q(\xi), \tag{3.4}$$

where the matrix $[Y]$ are determined in such way that the blocks $\left[M'_{ii}\right]$ and $\left[K'_{ii}\right]$ related to the internal modes of the mass and stiffness matrices are diagonal and determined as

$$\begin{aligned} \left[M'_{ii}\right] &= [Y]\,[M_{ii}]\,[Y]^T, \\ \left[K'_{ii}\right] &= [Y]\,[K_{ii}]\,[Y]^T. \end{aligned} \tag{3.5}$$

Consider $[L] = \left([X]\left[\Lambda_M^{-\frac{1}{2}}\right]\right)^T [K_{ii}]\left([X]\left[\Lambda_M^{-\frac{1}{2}}\right]\right)$, where $[X]$ and $[\Lambda_M]$ are respectively the matrices of eigenvectors and eigenvalues of $[M_{ii}]$. The matrix $[Y]$ are determined as

$$[Y] = \left([X]\left[\Lambda_M^{-\frac{1}{2}}\right][Z]\left[\Lambda_S^{-\frac{k}{2}}\right]\right)^T, \tag{3.6}$$

where $[Z]$ is the matrix of eigenvectors and $[\Lambda_S]$ is the diagonal matrix with the eigenvalues of $[L]$. Factor k influences the condition number of the matrices related to the internal modes (Zheng and Dong, 2011). The choice of $k = 1/2$ is convenient, since it yields the same condition number for the internal blocks of the one-dimensional mass and stiffness matrices.

The above transformation is applied to the internal modes. However, the vertex and internal modes are still coupled. In the next section we present a procedure to modify the one-dimensional boundary modes for the mass and stiffness matrices.

3.2.2 Newmark Method and the Minimum Energy Procedure

In general, the implicit methods for time integration have better numerical stability and accuracy when compared to explicit methods. They are unconditionally stable and allows the use of larger time steps. Consider the discrete equation of motion for a structural body given by

$$[M]\{\ddot{U}^t\} + [C]\{\dot{U}^t\} + [K]\{U^t\} = \{R^t\}, \tag{3.7}$$

where $[M]$, $[C]$ and $[K]$ are the global mass, damping and stiffness matrices. The terms $\{\ddot{U}^t\}$, $\{\dot{U}^t\}$ and $\{U^t\}$ are the acceleration, velocity and displacement vectors for a given time t. The vector $\{R^t\}$ contains the equivalent nodal loads.

In the Newmark method, the displacement at time $t + \triangle t$ can be approximated by (Bathe, 1996)

$$[\hat{K}]\{U^{t+\triangle t}\} = \{\hat{R}^{t+\triangle t}\}, \tag{3.8}$$

with the effective stiffness matrix $[\hat{K}]$ given by

$$[\hat{K}] = [K] + a_0[M] + a_1[C], \tag{3.9}$$

and

$$\{\hat{R}^{t+\triangle t}\} = \{R^{t+\triangle t}\} + [M]\left(a_0\{U^t\} + a_2\{\dot{U}^t\} + a_3\{\ddot{U}^t\}\right) + ... \tag{3.10}$$
$$+ [C]\left(a_1\{U^t\} + a_4\{\dot{U}^t\} + a_5\{\ddot{U}^t\}\right).$$

The constants used for the Newmark method are $a_0 = \frac{1}{\alpha\triangle t^2}$, $a_1 = \frac{\delta}{\alpha\triangle t}$, $a_2 = \frac{1}{\alpha\triangle t}$, $a_3 = \frac{1}{2\alpha}-1$, $a_4 = \frac{\delta}{\alpha} - 1$, $a_5 = \frac{\triangle t}{2}\left(\frac{\delta}{\alpha} - 2\right)$, $a_6 = \triangle t(1 - \delta)$, $a_7 = \delta\triangle t$, with $\delta \geq 0.50$ and $\alpha \geq 0.25(0.5 + \delta)^2$. For our analyses, we adopt $\alpha = 0.25$ and $\delta = 0.50$.

We propose a modification of the one-dimensional vertex modes based on the simultaneously diagonal and minimum energy (SDME) procedure with the Helmholtz norm. The minimum energy

extensions of the standard basis functions is computed as (Vejchodský, 2010)

$$\psi_k^{me} = \psi_k^v - \sum_{j=1}^{N_i} \alpha_{kj}\psi_j^i, \quad k = 1,...,N_v, \tag{3.11}$$

where N_v and N_i are the numbers of vertex and internal modes.

This formulation enables the construction of the minimum energy procedure according to the choice of the coefficients α_{kj}. The effective stiffness matrix without damping can be partitioned as

$$\left[\hat{K}\right] = \begin{bmatrix} [K_{vv}] & [K_{vi}] \\ [K_{vi}]^T & [K_{ii}] \end{bmatrix} + \lambda \begin{bmatrix} [M_{vv}] & [M_{vi}] \\ [M_{vi}]^T & [M_{ii}] \end{bmatrix} = \begin{bmatrix} \left[\hat{K}_{vv}\right] & \left[\hat{K}_{vi}\right] \\ \left[\hat{K}_{vi}\right]^T & \left[\hat{K}_{ii}\right] \end{bmatrix}, \tag{3.12}$$

where the subindices v and i identify the blocks relative to vertex and internal modes.

The Helmholtz energy norm of a function $v \in V$ is $\|v\|_E^2 = \langle v,v \rangle_E = \langle v,v \rangle_{L_2} + \lambda \langle v,v \rangle_{L_2}$. The L_2-inner product of functions f and g is defined as $\langle f,g \rangle_{L_2} = \int_{-1}^1 f(\xi)g(\xi)d\xi$. The coefficients α_{vj} in Eq. 3.11 are determined such that

$$\langle \psi_k^{me}, \psi_j^i \rangle_E = 0, \quad k = 1,...,N_v \text{ and } j = 1,...,N_i. \tag{3.13}$$

This condition decouples the boundary and internal blocks such of the one-dimensional effective stiffness matrix $[\hat{K}]$. In matrix notation, the coefficients α_{kj} are calculated as

$$\left[\alpha^{\hat{K}}\right] = \left[\hat{K}_{vi}\right] \left[\hat{K}_{ii}\right]^{-1}. \tag{3.14}$$

In this case, λ could be associated with coefficient a_0 in Eq. (3.9). For convenience, we take $\lambda = 1$ and then analyse later the effect of the choice of this parameter in the construction of the one-dimensional shape functions of the minimum energy.

Analogously , we can use a construction based on the terms of the mass matrix only and the respective coefficients $\left[\alpha^M\right]$ are

$$\left[\alpha^M\right] = [M_{vi}] [M_{ii}]^{-1}. \tag{3.15}$$

This construction decouples the internal and boundary modes of the one-dimensional mass matrix, but these modes remain coupled for the effective stiffness matrix. In Fig.3.1, we show the sparsity profiles of the one-dimensional effective stiffness matrix with the standard basis (ST) and the simultaneously diagonal and minimum energy bases (SDME). The boundary modes are numbered first followed by the internal modes.

The proposed basis considers the simultaneously diagonalization and minimum energy (SDME) procedures in linear dynamic analysis using the Newmark method. As in (Zheng and Dong, 2011), the proposed basis functions and their derivatives are not constructed analytically but calculated on the integration points.

| (a) | (b) | (c) |
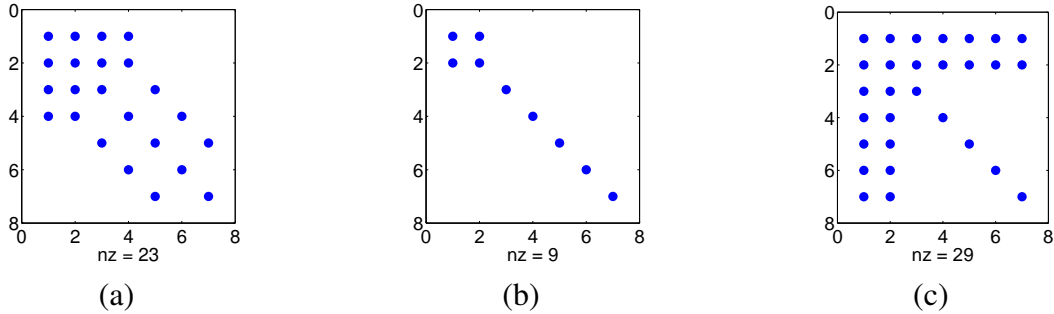
Figure 3.1: Sparsity patterns of the effective stiffness matrix for a polynomial order $P = 6$ with the standard basis (a), SDME basis with $\left[\alpha^{\hat{K}}\right]$ and $\lambda = 1$ (b) and SDME basis with $\left[\alpha^M\right]$ and $\lambda = 1$ (c).

3.3   Calculation Procedure for the Matrices of Quadrilaterals and Hexahedra

This section presents the 1D matrices procedure which obtains the coefficients of the mass and stiffness matrices of quadrilaterals and hexahedra using the product of the coefficientes of the one-dimensional matrices. As will be seen in Section 3.4.1, this procedure has performance gains in terms of speed and less memory allocation for the high-order FEM software. We write the coefficientes of the stiffness and mass matrices in explicit form, that is, we do not use the product of matrix operators as done in the standard procedure. This allows to simplify the obtained expressions for the stiffness matrix when the material is isotropic. The element matrices using the

standard procedure are calculated of

$$[M] = \rho \int_{\Omega_e} [N]^T [N] |J| d\Omega_e, \tag{3.16}$$

$$[K] = \int_{\Omega_e} [B]^T [D] [B] |J| d\Omega_e, \tag{3.17}$$

where ρ is the density, $[N]$ and $[B]$ respectively are the matrices of the shape functions and their global derivatives, $[D]$ is the constitutive matrix and $|J|$ is the determinant of the Jacobian matrix. We introduce the coefficients of the local one-dimensional element matrices, denoted as M_{ap}^{1D} for mass, K_{ap}^{1D} for stiffness and D_{ap}^{1D} for mixed:

$$M_{ap}^{1D}(\xi) = \int_{-1}^{1} \varphi_a(\xi)\varphi_p(\xi)d\xi,$$

$$K_{ap}^{1D}(\xi) = \int_{-1}^{1} \varphi_{a,1}(\xi)\varphi_{p,1}(\xi)d\xi, \tag{3.18}$$

$$D_{ap}^{1D}(\xi) = \int_{-1}^{1} \varphi_{a,1}(\xi)\varphi_p(\xi)d\xi.$$

For notation purposes, we rewrite the above expressions in terms of numerical integration as:

$$M_{ap}^{1D}(\xi) = \sum_{d=1}^{n_1} \varphi_a(\xi_d)\varphi_p(\xi_d)W_d,$$

$$K_{ap}^{1D}(\xi) = \sum_{d=1}^{n_1} \varphi_{a,1}(\xi_d)\varphi_{p,1}(\xi_d)W_d, \tag{3.19}$$

$$D_{ap}^{1D}(\xi) = \sum_{d=1}^{n_1} \varphi_{a,1}(\xi_d)\varphi_p(\xi_d)W_d,$$

where n_1 is the number of integration points in direction ξ, ξ_d is the corresponding integration coordinate and W_d the associated weight. The terms φ_a and φ_p are the one-dimensional shape functions, $\varphi_{a,1}$ and $\varphi_{p,1}$ are their derivatives relative to ξ. The indices a and p will be explained in Section 3.3.1. We define the terms inside the summation in Eq.(3.19) as the one-dimensional

matrices calculated for each integration point and given by

$$
\begin{aligned}
M_{ap}^{1D}(\xi_d) &= \varphi_a(\xi_d)\varphi_p(\xi_d), \\
K_{ap}^{1D}(\xi_d) &= \varphi_{a,1}(\xi_d)\varphi_{p,1}(\xi_d), \\
D_{ap}^{1D}(\xi_d) &= \varphi_{a,1}(\xi_d)\varphi_p(\xi_d).
\end{aligned}
\tag{3.20}
$$

3.3.1 Tensor product of one-dimensional matrices for quadrilaterals

The coefficients of the mass matrix for quadrilateral elements are given by

$$
M_{st}^{2D} = \rho \int_{-1}^{1}\int_{-1}^{1} N_s(\xi,\eta)N_t(\xi,\eta)|J|d\xi d\eta,
\tag{3.21}
$$

with $N_s(\xi,\eta)$ and $N_t(\xi,\eta)$ the local shape functions for quadrilaterals defined as (Karniadakis and Sherwin, 2005; Bittencourt *et al.*, 2007a)

$$
\begin{aligned}
N_s(\xi,\eta) &= \varphi_p(\xi)\varphi_q(\eta), \quad 0 \le p,q \le P, \\
N_t(\xi,\eta) &= \varphi_a(\xi)\varphi_b(\eta), \quad 0 \le a,b \le P,
\end{aligned}
\tag{3.22}
$$

where p,q,a,b are the tensor product indices associated with the topological entities of the element, P is the polynomial order in directions ξ and η, and $s,t = 1,\ldots,(P+1)^2$. Rewriting Eq.(3.21) in terms of numerical integration quadrature, we obtain

$$
M_{st}^{2D} = \rho \sum_{d=1}^{n_1}\sum_{e=1}^{n_2} N_s(\xi_d,\eta_e)N_t(\xi_d,\eta_e)|J|_{de}W_dW_e,
\tag{3.23}
$$

and n_2 is the number of integration points for direction η, W_e is the weight, and $|J|_{de}$ is the determinant of the Jacobian matrix on integration point (ξ_d,η_e). Recalling Eq.(3.19), the product of local shape functions for the quadrilateral can be written in terms of the local one-dimensional mass matrices for an integration point in the following way:

$$
N_s(\xi_d,\eta_e)N_t(\xi_d,\eta_e) = \varphi_p(\xi_d)\varphi_q(\eta_e)\varphi_a(\xi_d)\varphi_b(\eta_e) = M_{pa}^{1D}(\xi_d)M_{qb}^{1D}(\eta_e).
\tag{3.24}
$$

Substituting Eq.(3.24) into Eq.(3.23), we obtain the explicit expression for the coefficients of

the mass matrix in terms of the one-dimensional matrices as

$$M_{st}^{2D} = \rho \sum_{d=1}^{n_1} \sum_{e=1}^{n_2} M_{pa}^{1D}(\xi_d) M_{qb}^{1D}(\eta_e) |J|_{de} W_d W_e. \tag{3.25}$$

The coefficients of the stiffness matrix are written in index notation, because the derivative operators and constitutive terms assume different values according to the degrees of freedom. The expression is given by

$$K_{st}^{2D}(i,j) = \int_{-1}^{1} \int_{-1}^{1} C_{iljk} N_{s,k} N_{t,l} |J| d\xi d\eta, \tag{3.26}$$

with $i,j,k,l = 1,2$. The terms $N_{s,k}$ and $N_{t,l}$ are the global derivatives of the quadrilateral shape functions. The term C_{iljk} is the constitutive tensor given by

$$C_{iljk} = \lambda \delta_{il} \delta_{jk} + \mu \left(\delta_{ij} \delta_{lk} + \delta_{ik} \delta_{lj} \right). \tag{3.27}$$

The above equation is usually written in Voigt notation, which we present here for implementation purpose. We have for plane strain in linear isotropic elasticity:

$$[D] = \begin{bmatrix} C_{1111} & C_{1122} & C_{1112} \\ C_{1122} & C_{2222} & C_{2212} \\ C_{1112} & C_{2212} & C_{1212} \end{bmatrix} = \begin{bmatrix} 2\mu + \lambda & \lambda & 0 \\ \lambda & 2\mu + \lambda & 0 \\ 0 & 0 & \mu \end{bmatrix}, \tag{3.28}$$

where μ and λ are the Lamé coefficients. We can rewrite Eq.(3.26) in terms of numerical integration and obtain:

$$K_{st}^{2D}(i,j) = \sum_{d=1}^{n_1} \sum_{e=1}^{n_2} C_{iljk} N_{s,k}(\xi_d,\eta_e) N_{t,l}(\xi_d,\eta_e) |J|_{de} W_d W_e. \tag{3.29}$$

The global derivatives of the shape functions for each integration point are

$$N_{s,k}(\xi_d,\eta_e) = (j_{km})_{de} N_{s,m}(\xi_d,\eta_e), \tag{3.30}$$
$$N_{t,l}(\xi_d,\eta_e) = (j_{ln})_{de} N_{t,n}(\xi_d,\eta_e),$$

where $(j_{km})_{de}$ and $(j_{ln})_{de}$ are the coefficients of the inverse of the Jacobian matrices and $N_{s,m}(\xi_d,\eta_e)$ and $N_{t,n}(\xi_d,\eta_e)$ are the local derivatives of the quadrilateral shape functions for each integration

point. We can substitute Eq.(3.30) into Eq.(3.29) and obtain

$$K_{st}^{2D}(i,j) = \sum_{d=1}^{n_1} \sum_{e=1}^{n_2} C_{iljk}(j_{km}j_{ln})_{de} N_{s,m}(\xi_d,\eta_e) N_{t,n}(\xi_d,\eta_e)|J|_{de}W_dW_e. \tag{3.31}$$

Recalling Eq.(3.20), we can write the local derivatives of the quadrilateral shape functions in terms of the one-dimensional element matrices calculated for each integration point. For this purpose, the indices k, l are expanded and the following expressions are obtained:

$$\begin{aligned}
N_{s,1}(\xi_d,\eta_e)N_{t,1}(\xi_d,\eta_e) &= \varphi_{p,1}(\xi_d)\varphi_q(\eta_e)\varphi_{a,1}(\xi_d)\varphi_b(\eta_e) = K_{pa}^{1D}(\xi_d)M_{qb}^{1D}(\eta_e), \\
N_{s,1}(\xi_d,\eta_e)N_{t,2}(\xi_d,\eta_e) &= \varphi_{p,1}(\xi_d)\varphi_q(\eta_e)\varphi_a(\xi_d)\varphi_{b,2}(\eta_e) = D_{pa}^{1D}(\xi_d)D_{bq}^{1D}(\eta_e), \\
N_{s,2}(\xi_d,\eta_e)N_{t,1}(\xi_d,\eta_e) &= \varphi_p(\xi_d)\varphi_{q,2}(\eta_e)\varphi_{a,1}(\xi_d)\varphi_b(\eta_e) = D_{ap}^{1D}(\xi_d)D_{qb}^{1D}(\eta_e), \\
N_{s,2}(\xi_d,\eta_e)N_{t,2}(\xi_d,\eta_e) &= \varphi_p(\xi_d)\varphi_{q,2}(\eta_e)\varphi_a(\xi_d)\varphi_{b,2}(\eta_e) = M_{pa}^{1D}(\xi_d)K_{qb}^{1D}(\eta_e).
\end{aligned} \tag{3.32}$$

The terms $N_{s,1}(\xi_d,\eta_e)N_{t,2}(\xi_d,\eta_e)$ and $N_{s,2}(\xi_d,\eta_e)N_{t,1}(\xi_d,\eta_e)$ are different, since the one-dimensional mixed matrices D^{1D} are not symmetric. We expand the index notation to show the explicit form for $K_{st}^{2D}(1,1)$. Setting the free indices $i,j = 1$ in Eq.(3.31), we obtain

$$K_{st}^{2D}(1,1) = \sum_{d=1}^{n_1} \sum_{e=1}^{n_2} C_{1l1k}(j_{km}j_{ln})_{de} N_{s,m}(\xi_d,\eta_e) N_{t,n}(\xi_d,\eta_e)|J|_{de}W_dW_e. \tag{3.33}$$

Expanding the repeated indices m and n, and omitting ξ_d and η_e for simplicity, we obtain

$$K_{st}^{2D}(1,1) = \sum_{d=1}^{n_1} \sum_{e=1}^{n_2} C_{1l1k} \left[(j_{k1}j_{l1})_{de}N_{s,1}N_{t,1} + (j_{k1}j_{l2})_{de}N_{s,1}N_{t,2} + \right. \tag{3.34}$$

$$\left. (j_{k2}j_{l1})_{de}N_{s,2}N_{t,1} + (j_{k2}j_{l2})_{de}N_{s,2}N_{t,2} \right]|J|_{de}W_dW_e.$$

Expanding the repeated indices k and l, we obtain

$$K_{st}^{2D}(1,1) = \sum_{d=1}^{n_1}\sum_{e=1}^{n_2}\{\,C_{1111}\,[(j_{11}j_{11})_{de}N_{s,1}N_{t,1} + (j_{11}j_{12})_{de}N_{s,1}N_{t,2} +$$
$$(j_{12}j_{11})_{de}N_{s,2}N_{t,1} + (j_{12}j_{12})_{de}N_{s,2}N_{t,2}] +$$
$$C_{1211}\,[(j_{11}j_{21})_{de}N_{s,1}N_{t,1} + (j_{11}j_{22})_{de}N_{s,1}N_{t,2} +$$
$$(j_{12}j_{21})_{de}N_{s,2}N_{t,1} + (j_{12}j_{22})_{de}N_{s,2}N_{t,2}] + \qquad (3.35)$$
$$C_{1112}\,[(j_{21}j_{11})_{de}N_{s,1}N_{t,1} + (j_{21}j_{12})_{de}N_{s,1}N_{t,2} +$$
$$(j_{22}j_{11})_{de}N_{s,2}N_{t,1} + (j_{22}j_{12})_{de}N_{s,2}N_{t,2}] +$$
$$C_{1212}\,[(j_{21}j_{21})_{de}N_{s,1}N_{t,1} + (j_{21}j_{22})_{de}N_{s,1}N_{t,2} +$$
$$(j_{22}j_{21})_{de}N_{s,2}N_{t,1} + (j_{22}j_{22})_{de}N_{s,2}N_{t,2}]\,\}\,|J|_{de}W_dW_e.$$

Recalling that $C_{1211} = C_{1112} = 0$ from Eq.(3.28), we can simplify the above equation and rewrite it in terms of the one-dimensional matrices of Eq.(3.32) as

$$K_{st}^{2D}(1,1) = \sum_{d=1}^{n_1}\sum_{e=1}^{n_2}\{C_{1111}\,[\,(j_{11}^2)_{de}K_{pa}^{1D}M_{qb}^{1D} + (j_{11}j_{12})_{de}D_{pa}^{1D}D_{bq}^{1D} +$$
$$(j_{12}j_{11})_{de}D_{ap}^{1D}D_{qb}^{1D} + (j_{12}j_{12})_{de}M_{pa}^{1D}K_{qb}^{1D}] + \qquad (3.36)$$
$$C_{1212}\,[(j_{21}j_{21})_{de}K_{pa}^{1D}M_{qb}^{1D} + (j_{21}j_{22})_{de}D_{pa}^{1D}D_{bq}^{1D} +$$
$$(j_{22}j_{21})_{de}D_{ap}^{1D}D_{qb}^{1D} + (j_{22}j_{22})_{de}M_{pa}^{1D}K_{qb}^{1D}]\,\}\,|J|_{de}W_dW_e.$$

The other three stiffness terms can be obtained by changing the free indices i,j. The above procedure can be easily applied to plane stress, by just changing the plane strain constitutive matrix $[D]$ of Eq.(3.28) for the plane stress equivalent.

3.3.2 Tensor product of one-dimensional matrices for hexahedra

It is straightforward to extend the previous procedure to three dimensions. The coefficients of the mass matrix for hexahedra are defined as

$$M_{st}^{3D} = \int_{-1}^{1} \int_{-1}^{1} \int_{-1}^{1} N_s(\xi,\eta,\zeta) N_t(\xi,\eta,\zeta) |J| d\xi d\eta d\zeta, \tag{3.37}$$

where $N_s(\xi,\eta,\zeta)$ and $N_t(\xi,\eta,\zeta)$ are the local shape function, given by (Karniadakis and Sherwin, 2005; Bittencourt *et al.*, 2007a)

$$\begin{aligned} N_s(\xi,\eta,\zeta) &= \varphi_p(\xi)\varphi_q(\eta)\varphi_r(\zeta), \quad 0 \le p,q,r \le P, \\ N_t(\xi,\eta,\zeta) &= \varphi_a(\xi)\varphi_b(\eta)\varphi_c(\zeta), \quad 0 \le a,b,c \le P, \end{aligned} \tag{3.38}$$

where r is the tensor index for direction ζ, and $r,s,t = 1,\ldots,(P+1)^3$. Rewriting Eq.(3.37) in terms of numerical integration, we obtain

$$M_{st}^{3D} = \rho \sum_{d=1}^{n_1} \sum_{e=1}^{n_2} \sum_{f=1}^{n_3} N_s(\xi_d,\eta_e,\zeta_f) N_t(\xi_d,\eta_e,\zeta_f) |J|_{def} W_d W_e W_f, \tag{3.39}$$

where n_3 is the number of integration points for direction ζ, ζ_f is the corresponding integration coordinate and W_f is the weight. The product of the local shape functions for hexahedra on an integration point can be written in terms of the local one-dimensional mass matrices as

$$\begin{aligned} N_s(\xi_d,\eta_e,\zeta_f) N_t(\xi_d,\eta_e,\zeta_f) &= \varphi_p(\xi_d)\varphi_q(\eta_e)\varphi_r(\zeta_f)\varphi_a(\xi_d)\varphi_b(\eta_e)\varphi_c(\zeta_f) \\ &= M_{pa}^{1D}(\xi_d) M_{qb}^{1D}(\eta_e) M_{rc}^{1D}(\zeta_f). \end{aligned} \tag{3.40}$$

Substituting Eq.(3.40) into Eq.(3.39), we obtain the explicit expression for the coefficients of the three dimensional mass matrix in terms of the one-dimensional matrices:

$$M_{st}^{3D} = \rho \sum_{d=1}^{n_1} \sum_{e=1}^{n_2} \sum_{f=1}^{n_3} M_{pa}^{1D}(\xi_d) M_{qb}^{1D}(\eta_e) M_{rc}^{1D}(\zeta_f) |J|_{def} W_d W_e W_f. \tag{3.41}$$

The coefficients of the stiffness matrix for hexahedrical elements in index notation can be written as

$$K_{st}^{3D}(i,j) = \int_{-1}^{1} \int_{-1}^{1} \int_{-1}^{1} C_{iljk} N_{s,k} N_{t,l} |J| d\xi d\eta d\zeta, \tag{3.42}$$

where $i,j,k,l = 1,2,3$. Rewriting the above equation using numerical integration, we obtain

$$K_{st}^{3D}(i,j) = \sum_{d=1}^{n_1} \sum_{e=1}^{n_2} \sum_{f=1}^{n_3} C_{iljk} N_{s,k}(\xi_d, \eta_e, \zeta_f) N_{t,l}(\xi_d, \eta_e, \zeta_f) |J|_{def} W_d W_e W_f, \tag{3.43}$$

The global derivatives for three dimensions are

$$N_{s,k}(\xi_d, \eta_e, \zeta_f) = (j_{km})_{def} N_{s,m}(\xi_d, \eta_e, \zeta_f), \tag{3.44}$$

$$N_{t,l}(\xi_d, \eta_e, \zeta_f) = (j_{ln})_{def} N_{t,n}(\xi_d, \eta_e, \zeta_f).$$

Substituting Eq.(3.44) in Eq.(3.43), we obtain

$$K_{st}^{3D}(i,j) = \sum_{d=1}^{n_1} \sum_{e=1}^{n_2} \sum_{f=1}^{n_3} C_{iljk}(j_{km}j_{ln})_{def} N_{s,m}(\xi_d, \eta_e, \zeta_f) N_{t,n}(\xi_d, \eta_e, \zeta_f) |J|_{def} W_d W_e W_f. \tag{3.45}$$

Analogously to quadrilateral elements, we can expand the indices k and l and rewrite the local hexahedron shape functions in terms of the one-dimensional element matrices as

$$
\begin{aligned}
N_{s,1}(\xi_d, \eta_e, \zeta_f) N_{t,1}(\xi_d, \eta_e, \zeta_f) &= \varphi_{p,1}(\xi_d)\varphi_q(\eta_e)\varphi_r(\zeta_f)\varphi_{a,1}(\xi_d)\varphi_b(\eta_e)\varphi_c(\zeta_f) \\
&= K_{pa}^{1D}(\xi_d) M_{qb}^{1D}(\eta_e) M_{rc}^{1D}(\zeta_f), \\
N_{s,1}(\xi_d, \eta_e, \zeta_f) N_{t,2}(\xi_d, \eta_e, \zeta_f) &= \varphi_{p,1}(\xi_d)\varphi_q(\eta_e)\varphi_r(\zeta_f)\varphi_a(\xi_d)\varphi_{b,2}(\eta_e)\varphi_c(\zeta_f) \\
&= D_{pa}^{1D}(\xi_d) D_{bq}^{1D}(\eta_e) M_{rc}^{1D}(\zeta_f), \\
N_{s,1}(\xi_d, \eta_e, \zeta_f) N_{t,3}(\xi_d, \eta_e, \zeta_f) &= \varphi_{p,1}(\xi_d)\varphi_q(\eta_e)\varphi_r(\zeta_f)\varphi_a(\xi_d)\varphi_b(\eta_e)\varphi_{c,3}(\zeta_f) \\
&= D_{pa}^{1D}(\xi_d) M_{qb}^{1D}(\eta_e) D_{cr}^{1D}(\zeta_f), \\
N_{s,2}(\xi_d, \eta_e, \zeta_f) N_{t,1}(\xi_d, \eta_e, \zeta_f) &= \varphi_p(\xi_d)\varphi_{q,2}(\eta_e)\varphi_r(\zeta_f)\varphi_{a,1}(\xi_d)\varphi_b(\eta_e)\varphi_c(\zeta_f) \\
&= D_{ap}^{1D}(\xi_d) D_{qb}^{1D}(\eta_e) M_{rc}^{1D}(\zeta_f), \\
N_{s,2}(\xi_d, \eta_e, \zeta_f) N_{t,2}(\xi_d, \eta_e, \zeta_f) &= \varphi_p(\xi_d)\varphi_{q,2}(\eta_e)\varphi_r(\zeta_f)\varphi_a(\xi_d)\varphi_{b,2}(\eta_e)\varphi_c(\zeta_f) \\
&= M_{pa}^{1D}(\xi_d) K_{qb}^{1D}(\eta_e) M_{rc}^{1D}(\zeta_f), \\
N_{s,2}(\xi_d, \eta_e, \zeta_f) N_{t,3}(\xi_d, \eta_e, \zeta_f) &= \varphi_p(\xi_d)\varphi_{q,2}(\eta_e)\varphi_r(\zeta_f)\varphi_a(\xi_d)\varphi_b(\eta_e)\varphi_{c,3}(\zeta_f) \\
&= M_{pa}^{1D}(\xi_d) D_{qb}^{1D}(\eta_e) D_{cr}^{1D}(\zeta_f), \\
N_{s,3}(\xi_d, \eta_e, \zeta_f) N_{t,1}(\xi_d, \eta_e, \zeta_f) &= \varphi_p(\xi_d)\varphi_q(\eta_e)\varphi_{r,3}(\zeta_f)\varphi_{a,1}(\xi_d)\varphi_b(\eta_e)\varphi_c(\zeta_f) \\
&= D_{ap}^{1D}(\xi_d) M_{qb}^{1D}(\eta_e) D_{rc}^{1D}(\zeta_f), \\
N_{s,3}(\xi_d, \eta_e, \zeta_f) N_{t,2}(\xi_d, \eta_e, \zeta_f) &= \varphi_p(\xi_d)\varphi_q(\eta_e)\varphi_{r,3}(\zeta_f)\varphi_a(\xi_d)\varphi_{b,2}(\eta_e)\varphi_c(\zeta_f) \\
&= M_{pa}^{1D}(\xi_d) D_{bq}^{1D}(\eta_e) D_{rc}^{1D}(\zeta_f), \\
N_{s,3}(\xi_d, \eta_e, \zeta_f) N_{t,3}(\xi_d, \eta_e, \zeta_f) &= \varphi_p(\xi_d)\varphi_q(\eta_e)\varphi_{r,3}(\zeta_f)\varphi_a(\xi_d)\varphi_b(\eta_e)\varphi_{c,3}(\zeta_f) \\
&= M_{pa}^{1D}(\xi_d) M_{qb}^{1D}(\eta_e) K_{rc}^{1D}(\zeta_f).
\end{aligned} \tag{3.46}
$$

The constitutive tensor in matrix form for general linear isotropic elasticity is given by

$$
[D] = \begin{bmatrix}
C_{1111} & C_{1122} & C_{1133} & C_{1112} & C_{1113} & C_{1123} \\
C_{1122} & C_{2222} & C_{2233} & C_{2212} & C_{2213} & C_{2223} \\
C_{1133} & C_{2233} & C_{3333} & C_{3312} & C_{3313} & C_{3323} \\
C_{1112} & C_{2212} & C_{3312} & C_{1212} & C_{1213} & C_{1223} \\
C_{1113} & C_{2213} & C_{3313} & C_{1213} & C_{1313} & C_{1323} \\
C_{1123} & C_{2223} & C_{3323} & C_{1223} & C_{1323} & C_{2323}
\end{bmatrix}
$$

$$
= \begin{bmatrix}
2\mu + \lambda & \lambda & \lambda & 0 & 0 & 0 \\
\lambda & 2\mu + \lambda & \lambda & 0 & 0 & 0 \\
\lambda & \lambda & 2\mu + \lambda & 0 & 0 & 0 \\
0 & 0 & 0 & \mu & 0 & 0 \\
0 & 0 & 0 & 0 & \mu & 0 \\
0 & 0 & 0 & 0 & 0 & \mu
\end{bmatrix}. \tag{3.47}
$$

The Jacobian matrix is calculated using the same tensorization procedure. The general expression is given by

$$
[J]_{def} = \begin{bmatrix}
\sum_{s=1}^{n} N_{s,1}(\xi_d, \eta_e, \zeta_f)X_s & \sum_{s=1}^{n} N_{s,1}(\xi_d, \eta_e, \zeta_f)Y_s & \sum_{s=1}^{n} N_{s,1}(\xi_d, \eta_e, \zeta_f)Z_s \\
\sum_{s=1}^{n} N_{s,2}(\xi_d, \eta_e, \zeta_f)X_s & \sum_{s=1}^{n} N_{s,2}(\xi_d, \eta_e, \zeta_f)Y_s & \sum_{s=1}^{n} N_{s,2}(\xi_d, \eta_e, \zeta_f)Z_s \\
\sum_{s=1}^{n} N_{s,3}(\xi_d, \eta_e, \zeta_f)X_s & \sum_{s=1}^{n} N_{s,3}(\xi_d, \eta_e, \zeta_f)Y_s & \sum_{s=1}^{n} N_{s,3}(\xi_d, \eta_e, \zeta_f)Z_s
\end{bmatrix}, \tag{3.48}
$$

where n is the number of element nodes/modes and X_s, Y_s, Z_s are the nodal/modal coordinates. The local shape function derivatives calculated on the integration point coordinates are written in terms of the one-dimensional shape functions as

$$
\begin{aligned}
N_{s,1}(\xi_d, \eta_e, \zeta_f) &= \varphi_{p,1}(\xi_d)\varphi_q(\eta_e)\varphi_r(\zeta_f), \\
N_{s,2}(\xi_d, \eta_e, \zeta_f) &= \varphi_p(\xi_d)\varphi_{q,2}(\eta_e)\varphi_r(\zeta_f), \\
N_{s,3}(\xi_d, \eta_e, \zeta_f) &= \varphi_p(\xi_d)\varphi_q(\eta_e)\varphi_{r,3}(\zeta_f).
\end{aligned} \tag{3.49}
$$

In the case of non-distorted elements, the Jacobian matrix is diagonal, given by

$$
[J]_{def} = \begin{bmatrix}
\sum_{s=1}^{n} N_{s,1}(\xi_d, \eta_e, \zeta_f)X_s & 0 & 0 \\
0 & \sum_{s=1}^{n} N_{s,2}(\xi_d, \eta_e, \zeta_f)Y_s & 0 \\
0 & 0 & \sum_{s=1}^{n} N_{s,3}(\xi_d, \eta_e, \zeta_f)Z_s
\end{bmatrix}, \tag{3.50}
$$

Notice that the Jacobian matrix is not written in terms of the one-dimensional matrices. This is because the Jacobian operator has only one shape function derivative operator $N_{s,m}$.

3.4   Numerical Examples

3.4.1   1D matrices procedure benchmarks

The purpose here is to show the speedup obtained using the 1D matrices procedure compared to the standard one. We implemented the procedure in the C++ high-order finite element code $(hp)^2$FEM and computed the runtime ratio to calculate the element matrices.

We measured the calculation time of the stiffness matrix for plane stress/strain (quadrilaterals), axisymmetric (quadrilaterals) and 3D elasticity (hexahedra) problems with the increase of the element order. The number of time measurements was taken according to the number of elements of the mesh: 9 for plane stress/strain, 8 for axisymmetric, and 8 for solid. This procedure was performed for distorted and non-distorted meshes.

Fig.3.2 shows the time ratio between the standard and the 1D procedures for the stiffness matrices with distorted elements. Notice that the overall time ratio is in the range of 2-3. The calculation of quadrilateral elements with the 1D matrices procedure was about 2 times faster and for hexahedrical elements it was approximately 2.5 times faster.

The results for non-distorted elements are shown in Fig.3.3. The very high time ratio is because the Jacobian matrix is constant for all integration points. Therefore, we can sum up the one-dimensional matrices calculated for all integration points, and use the resulting matrix to perform the tensor product procedure by only indexing the shape function indices, and without the summation on the integration points of Eq.(3.33). The same implementation cannot be performed for the standard procedure, because the matrix $[B]$ with global derivatives is not constant, as the local derivatives change with the integration point coordinates. Also, when implementing the explicit expressions, we excluded the inverse Jacobian matrix terms j_{12} and j_{21}, since they are zero for non-distorted meshes (see Eq.3.50). We did not show the results for non-distorted meshes in axisymmetric problems, since the radial coordinate r must be calculated for each integration point. Therefore, it would be necessary to loop all integration points, and this would make the above
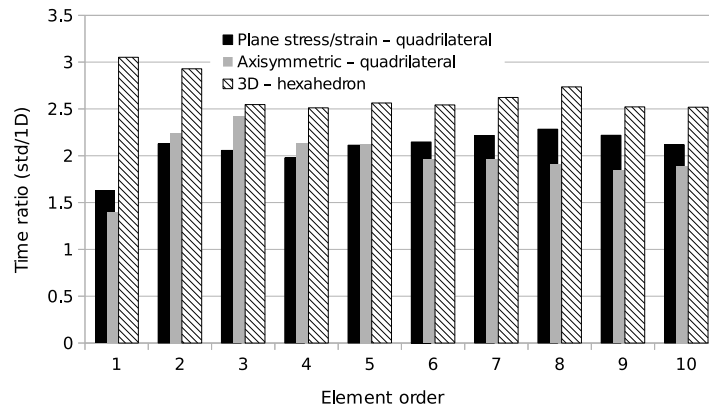
Figure 3.2: Mean time ratio between the standard and 1D matrices procedures to calculate the element stiffness matrix for distorted meshes. The average time ratio values are approximately 2.5 for hexahedra and 2 for quadrilaterals, without much variation for different element orders.

procedure troublesome to implement, possibly without significant speed up.
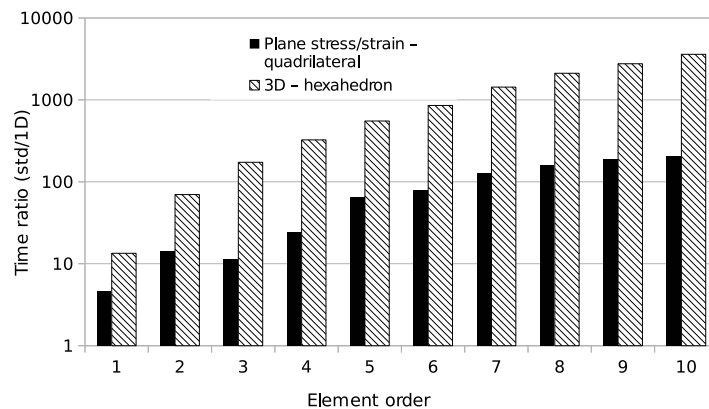
Figure 3.3: Mean time ratio in logarithmic scale between the standard and 1D matrices procedures to calculated the element stiffness matrix for undistorted meshes. The time ratio reache values of 300 for quadrilateral and 4000 for hexahedrical elements.

The time ratio measurements for the mass matrix were also performed for two- and three-dimensional problems, using meshes with 16 quadrilateral and 16 hexahedrical elements. Figs. 3.4 and 3.5 respectively show the results for distorted and undistorted element meshes. Note the increasing time ratio with the element order for hexahedra.

We measured the memory consumption of the class that calculates the shape functions and their derivatives and the class that allocates the entire finite element model. The shape function class has a high memory consumption in high-order FE codes, since the number of shape functions
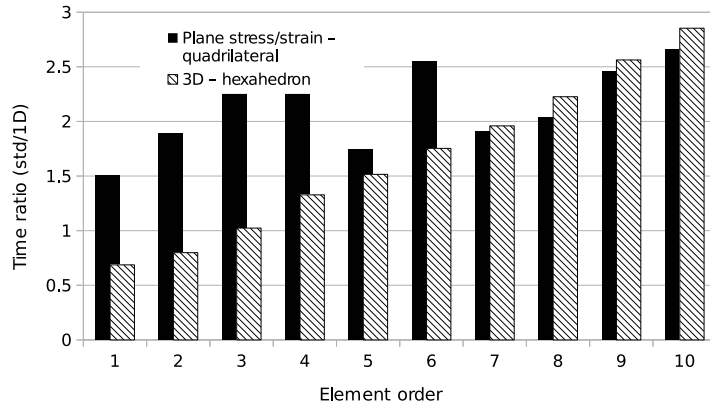
Figure 3.4: Mean time ratio between the standard and 1D matrices procedures to calculate the element mass matrix for distorted meshes. The ratio ranges from 1.5 to 2.5 for quadrilaterals and 0.7 to 2.8 for hexahedrical elements. Notice that different to the stiffness matrix for distorted elements, the ratio increases with the element interpolation order.
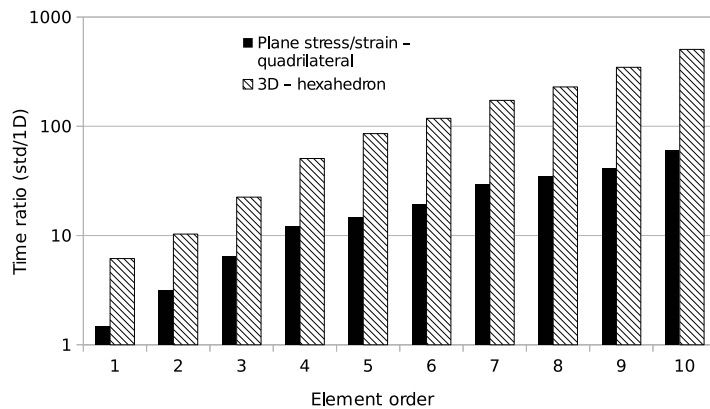
Figure 3.5: Mean time ratio between the standard and 1D matrices procedures to calculate the element mass matrix for non-distorted element meshes. The ratio reaches 60 for quadrilaterals and 500 for hexahedra.

and their derivatives, as well as the number of integration points greatly increase with the element interpolation order.

For a projection problem with 32 hexahedrical elements of interpolation order $P = 13$, the class with shape functions represents 44.87% (1.629 Gigabytes) of the total memory allocated by the entire FE model for the standard procedure. The 1D matrices procedure reduced this allocation to 0.02% (0.4 Megabytes), representing 4019 times less memory consumption. The class with the FE model had a reduction from 3.6 Gigabytes to 2.1 Gigabytes, representing a total reduction of 43% in memory allocation.

3.4.2 Simultaneously diagonal and minimum energy bases

In this section we present the numerical efficiency of the minimum energy basis applied to three-dimensional linear elastic dynamic problems integrated with the Newmark method. Consider the following definition for the energy norm:

$$\|\mathbf{u}^t\|_E^2 = \int_\Omega \mathbf{E}(\mathbf{u}^t) : \mathbf{T}(\mathbf{u}^t) d\Omega, \tag{3.51}$$

where $\mathbf{u}^t$ is the analytic solution for time t, $\mathbf{E}$ the infinitesimal strain tensor and $\mathbf{T}$ the Cauchy stress tensor. The relative error in the energy norm is calculated as

$$\|e_{rel}\|_E^2 = \frac{\|\mathbf{u}^t\|_E^2 - \|\mathbf{u}_{app}^t\|_E^2}{\|\mathbf{u}^t\|_E^2} \tag{3.52}$$

with the energy norm of the approximated solution $\mathbf{u}_{app}^t$ at time t given by

$$\|\mathbf{u}_{app}^t\|_E^2 = \{U^t\}^T \left[\hat{K}\right] \{U^t\}.$$

The errors in the L_2 and L_∞ norms are respectively

$$\|e\|_{L_2}^2 = \int_\Omega \left(\mathbf{u}^t - \mathbf{u}_{app}^t\right)^2 d\Omega, \tag{3.53}$$

$$\|e\|_{L_\infty} = max|\mathbf{u}^t - \mathbf{u}_{app}^t|. \tag{3.54}$$

We use the conjugate gradient method to solve the linear systems of equations with tolerance 10^{-11} after applying the Schur complement (Axelsson, 1994). The numerical conditioning of the effective stiffness matrix and the number of iterations are analyzed.
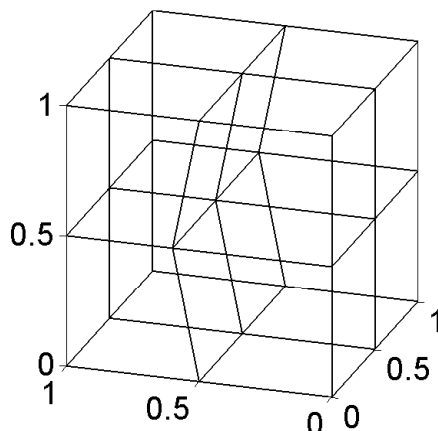
Figure 3.6: Distorted mesh for $3D$ linear elasticity.

Consider the domain $\Omega = [0,1] \times [0,1] \times [0,1]$ discretized with 8 elements as shown in Fig.3.6, with material properties $E = 1 \ [UF]/[UL]^2$, $\rho = 1 \ [UM]/[UL]^3$ and $\nu = 0.3$, where UF, UL and UM respectively indicate units of force, units of length and units of mass. We use the following fabricated solution for the displacement field:

$$
\begin{aligned}
u_x(\mathbf{x},t) &= 10^{-4} x^4 \sin(2\pi t), \\
u_y(\mathbf{x},t) &= 0, \\
u_z(\mathbf{x},t) &= 0.
\end{aligned}
\tag{3.55}
$$

The face at $x = 0$ is clamped and the following surface tractions are applied on the other faces

$$
\begin{aligned}
t_x(\mathbf{x},t) &= 7x^3 n_x \sin(2\pi t)\frac{1}{13}, \\
t_y(\mathbf{x},t) &= 3x^3 n_y \sin(2\pi t)\frac{1}{13}, \\
t_z(\mathbf{x},t) &= 3x^3 n_z \sin(2\pi t)\frac{1}{13},
\end{aligned}
\tag{3.56}
$$

70

where $\mathbf{n} = [n_x, n_y, n_z]^T$ is the normal vector. The respective body force field is given by

$$
\begin{aligned}
f_x(\mathbf{x},t) &= -\sin(2\pi t)\left(\frac{\pi^2 x^4}{2500} + \frac{21}{13}x^2\right), \\
f_y(\mathbf{x},t) &= 0, \\
f_z(\mathbf{x},t) &= 0.
\end{aligned}
\tag{3.57}
$$

The initial condition in terms of displacement is $\mathbf{u}(\mathbf{x},t) = [0,0,0]^T$. The initial velocities are given by

$$
\begin{aligned}
\dot{u}_x(\mathbf{x},0) &= \frac{\pi x^4}{5000}\cos(2\pi t), \\
\dot{u}_y(\mathbf{x},0) &= 0, \\
\dot{u}_z(\mathbf{x},0) &= 0.
\end{aligned}
$$

We investigated the spatial convergence rate by varying the element order P using the standard (ST) and simultaneously diagonal and minimum energy (SDME) bases with $\left[\alpha^{\hat{K}}\right]$ and $\lambda = 1$. The convergence of the approximated energy norm in terms of the polynomial order is illustrated in Fig. 3.7(a). The exponential convergence rates of the relative error in the energy norm is shown in Fig. 3.7(b). We considered four possibilities: the standard basis with diagonal preconditioner (DP-ST), the simultaneously diagonal and minimum energy basis with diagonal precontitioner (DP-SDME), the standard basis with symmetric successive over relaxation preconditioner (SSOR-ST) and SDME basis with symmetric successive over relaxation preconditioner (SSOR-SDME) (Axelsson, 1994), with relaxation parameter $\omega = 1$. Fig. 3.8(a) shows the L_2 and L_∞ error norms for displacement components in terms of the polynomial order to the time interval $[t_0; t_f] = [0; 0.25]$ and 30 time steps. There is an exponential convergence rate for the error as the element order increases. Also note that when $P = 5$, the convergence rate does not change, since we have achieved the order of the analytical solution defined in Eq.(3.55). Fig.3.8(b) shows the quadratic convergence rate for the Newmark method with $P = 4$.

Fig.3.9 shows the sparsity profiles of the Schur-complemented global effective stiffness matrices with element order $P = 4$ obtained with the standard, SDME basis with $\left[\alpha^{\hat{K}}\right]$ and SDME basis with $\left[\alpha^M\right]$. The sparsity profile of the SDME basis with $\left[\alpha^{\hat{K}}\right]$ is slightly different from that of the standard basis. Note that the profile with SDME contains a smaller number of non-zeros (nz) than the standard basis. The number of non-zeros was smaller when using the SDME basis with
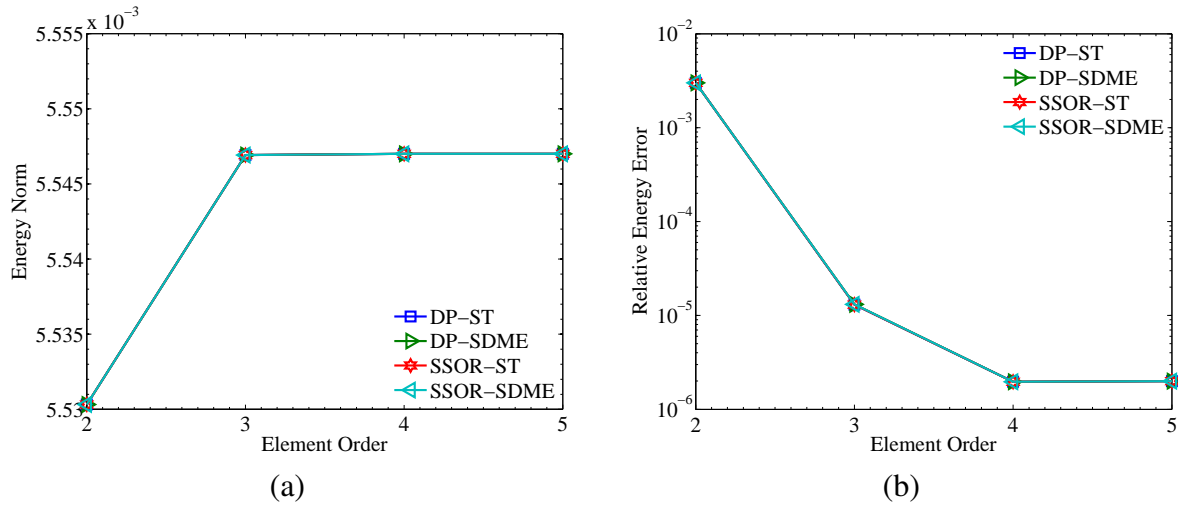
Figure 3.7: Convergence of the energy norm (a) with ST and SDME bases with $\left[\alpha^{\hat{K}}\right]$ and $\lambda = 1$ in terms of the element order with 30 time steps. Convergence rates of the relative energy error norm (b) in terms of the element order.
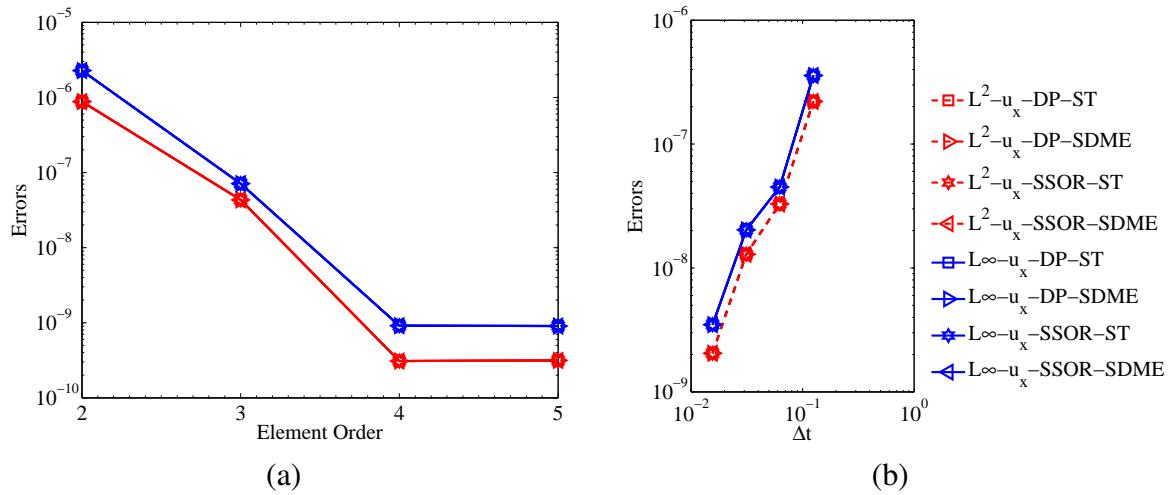
Figure 3.8: Exponential convergence rates of the error for L_2 and L_∞ norms with ST and SDME bases with $\left[\alpha^{\hat{K}}\right]$ and $\lambda = 1$ in terms of the element order with 30 time steps (a) and quadratic convergence rate of the error in terms of Δt with $P = 4$ (b).

$\left[\alpha^M\right]$.

(a)   (b)   (c)
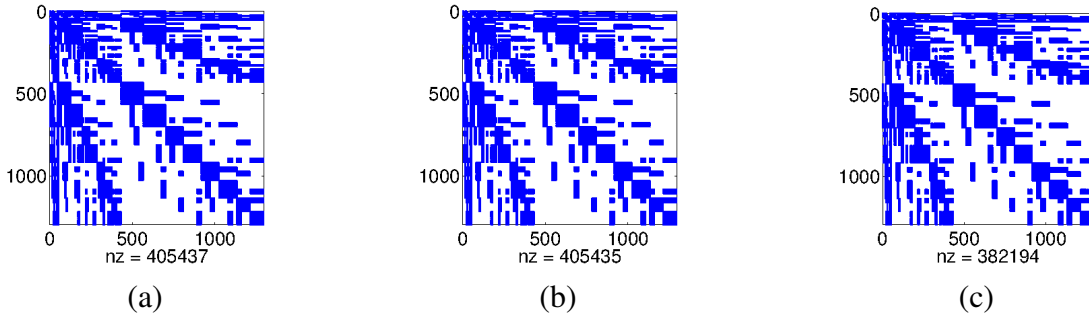
Figure 3.9: Sparsity profiles of the global effective stiffness matrices for $P = 4$ using the standard basis (a), SDME basis with $\left[\alpha^{\hat{K}}\right]$ with $\lambda = 1$ (b), SDME basis with $\left[\alpha^M\right]$ (c).

Fig.3.10 shows the total number of iterations for all time steps in terms of Δt with $P = 4$. For comparison, the number of iterations using the standard basis is considered. The total number of iterations is computed as the sum of the number os iterations for each time step. Consequently the number of iterations decreases when of the time step size is increased. We observed that the SDME basis has a superior numerical efficiency. The conjugate gradient algorithm using the SSOR preconditioner had the smallest number of iterations compared to all other cases.
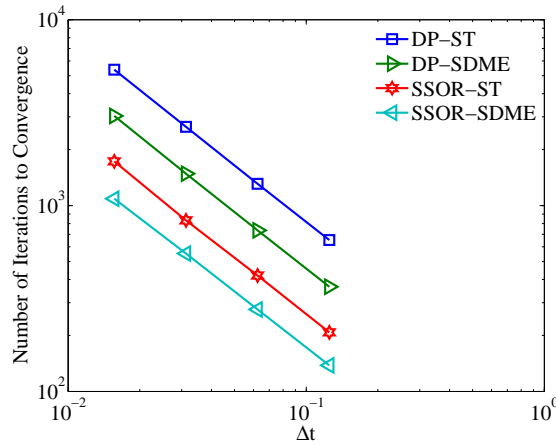
Figure 3.10: Number of iterations in terms of the time step size with $P = 4$ for the standard and SDME basis with $\left[\alpha^{\hat{K}}\right]$ and $\lambda = 1$, using the diagonal and symmetric successive over relaxation (SSOR) preconditioners.

Next, we consider at the condition number and number of iterations in terms of the polynomial order. We used 30 time steps and increased the element order. Fig. 3.11(a) illustrates the

condition number. Notice that the condition numbers for the standard basis are larger than using the SDME basis by two orders of magnitude, for both diagonal and SSOR preconditioners. Also notice that the condition number with the diagonal preconditioner for the SDME basis was lower even when compared to the standard basis using the SSOR preconditioner.

Figure 3.11: Condition number of the effective stiffness matrix (a) and number of iterations (b) using standard and SDME bases with $\left[\alpha^{\hat{K}}\right]$ with $\lambda = 1$ in terms of the element order with diagonal and SSOR preconditioners and 30 time steps.

Fig. 3.11(b) shows the number of iterations in terms of the element order. Notice that the SDME basis required less iterations than the standard basis for all element orders. For $P = 4$, there was an average of 369 iterations using the diagonal preconditioner for the standard basis. This number lowered to 202 when using the same preconditioner for the SDME basis, representing a reduction of approximately 45%. The same behavior is observed when comparing both bases with the SSOR preconditioner. In this case, the reduction in the number of iterations was approximately 39%. The use of SSOR preconditioner for the SDME bases reduction the number of iterations of the 202 to 74 for $P = 4$. This represent the improvement of the 63%.

3.4.3 Analysis of the λ-parameter

As shown in Eq. (3.12), the construction of the SDME basis with $\left[\alpha^{\hat{K}}\right]$ involves the choice of the parameter λ and until now we have used $\lambda = 1$. Now we investigate the influence of λ in the numerical conditioning of the effective stiffness matrix and the number of iterations to convergence.

We consider the same previous problem with $P = 4$ and 30 time steps and calculate the condition number of the effective stiffness matrix using the diagonal preconditioner. Notice in Fig.3.12(a) that there is a value of λ that yields a minimum condition number. Values of λ close to 100 resulted in a better conditioned matrix. This choice results in a decrease in the number of iterations required for convergence as shown in Fig. 3.12(b). The reduction in the number of interations for $\lambda = 100$ was nearly 88% when compared to $\lambda = 0.1$. Note also that the further increase of λ results in the increase of the condition number and number of iterations. For $\lambda = 1000$, we observed an increase in the number of iterations of nearly 25% when compared to $\lambda = 100$.
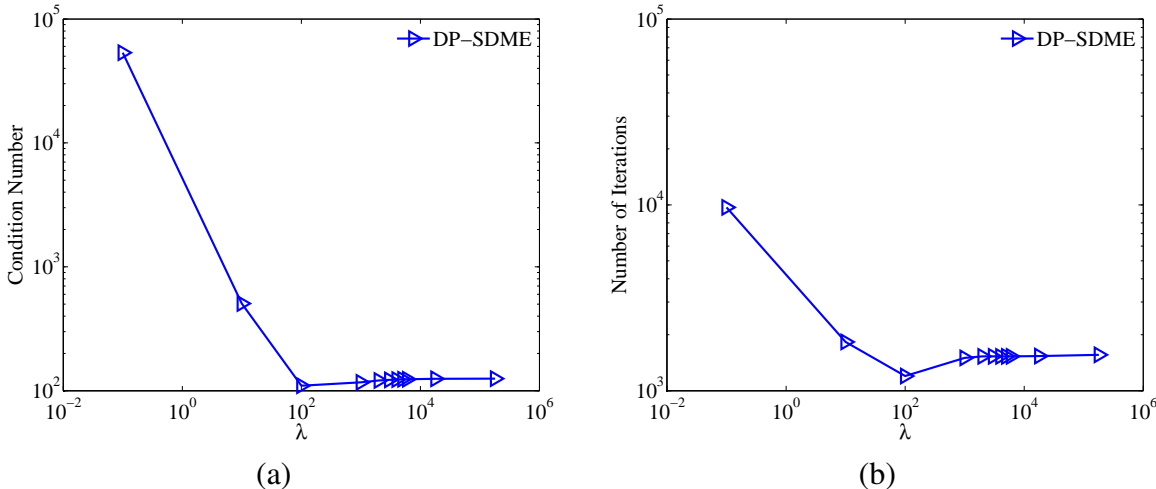
Figure 3.12: Condition number (a) and number of iterations (b) of the effective stiffness matrix in terms of λ with $P = 4$, 30 time steps, using the SDME basis with the diagonal preconditioner.

This behavior is significant when analyzing the influence of λ in terms of the polynomial order. Now we investigate an arbitrary choice of $\lambda = [0.1, 1, 100, 1000]$ for different polynomial orders. Fig.3.13(a) shows that the choice of $\lambda = 100$ or $\lambda = 1000$ makes the condition number of the effective stiffness matrix nearly constant. This value is significantly lower when compared with the standard basis. The choice of the $\lambda = 100$ is better than $\lambda = 1$ even for the SDME basis with $\left[\alpha^{\hat{K}}\right]$. This result influences the number of iterations as shown in Fig.3.13(b). For $\lambda = 1000$ and $P = 4$, we observed that the reduction in the number of iterations is approximately 86% compared to the standard basis. For $\lambda = 100$ this reduction is even larger, nearly 89%. These results suggest a stronger influence of the mass matrix on the conditioning reduction of the effective stiffness matrix when constructing the SDME basis. In fact, the higher the value of λ, the greater the contribution of the mass matrix to the conditioning.
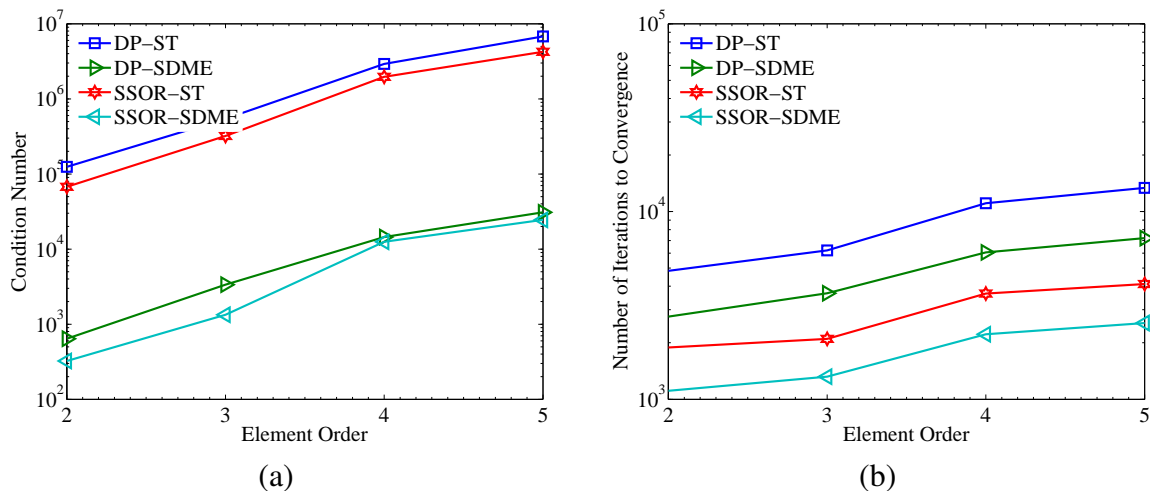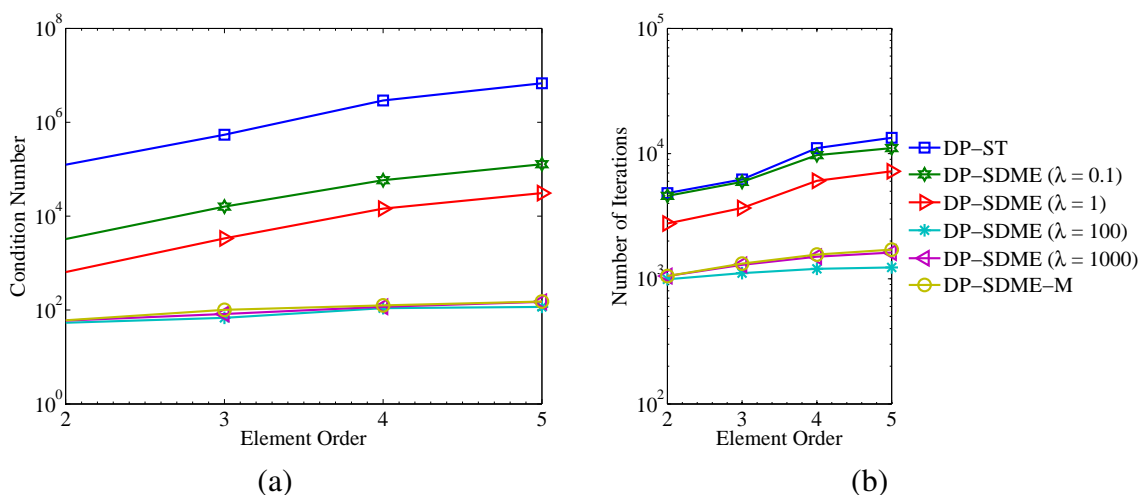
Figure 3.13: Condition number of the effective stiffness matrix (a) and number of iterations (b) for SDME basis with $\left[\alpha^{\hat{K}}\right]$ and $\left[\alpha^{M}\right]$ in terms of P. 30 time steps and $\lambda = [0.1, 1, 100, 1000]$ was used with diagonal preconditioner.

Fig.3.13 shows also the behavior of the condition number and the number of iterations in terms of the polynomial order to compare the construction of the SDME basis using $\left[\alpha^{M}\right]$ and $\left[\alpha^{\hat{K}}\right]$. The condition number of the effective stiffness matrix using SDME with $\left[\alpha^{M}\right]$ is nearly constant when compared to the SDME basis with $\left[\alpha^{\hat{K}}\right]$ and $\lambda = 1$. Similar results are observed for the number of iterations in Fig. 3.13(b). For $P = 5$, the reduction in the number of iterations with the SDME basis with $\left[\alpha^{M}\right]$ is approximately 76% compared to the SDME basis with $\left[\alpha^{\hat{K}}\right]$ and $\lambda = 1$. But the number of iterations obtained with SDME basis with $\left[\alpha^{\hat{K}}\right]$ and $\lambda = 100$ is smaller than obtained using SDME basis with $\left[\alpha^{M}\right]$, for the range considered for P. This reduction reaches 28% for $P = 5$.

We observed a similar behavior when using the undistorted mesh illustrated in Fig.3.14. The sparsity profile of the global effective stiffness matrix is illustrated in Fig.3.15 after applying the Schur-complement for the undistorted mesh. The results for the standard basis and SDME basis with $\left[\alpha^{M}\right]$ are respectively shown in Figs.3.15(a) and 3.15(c). In this case, despite the similar sparsity profiles, the number of non-zeros of the standard basis is smaller than the SDME basis with $\left[\alpha^{\hat{K}}\right]$ with $\lambda = 1$ as illustrated in Fig. 3.15(b). The SDME basis with $\left[\alpha^{M}\right]$ provided a significant reduction in the number of zeros and lower than the standard basis.

The results for the condition number and number of iterations in terms of the polynomial
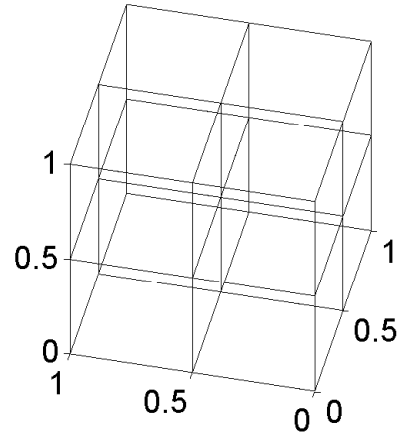
Figure 3.14: Undistorted mesh for $3D$ linear elasticity.

(a)

(b)

(c)
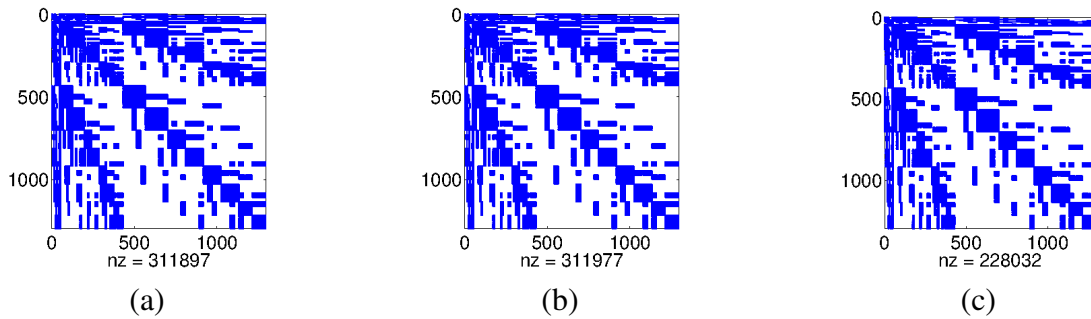
Figure 3.15: Sparsity profiles of the global effective stiffness matrices using the standard basis (a), SDME basis with $\left[\alpha^{\hat{K}}\right]$ with $\lambda = 1$ (b), ME basis with $\left[\alpha^{M}\right]$ (c). Interpolation order is $P = 4$ using the undistorted mesh.
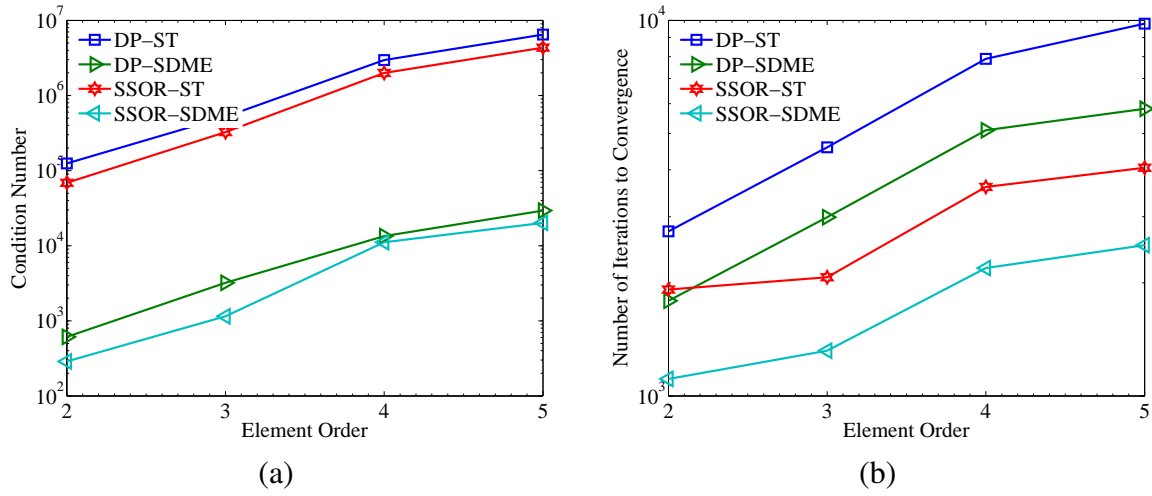
Figure 3.16: Condition number of the effective stiffness matrix (a) and number of iterations (b) with standard and SDME bases with $\left[\alpha^{\hat{K}}\right]$ and $\lambda = 1$ in terms of the polynomial order using the diagonal and SSOR preconditioners with 30 time steps, undistorted mesh.

order are respectively illustrated in Figs.3.16(a) and 3.16(b). Notice the lower values obtained with the SDME basis for the range of P used. For $P = 4$, the preconditioned standard basis has an average number of 263 iterations per time step, while the preconditioned SDME basis has an average of 170 iterations, representing a 35% reduction. A similar behavior is observed using the SSOR preconditioner, with a reduction of approximately 39% in the number of iterations.

We performed the same analysis with the preconditioned SDME bases using $\left[\alpha^{M}\right]$ and $\left[\alpha^{\hat{K}}\right]$ with $\lambda = 1$ and $\lambda = 100$. Similar to distorted meshes, the condition number using the SDME basis with $\left[\alpha^{M}\right]$ is almost constant for the range of P used, as illustrated in Fig.3.17(a). Likewise, we found that the number of iterations is lower than the SDME basis with $\left[\alpha^{\hat{K}}\right]$ and $\lambda = 1$, as shown in Fig. 3.17(b). For $P = 5$ the reduction in the number of iterations was approximately 74% compared to the SDME basis with $\left[\alpha^{\hat{K}}\right]$ with $\lambda = 1$. But when $\lambda = 100$ the condition number and the number of iterations is smaller than presented with SDME basis with $\left[\alpha^{M}\right]$. For all range of P analysed, the number of iterations using the standard basis was higher than the SDME bases.
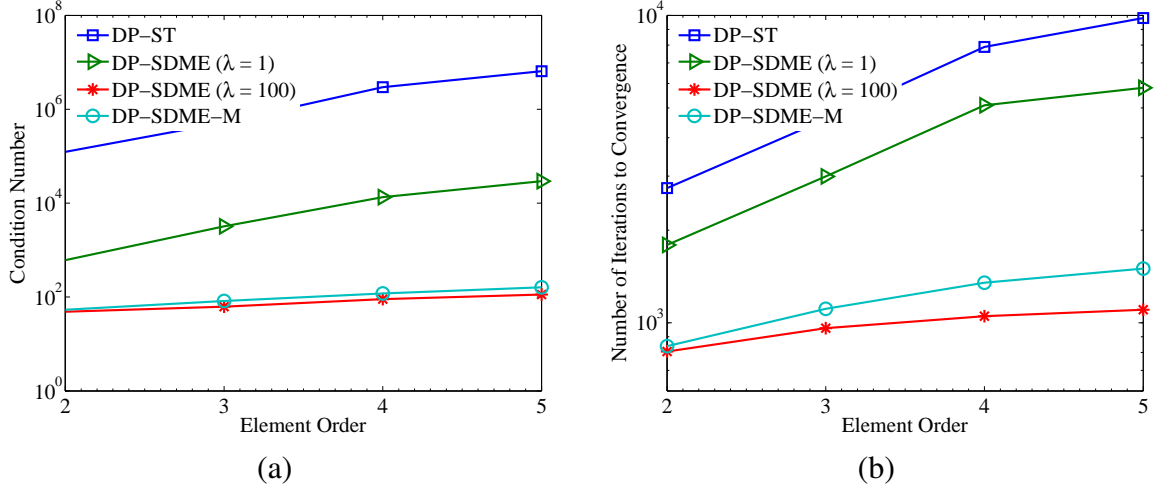
Figure 3.17: Condition number of the effective stiffness matrix (a) and number of iterations (b) with the standard and SDME bases with $\left[\alpha^{\hat{K}}\right]$ and $\left[\alpha^{M}\right]$ in terms of the polynomial order with 30 time steps, using the diagonal preconditioner and the undistorted mesh.

3.4.4 Minimum Energy Local Mass Preconditioner

We have used the the diagonal and SSOR preconditioners in the CG method. For a general preconditioning matrix $[P]$, we replace the original system of equation in Eq.(3.8) by

$$[P]^{-1}\left[\hat{K}\right]\left\{U^{t+\Delta t}\right\} = [P]^{-1}\left[\hat{R}^{t+\Delta t}\right]. \tag{3.58}$$

We will now investigate the numerical efficiency using the undistorted local mass matrix obtained with the SDME basis as the preconditioner. First we do not consider the Jacobian and the preconditioner matrix $[P]$ is given by the assembly of the local mass matrices as

$$[P] = a_0 \bigcup_{e=1}^{nel} [M_L]_e , \tag{3.59}$$

where a_0 is a Newmark constant and $[M_L]$ is the local undistorted mass matrix. The second preconditioned matrix uses the average Jacobian for each element and assembles the global matrix as

$$[P] = a_0 \bigcup_{e=1}^{nel} [M_{av}]_e \, . \tag{3.60}$$

This choice is interesting since the sparsity profile of the local mass matrix after Schur complement is very sparse. Fig. 3.18(a) shows the sparsity profile of the preconditioner mass matrix using $[\alpha^M]$ with polynomial order $P = 4$ for the all elements of the mesh of the Fig. 3.6. Fig. 3.18(b) shows the sparsity profile of the inverse preconditioner mass matrix. In this case, we observed that the local preconditioner mass matrix using $[\alpha^M]$ is very sparse. When using the average Jacobian in the construction of preconditioner, the sparsity profile is similar to the local preconditioner mass without average Jacobian.

(a) (b)
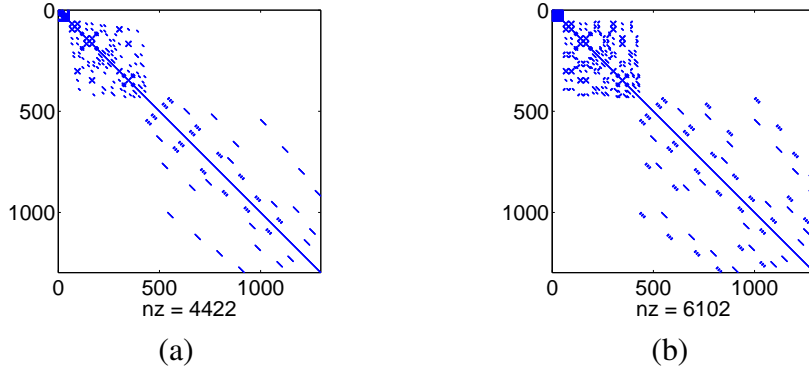
Figure 3.18: Sparsity profile of the preconditioner global mass matrix using $[\alpha^M]$ without consider the Jacobian (a), and the inverse preconditioner global mass matrix (b).

We can verify the influence of λ in the sparsity profile of the local mass matrix using $[\alpha^{\hat{K}}]$. Fig. 3.19 illustrates the number of non-zeros (nz) in terms of λ using the preconditioner local mass matrix, its inverse, and the effective stiffness matrix with and without preconditioning. Notice that the number of non-zeros reduces with increasing λ and consequently a better sparsity profile of $[P]$. When the order of magnitude of λ gets closer to the tolerance used to construct the matrices, the sparsity of $[P]$ increases. Fig. 3.19 shows that the sparsity of $[P]^{-1} \hat{K}$ was nearly constant for $\lambda < 10^{10}$.

We perform the tests for the problem of the previous sections using the same mesh, number of time steps, and analyze the condition number and number of iterations in terms of the polynomial order using the preconditioners defined in Eqs.(3.59) and (3.60) after applying the Schur complement to the effective stiffness matrix.
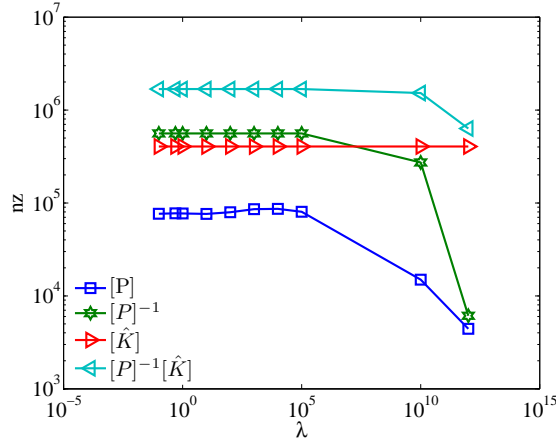
Figure 3.19: Number of the non-zeros in terms of λ for effective stiffness and preconditioner matrices.

Fig. 3.20 shows the results for the effective stiffness matrix for the SDME basis using $\left[\alpha^{\hat{K}}\right]$ with $\lambda = 1$ and $\lambda = 100$ and the standard basis. We considered diagonal and SSOR preconditioners and included the results using the local mass preconditioner (LP-SDME) and the local mass preconditioner with average Jacobian (LP-SDME$_{av}$). Notice that the condition number using the local mass matrix as preconditioner with the SDME basis is smaller than the using the standard basis with diagonal and SSOR preconditioners. Likewise the number of iterations was smaller when compared to the standard basis.

Fig. 3.21 shows the results using the local diagonal mass preconditioner with $\left[\alpha^{\hat{K}}\right]$ and $\lambda = 100$. For comparison, we also consider the results using the local mass preconditioner. In this case, the condition number of the effective stiffness matrix has a similar behavior to both preconditioners. However, there is a slight reduction in the number of iterations when using the local diagonal mass preconditioner, compared to the local mass preconditioner.

Fig. 3.22 shows the condition number and number of iterations of the effective stiffness matrix using the SDME with $\left[\alpha^{M}\right]$. The results with the standard basis are also included. The condition number obtained with LP-SDME-M and LP-SDME-M$_{av}$ is smaller than the standard cases with diagonal and SSOR preconditioner. However, the results obtained are larger than the ones obtained with diagonal and SSOR preconditioners for the SDME basis, as show in Fig. 3.22(a). Fig. 3.22(b) shows similar behavior to number of iterations when using LP-SDME-M and LP-SDME-M$_{av}$. Similarly, we find that the number of iterations is smaller when we use the diagonal or SSOR preconditioners.
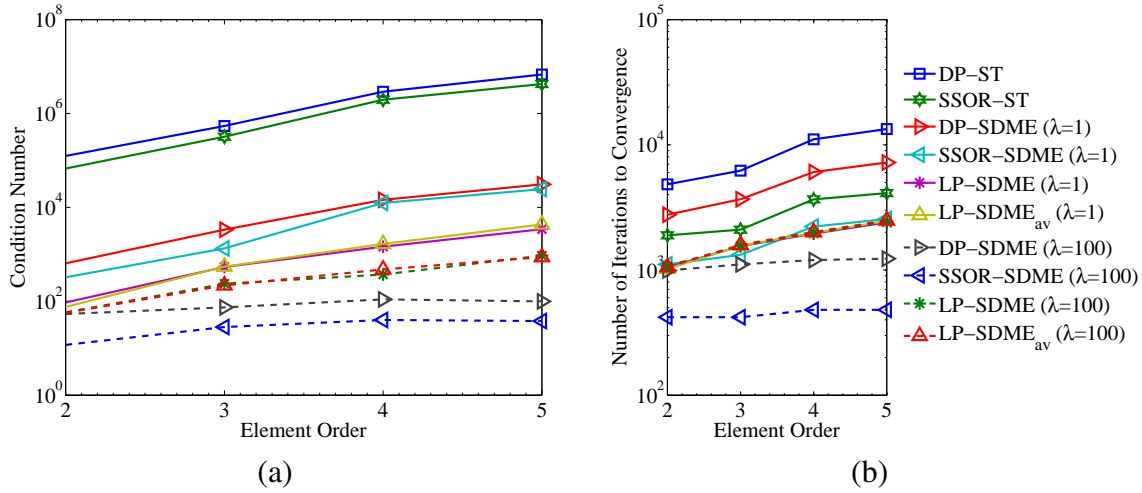
Figure 3.20: Condition number of the effective stiffness matrix (a) and number of iterations (b) using standard and SDME basis with $\left[\alpha^{\hat{K}}\right]$ and $\lambda = 1$ and $\lambda = 100$. Diagonal, SSOR, local mass and local mass matrix with average Jacobian preconditioners are considered. We used undistorted mesh and 30 time steps.

Figure 3.21: Condition number of the effective stiffness matrix (a) and number of iterations (b) using the standard and SDME bases with $\left[\alpha^{\hat{K}}\right]$ with $\lambda = 100$. Diagonal, SSOR, local mass and local diagonal mass matrix preconditioners, with and without average Jacobian, are considered. We used undistorted mesh and 30 time steps.
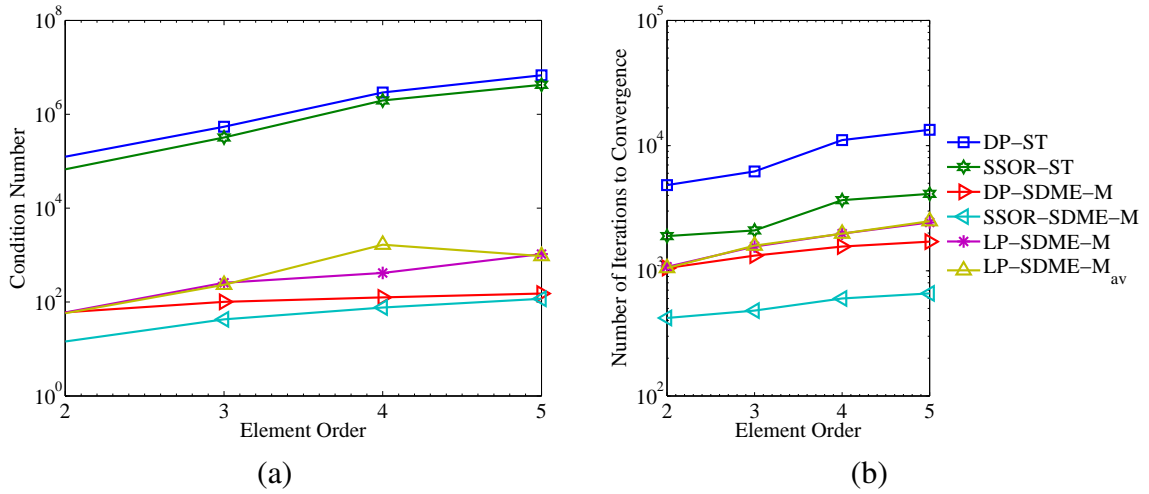
Figure 3.22: Condition number of the effective stiffness matrix (a) and number of iterations (b) with standard and SDME basis with $[\alpha^M]$ using diagonal, SSOR, local mass and local mass with average Jacobian preconditioners in terms of the polynomial order with 30 time steps, undistorted mesh.

Fig. 3.23 shows the results using the local lumped mass preconditioner with $[\alpha^M]$. We also show the results using the local mass preconditioner for comparison. Notice that the condition number using the lumped preconditioner was lower than the full preconditioner for the range of considered polynomial orders. The number of iterations for both preconditioners showed a similar behavior. This suggests that the use of the lumped diagonal preconditioner can be an appropriate choice when using the SDME basis with $[\alpha^M]$.

We observe that the local mass preconditioner using $[\alpha^M]$ or $[\alpha^{\hat{K}}]$ is an alternative as preconditioner for SDME bases. The sparsity patterns of the local mass preconditioners with $[\alpha^M]$ have a smaller number of the non-zeros coefficients nz, when comparing with use of the $[\alpha^{\hat{K}}]$, for any choice of the λ. We obtained good results with the diagonal local mass preconditioner with $[\alpha^{\hat{K}}]$ and $\lambda = 100$. The lumped local mass preconditioner was more interesting with $[\alpha^M]$.

3.4.5 Application

In the previous sections we applied the proposed bases to a fabricated smooth solution. Now we consider a larger problem with a complex geometry. Consider the conrod of an internal com-
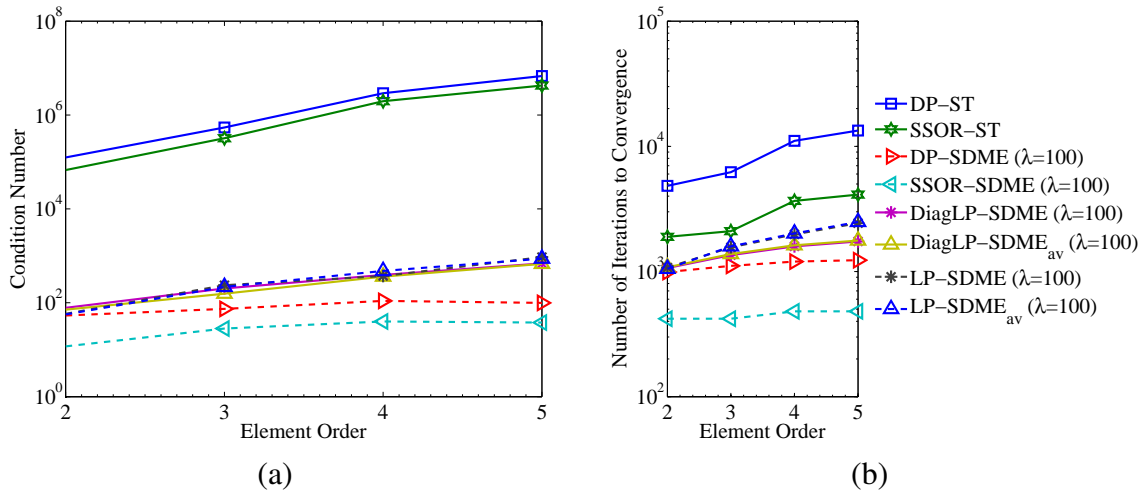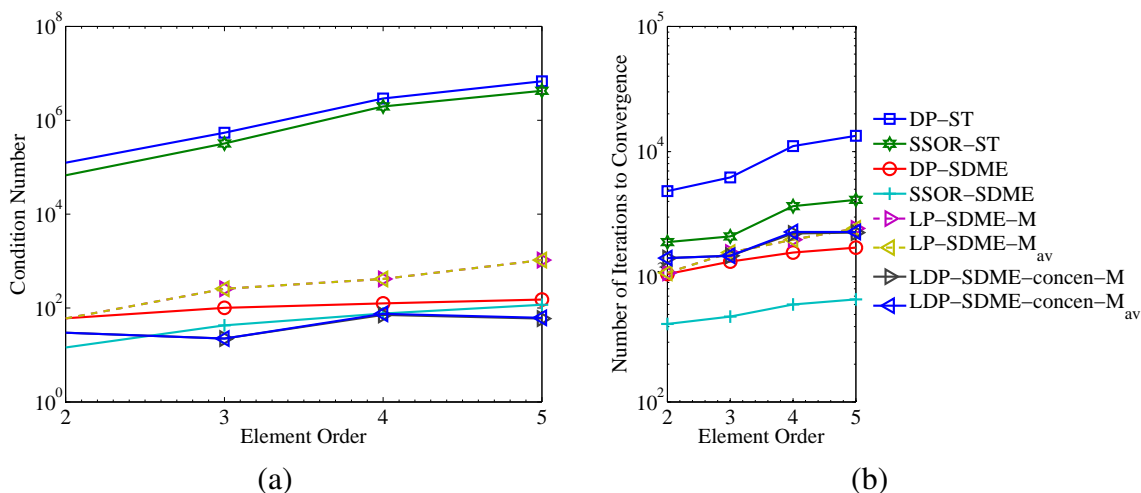
Figure 3.23: Condition number of the effective stiffness matrix (a) and number of iterations (b) with standard and minimum energy basis using $\left[\alpha^M\right]$. We considered diagonal, SSOR, local mass and local diagonal concentrated mass preconditioners, with and without average Jacobian, in terms of the polynomial order. We used undistorted mesh and 30 time steps.

bustion engine discretized with a mesh of 768 hexahedrical elements, as shown in Fig. 3.24(a). The internal nodes of the small end are clamped while the internal nodes of the big end are subjected to surface tractions in x and y. The loads corresponds to a complete cycle and are obtained using a dynamic rigid body model for the piston-conrod-crankshaft system (Carbonara *et al.*, 2009).
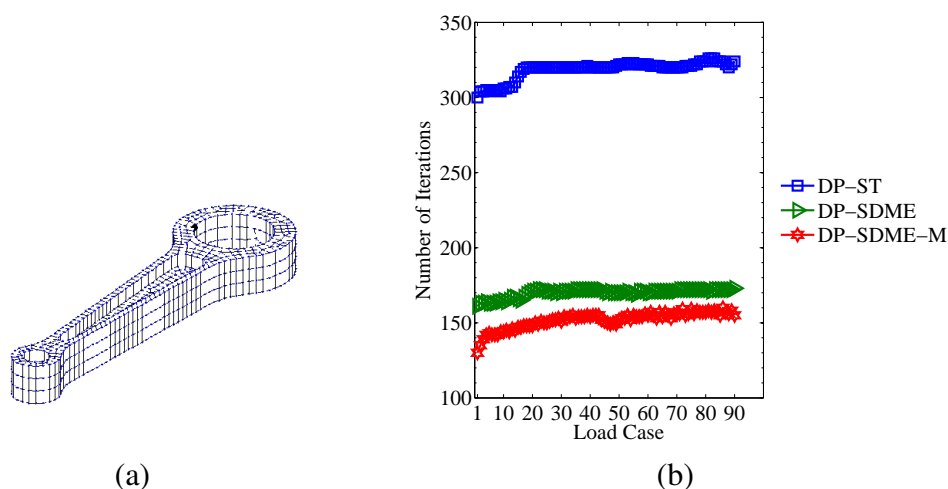
Figure 3.24: Mesh used for the conrod (a) and number of iterations per load step to standard and ME bases with $\left[\alpha^{\hat{K}}\right]$ with $\lambda = 1$ and $\left[\alpha^M\right]$ (b), and $P = 3$.

The time interval used was $[t_0; t_f] = [0; 5.454 \times 10^{-3}]$ and $\Delta t = 6.06 \times 10^{-5}$. We applied

the Schur complement to obtain the solution and used the diagonal preconditioner on the standard and SDME bases with $\left[\alpha^{\hat{K}} \right]$ and $\lambda = 1$ and also the SDME basis with $\left[\alpha^M \right]$. We computed the number of iterations for each load step with a total of 90 load steps. The results are shown in Fig.3.24(b). Notice that the numbers of iterations using the SDME bases are significantly lower than the standard basis along the load steps. The average number of iterations were 319 for the standard basis, 170 for the SDME basis with $\left[\alpha^{\hat{K}} \right]$ and 152 for the SDME basis with $\left[\alpha^M \right]$. The reduction in the number of iterations is about 46.7% between DP-ST and DP-SDME with $\left[\alpha^{\hat{K}} \right]$ and 52% between DP-ST and DP-SDME-M. This clearly demonstrates a higher numerical efficiency when using the proposed minimum energy bases.

3.5 Concluding remarks

In this paper we presented the simultaneously diagonal and minimum energy high-order expansion bases applied to transient analysis in linear elasticity using structured elements. A special construction for the one-dimensional basis functions was used. This formulation is suitable for application to dynamic problems using the Newmark method because considers use of the Helmholtz norm for minimum energy procedure. The internal modes of the one-dimensional mass and stiffness matrices are made simultaneously diagonal.

We also consider the mass norm in orthogonalization minimum energy procedure for boundary modes and compared with the use of Helmhotz norm. Numerical tests demonstrated a superior efficiency of the proposed bases in terms of number of iterations and condition number. We also observed that the use of the diagonal and SSOR preconditioners improved the numerical efficiency of the SDME bases. This makes the application of diagonal preconditioners preferable. Furthermore, the proposed bases can be efficiently preconditioned with the undistorted local mass matrix. In our tests we found advantages using this type of preconditioner, even compared to the standard diagonal preconditioner using SDME basis with $\left[\alpha^{\hat{K}} \right]$.

The use of the $1D$ matrices procedure allowed us to obtain a significant speedup ratio compared to the standard procedure, for distorted and undistorted meshes. In the case of undistorted meshes, the speedup was very high, due to a factorization of the one-dimensional element matrices. This procedure also consumes less memory for the solver, since we only need to store the one-dimensional shape functions and their derivatives calculated on one-dimensional integration

points.

We have considered in this work only structured elements. The extension to unstructured elements will be the focus of future work. Also, we also have interest on extending the $1D$ matrices procedure for nonlinear problems with large displacements and strains.

3.6 Acknowledgements

4 Conclusions

This work presented the construction of high-order bases for structured elements considering the procedure of simultaneous diagonalization for internal modes and minimum energy orthogonalization to boundary modes. The choice of the appropriate norm was used to generalize the minimum energy orthogonalization procedure. We show that, in accordance with the norm, some high-order bases proposed in the literature can be constructed considering the simultaneously diagonal of internal modes and orthogonalization of the boundary modes procedure. In addition, we proposed the use of the Helmholtz norm for construction of boundary modes with minimum energy orthogonalization. This particular basis for the one-dimensional Helmholtz problem uncoupled vertex and internal matrix blocks and is dependent of the parameter λ. For a given choice of this parameter, a smaller condition number is obtained when comparing with standard or Dong bases. Similar results are obtained for $3D$ Helmholtz problems and better efficiency in terms of the number of iterations and numerical conditioning of the global matrices compared to the standard basis.

We also showed that this special construction for the one-dimensional basis functions, using Helmholtz norm with $\left[\alpha^{H}\right]$ or $\left[\alpha^{\hat{K}}\right]$, is suitable for application to dynamic problems using the Newmark method for time integration. In transient linear elastic problems with explicit central difference methods, the use of the $\left[\alpha^{M}\right]$ is more convenient due to the use of the mass matrix in this procedure.

In projection and Poisson problems, the application of the procedure of the minimum energy with $\left[\alpha^{M}\right]$ and $\left[\alpha^{K}\right]$ is more efficient in terms of the condition number and number of iterations when compared to the standard bases. The results are similar to those ones presented in literature. We also showed that for $3D$ projection problems, the choice of the parameter $k = 0$ in the procedure of the simultaneous diagonalization can improve the number of iterations for convergence. For $3D$ Poisson problems, the use of the parameter $k = 1$ in the procedure of the simultaneous diagonalization did not improve the number of iterations for convergence because the condition number of the one-dimensional mass matrix is larger than that obtained with $k = 0$.

This work also presented the calculation of the coefficients of the $2D$ and $3D$ elemental operators as a combination of the coefficients of the $1D$ mass and stiffness matrices and the Jacobian matrix for quadrilateral and hexahedral elements in distorted domains. This procedure is interesting because consumes less memory, since we only need to store the one-dimensional shape functions

and their derivatives calculated on one-dimensional integration points. The use of the $1D$ matrices procedure allowed us to obtain a significant speedup ratio compared to the standard procedure, for distorted and undistorted meshes. In the case of undistorted meshes, the speedup was very high, due to a factorization of the one-dimensional element matrices.

We observed that the use of the diagonal and SSOR preconditioners improved the numerical efficiency of the SDME bases. Furthermore, the local mass preconditioner using $\left[\alpha^M\right]$ or $\left[\alpha^{\hat{K}}\right]$ is an alternative as preconditioner for SDME bases. The SDME bases can be efficiently preconditioned with the undistorted local mass matrix. In our tests we found advantages using this type of preconditioner, even compared to the standard diagonal preconditioner using SDME basis with $\left[\alpha^{\hat{K}}\right]$. In addition, the lumped local mass preconditioner was more interesting when we use $\left[\alpha^M\right]$.

4.1 Future work

We show that the use of the simultaneously diagonal and minimum energy basis is interesting for the considered problems. The a suggestions of work include:

○ The extension to unstructured elements.

○ Extending the $1D$ matrices procedure for nonlinear problems with large displacements and strains.

○ Consider the application of the simultaneously diagonal and minimum energy (SDME) bases for unstructured elements using local solution.

○ Analysis of performance of the preconditioners in parallel computer

○ Study and application of SDME bases in seismic modeling problems with a high degree of complexity and large number of degrees of freedom.

○ Application to contact problems.

References

ABDUL-RAHMAN, R. and KASPER, M. Higher-order triangular basis functions and solution performance of the CG method. **Comput. Methods Appl. Mech. Engrg**, v. 197, 115–127, 2007.

AUGUSTO, R. A. **Arquitetura de Software Orientada por Objetos para o Método de Elementos Finitos de Alta Ordem**. 2012. PhD Thesis. Faculdade de Engenharia Mecânica, Universidade Estadual de Campinas.

AXELSSON, O. **Iterative Solution Methods**. Cambridge University Press, 1994. Cambridge Books Online.

BABUSKA, I. and GUO, B.Q. The *h-p* version of the finite element method for problems with nonhomogeneous essential boundary condition. **Computer Methods in Applied Mechanics and Engineering**, v. 74, 1–28, 1989.

BABUSKA, I. and SURI, M. The optimal convergence rate of the p-version of the finite element method. **SIAM J. Numer. Anal.**, v. 24, 750–776, 1987.

BABUSKA, I. and SURI, M. The *p* and *h-p* versions of the finite element method, an overview. **Computer Methods in Applied Mechanics and Engineering**, v. 80, 5–26, 1990.

BABUSKA, I.; SZABÓ, B.A. and KATZ, I.N. The p-version of the finite element method. **SIAM J. Numer. Anal.**, v. 18, n. 3, 515–545, 1981.

BARGOS, F. F. **Implementação de elementos finitos de alta ordem baseado em produto tensorial**. 2009. Tese (mestrado). Faculdade de Engenharia Mecânica, Universidade Estadual de Campinas, Campinas, Brasil.

BATHE, K. **Finite Element Procedures**. Prentice Hall, Englewood Cliffs, 1996.

BESKOK, A. and WARBURTON, T.C. An unstructured hp finite-element scheme for fluid flow and heat transfer in moving domains. **Journal of Computational Physics**, v. 174, 492–509, 2001.

BEUCHLER, S. and SCHÖBERL, J. New shape functions for triangular p-fem using integrated jacobi polynomials. **Numerische Mathematik**, v. 103, 339–366, 2006.

BITTENCOURT, M. and VAZQUEZ, T. Local eigenvalue decomposition for projection problems using the high-order fem (submitted). **Journal of Computational Physics**, 2010.

BITTENCOURT, M.L.; VAZQUEZ, M.G. and VAZQUEZ, T.G. Construction of shape functions for the h- and p-versions of the fem using tensorial product. **International Journal for Numerical Methods in Engineering**, v. 71, 529–563, 2007a.

BITTENCOURT, M.L. and VAZQUEZ, T.G. Tensor-based gauss-jacobi numerical integration for high-order mass and stiffness matrices. **International journal for numerical methods in engineering**, v. 79, n. 5, 599–638, 2009.

BITTENCOURT, M.L.; VAZQUEZ, T.G. and NOGUEIRA JR, A.C. High-order finite elements applied to structural elastic problems. **Mechanics of solids in Brazil**, 2007b.

CARBONARA, A.F.; DUARTE JR, D. and BITTENCOURT, M.L. Comparison of journal orbits under hydrodynamic lubrication regime for traditional and newton-euler loads in combustion engines. **Latin American Journal of Solids and Structures**, v. 6, n. 1, 13–33, 2009.

CARNEVALI, P.; MORRIS, R.B.; TSUJI, Y. and TAYLOR, G. New basis functions and computational procedures for p-version finite element analysis. **International Journal for Numerical Methods in Engineering**, v. 36, 3759–3779, 1993.

CASARIN, M.A. Diagonal edge preconditioners in p-version and spectral element methods. **SIAM J. Sci. Comput.**, v. 18, n. 2, 610–620, 1997.

CLOUGH, R. The finite element method in plane stress analysis. **Proceedings 2nd ASCE Conference on Electronic Computation**, 1960.

CLOUGH, R.W. Thoughts about the origin of the finite element method. **Computers & Structures**, v. 79, 2029–2030, 2001.

DA COSTA, G. L. Valente. hp^2**FEM - Uma Arquitetura de *Software* p Não-Uniforme para o Método de Elementos Finitos de Alta Ordem**. 2012. Master Thesis. Faculdade de Engenharia Mecânica, Universidade Estadual de Campinas.

DEMKOWICZ, L. and VARDAPETYAN, L. Modeling of electromagnetic absorption / scattering problems using hp-adaptive finite elements. **Computer Methods in Applied Mechanics and Engineering**, v. 152, 103–124, 1998.

DONG, S. and KARNIADAKIS, G.E. Dual-level parallelism for high-order cfd methods. **Parallel Computing**, v. 30, 1–20, 2004.

DONG, S. and YOSIBASH, Z. A parallel spectral element method for dynamic three-dimensional nonlinear elasticity problems. **Computers and Structures**, v. 87, 59–72, 2009.

DONG, S. and YOSIBASHI, Z. A parallel spectral element method for dynamic three-dimensional nonlinear elasticity problems. **Computers and Structures**, v. 87, 59–72, 2009.

FURLAN, F. A. C. **Métodos Locais de Integração Explícito e Implícito aplicados ao Método de Elementos Finitos de Alta Ordem**. 2011. Master Thesis. Faculdade de Engenharia Mecânica, Universidade Estadual de Campinas.

GHARTI, H.; KOMATITSCH, D.; OYE, V.; MARTIN, R. and TROMP, J. Application of an elasto-plastic spectral-element method to 3d slope stability analysis. **International Journal for Numerical Methods in Engineering**, v. 91, n. 1, 1–26, 2012.

HEISSERER, U.; HARTMANN, S.; DÜSTER, A.; YOSIBASH, Z.; BIER, W. and RANK, E. p-

fem for finite deformation powder compaction. **Comput. Methods Appl. Mech. Engrg**, v. 197, n. 6-8, 727–740, 2008.

HUGHES, T.J.R. **The Finite Element Method: Linear Static and Dynamic Finite Element Analysis**. New York, 1987.

JOHNSON, C. **Numerical Solution of Partial Differential Equations by the Finite Element Method**. Cambridge University Press, Cambridge, 1990.

KARNIADAKIS, G.E. and SHERWIN, S.J. **Spectral/hp Element Methods for CFD**. Oxford University Press, Oxford, 1999.

KARNIADAKIS, G.E. and SHERWIN, S.J. **Spectral/hp Element Methods for Computational Fluid Dynamics**. Oxford University Press, Oxford, second edition ed., 2005.

KONYUKHOV, A. and SCHWEIZERHOF, K. Incorporation of contact for high-order finite elements in covariant form. **Computer Methods in Applied Mechanics and Engineering**, v. 198, n. 13-14, 1213–1223, 2009.

KRAUSE, R.; MUCKE, R. and RANK, E. hp-Version Finite-Elements for Geometrically Nonlinear Problems. **Communications in Numerical Methods in Engineering**, v. 11, n. 11, 887–897, NOV 1995.

LOMTEV, I.; QUILLEN, C.B. and KARNIADAKIS, G.E. Spectral/hp methods for viscous compressible flows on unstructured 2d meshes. **Journal of Computational Physics**, v. 144, 325–357, 1998.

NOELS, L.; STAINIER, L. and PONTHOT, J.P. Combined implicit/explicit algorithms for crashworthiness analysis. **International Journal of Impact Engineering**, v. 30, 1161–1177, 2004.

NOGUEIRA JR., A.C. and BITTENCOURT, M. Hierarchical basis functions for the p-version of the finite element method (in portuguese). **Revista Internacional de Métodos Numéricos para**

Cálculo y Diseño en Ingeniería, v. 17, n. 1, 37–59, 2001.

NOGUEIRA JR, A.C. and BITTENCOURT, M.L. Spectral/hp finite elements applied to linear and non-linear structural elastic problems. **Latin American Journal of Solids and Structures**, v. 4, n. 1, 61–85, 2007.

ODEN, J.; CAREY, G. and BECKER, E. **Finite Elements: An Introduction**, v. 1 of *Texas Finite Element Series*. Englewood-Cliffs, New Jersey, USA, 1981.

ODEN, J.T. Some historic comments on finite elements. **Proceedings of the ACM conference on History of scientific and numeric computation**, v. 79, 125–130, 1987.

PEANO, A. Hierarchies of conforming finite elements for plane elasticity and plate bending. **Computers and Mathematics with Applications.**, v. 2, 211–224, 1976.

SHEN, J. and WANG, L.L. Fourierization of the legendre–galerkin method and a new space–time spectral method. **Applied numerical mathematics**, v. 57, n. 5, 710–720, 2007.

SHERWIN, S.J. and KARNIADAKIS, G. A new triangular and tetrahedral basis for high-order (hp) finite element methods. **International Journal for Numerical Methods in Engineering**, v. 38, 3775–3802, 1995.

ŠOLíN, P. and VEJCHODSKÝ, T. Higher-order finite elements based on generalized eigenfunctions of the laplacian. **International journal for numerical methods in engineering**, v. 73, n. 10, 1374–1394, 2008.

SZABÓ, B. and BABUSKA, I. **Finite Element Analysis**. Wiley Interscience, New York, 1991.

TURNER, M. Stiffness and deflection analysis of complex structures. **Journal of the Aeronautical Sciences**, v. 23, 805–823, 1956.

VAZQUEZ, M. **Tensorização de matrizes de rigidez unidimensionais para quadrados e hexae-dros usando método de Elementos Finitos de Alta Ordem**. 2009. Tese (doutorado). Faculdade de Engenharia Mecânica, Universidade Estadual de Campinas, Campinas, Brasil.

VEJCHODSKỲ, T. Higher-order discrete maximum principle for 1d diffusion–reaction problems. **Applied numerical mathematics**, v. 60, n. 4, 486–500, 2010.

VIRIEUX, J.; ETIENNE, V.; CRUZ-ATIENZA, V.; BROSSIER, R.; CHALJUB, E.; COUTANT, O.; S.GARAMBOIS; D.MERCERAT; PRIEUX, V.; OPERTO, S. and ET AL. Modelling seismic wave propagation for geophysical imaging. **Seismic Waves - Research and Analysis**, Jan 2012.

VOS, P.; SHERWIN, S. and KIRBY, R. From h to p efficiently: Implementing finite and spec-tral/hp element methods to achieve optimal performance for low-and high-order discretisations. **JOURNAL OF COMPUTATIONAL PHYSICS**, v. 229, 5161–5181, 2010.

YU, Y.; BAEK, H.; BITTENCOURT, M. and KARNIADAKIS, G. Mixed spectral/hp element for-mulation for nonlinear elasticity. **Computer Methods in Applied Mechanics and Engineering**, v. 213-216, n. 0, 42 – 57, 2012.

YU, Y.; BITTENCOURT, M.L. and KARNIADAKIS, G. A semi-local spectral/hp element solver for linear elasticity problems. **Int. J. Numer. Meth. Engng**, v. 100, n. 5, 347–373, Jul 2014.

ZHENG, X. and DONG, S. An eigen-based high-order expansion basis for structured spectral elements. **Journal of Computational Physics**, v. 230, n. 23, 8573–8602, 2011.

ZIENKIEWICZ, O.; IRONS, B.; SCOTT, F. and CAMPBELL, J. Tree-dimensional stress analysis. **In Symposium on High Speed Computing of Elastic Structures (IUTAM)**, pp. 413–431, 1970.